NASA Tech Briefs

Official Publication of
National Aeronautics and
Space Administration
March 1990

Transferring Technology to
American Industry
and Government
Volume 14 Number 3

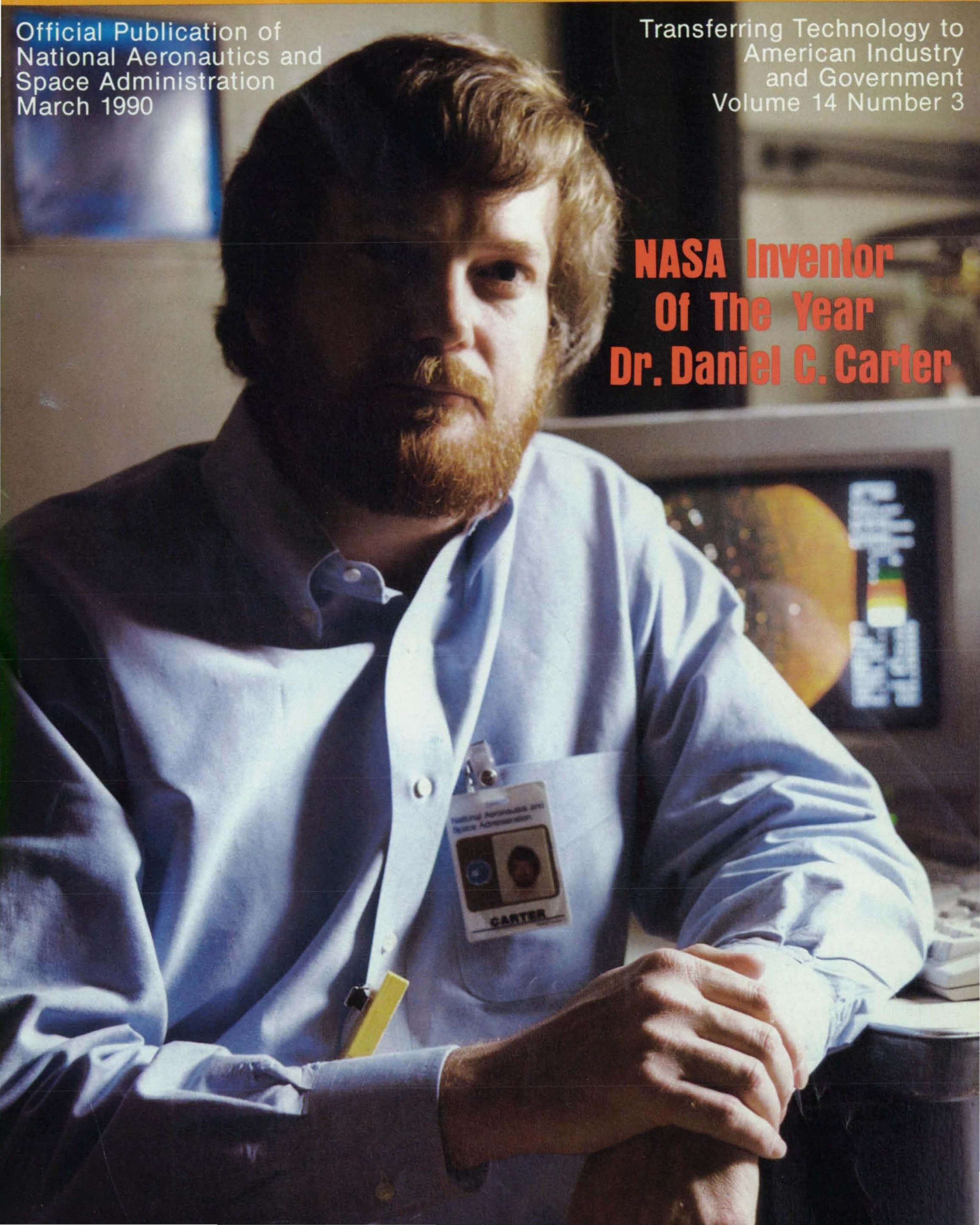

NASA Inventor Of The Year Dr. Daniel C. Carter

or Datalogger for Any Application...

For more information on these products

Circle Reader Action No. 619

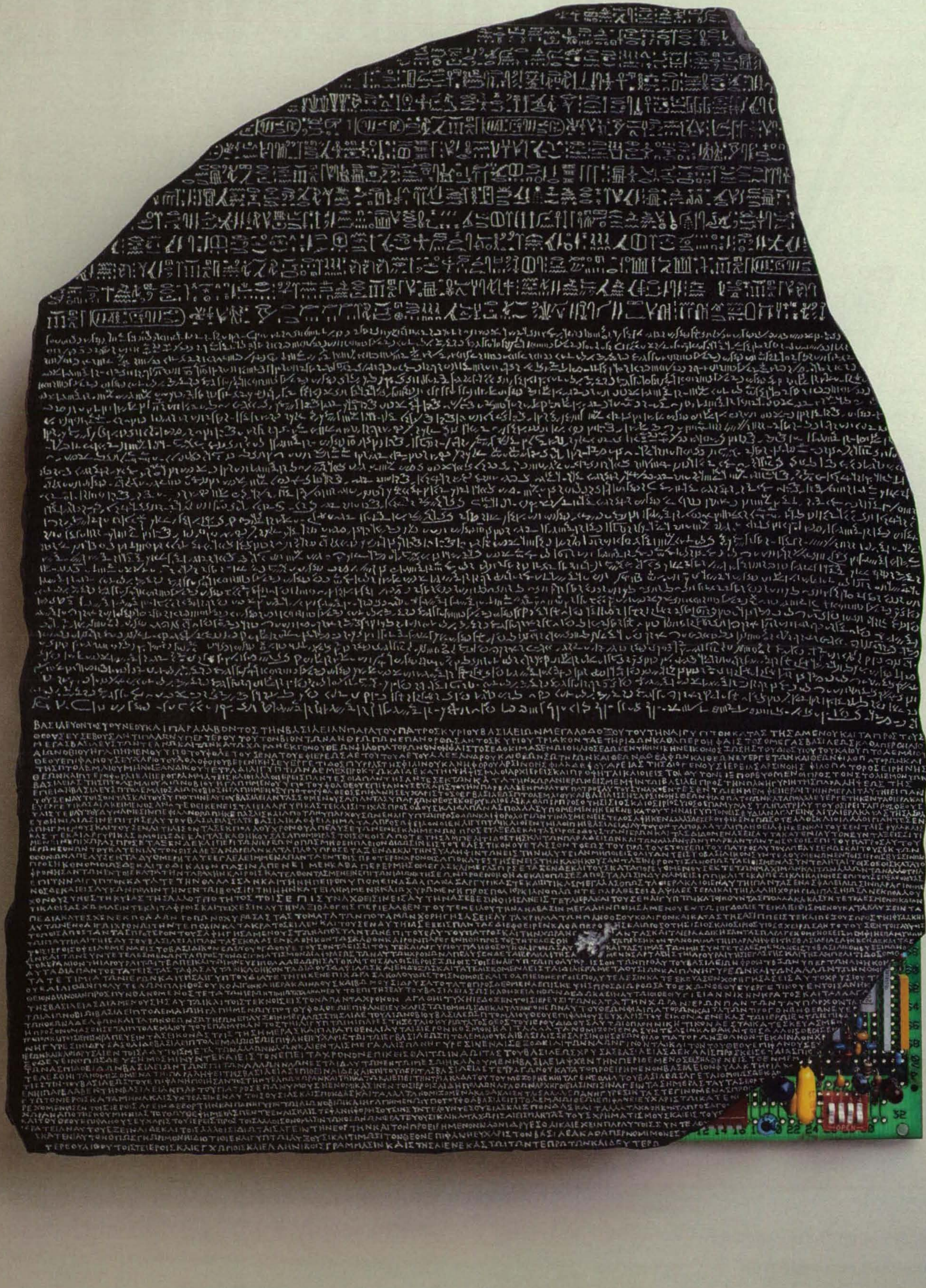

NASA Tech Briefs

Transferring Technology to
American Industry and Government

MARCH 1990
Volume 14 Number 3

SPECIAL FEATURES

NASA's Inventor Of The Year 14

The 1990 Award Finalists 15

Photo courtesy NASA

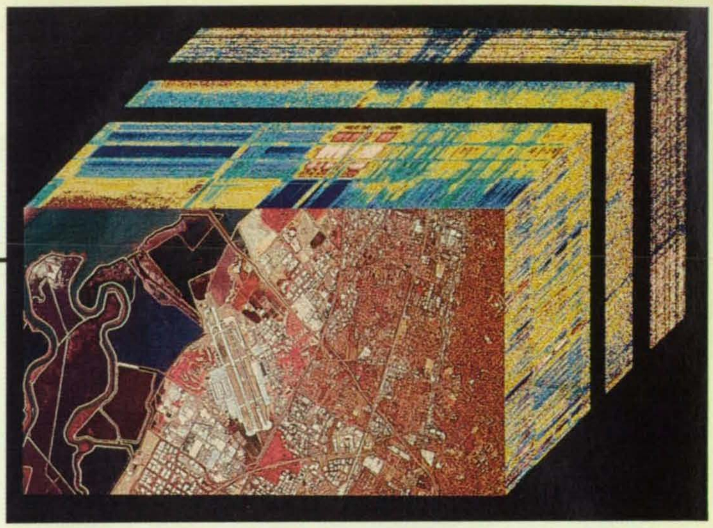

This image cube was acquired with the Airborne Visible/Infrared Imaging Spectrometer, which collects data in 220 narrow spectral bands in the wavelength region from 0.4 to 2.5 micrometers. The top of the cube is a false-color composite showing Palo Alto, California. Healthy vegetation appears red in the image, while the water of San Francisco Bay appears green. The two black bands are the atmospheric water absorption regions at 1.4 and 1.9 micrometers. For more on terrestrial-imaging spectroscopy, see page 65.

TECHNICAL SECTION

New Product Ideas 12

NASA TU Services 22

Electronic Components and Circuits 26

Electronic Systems 42

Physical Sciences 58

Materials 66

Computer Programs 68

Mechanics 70

Machinery 86

Fabrication Technology 89

Mathematics and Information Sciences 95

Subject Index 108

ABP BPA

DEPARTMENTS

On The Cover: Using a technique called x-ray crystallography, a Marshall Center research team headed by Dr. Daniel Carter has solved the three-dimensional structure of human serum albumin, the principal plasma protein in the circulatory system. This breakthrough, which could lead to the development of new or improved disease-fighting drugs, has earned Dr. Carter NASA's Inventor of the Year Award. Turn to page 14. (Photo courtesy NASA)

Editorial Notebook . . . 10

New on the Market 104

New Literature . . . 106

Advertisers Index 114

Photo courtesy NASA

The Orbiter Escape Pole, developed by this engineering group at the Johnson Space Center, will enable shuttle astronauts to quickly and safely bail out of a descending orbiter in the event of an aborted launch or other mission failure (page 18).

NASA Tech Briefs, ISSN 0145-319X, USPS 750-070, copyright © 1990 in U.S., is published monthly by Associated Business Publications Co., Ltd. 41 E. 42nd St., New York, NY 10017-5391. The copyrighted information does not include the individual Tech Briefs which are supplied by NASA. Editorial, sales, production and circulation offices at 41 E. 42nd Street, New York, NY 10017-5391. Subscriptions for non-qualified subscribers in the U.S., Panama Canal Zone, and Puerto Rico, $75.00 for 1 year; $125.00 for 2 years; $200 for 3 years. Single copies $10.00. Remit by check, draft, postal or express orders. Other remittances at sender's risk. Address all communications for subscriptions or circulation to NASA Tech Briefs, 41 E. 42nd Street, New York, NY 10017-5391. Second-class postage paid at New York, NY and additional mailing offices.

POSTMASTER: please send address changes to NASA Tech Briefs, 41 E. 42nd Street, Suite 921, New York, NY 10017-5391.

CLOSER SHEET AND STRIP TOLERANCES. JUST ONE FORM INCO ALLOYS INTERNATIONAL TECHNOLOGY TAKES.

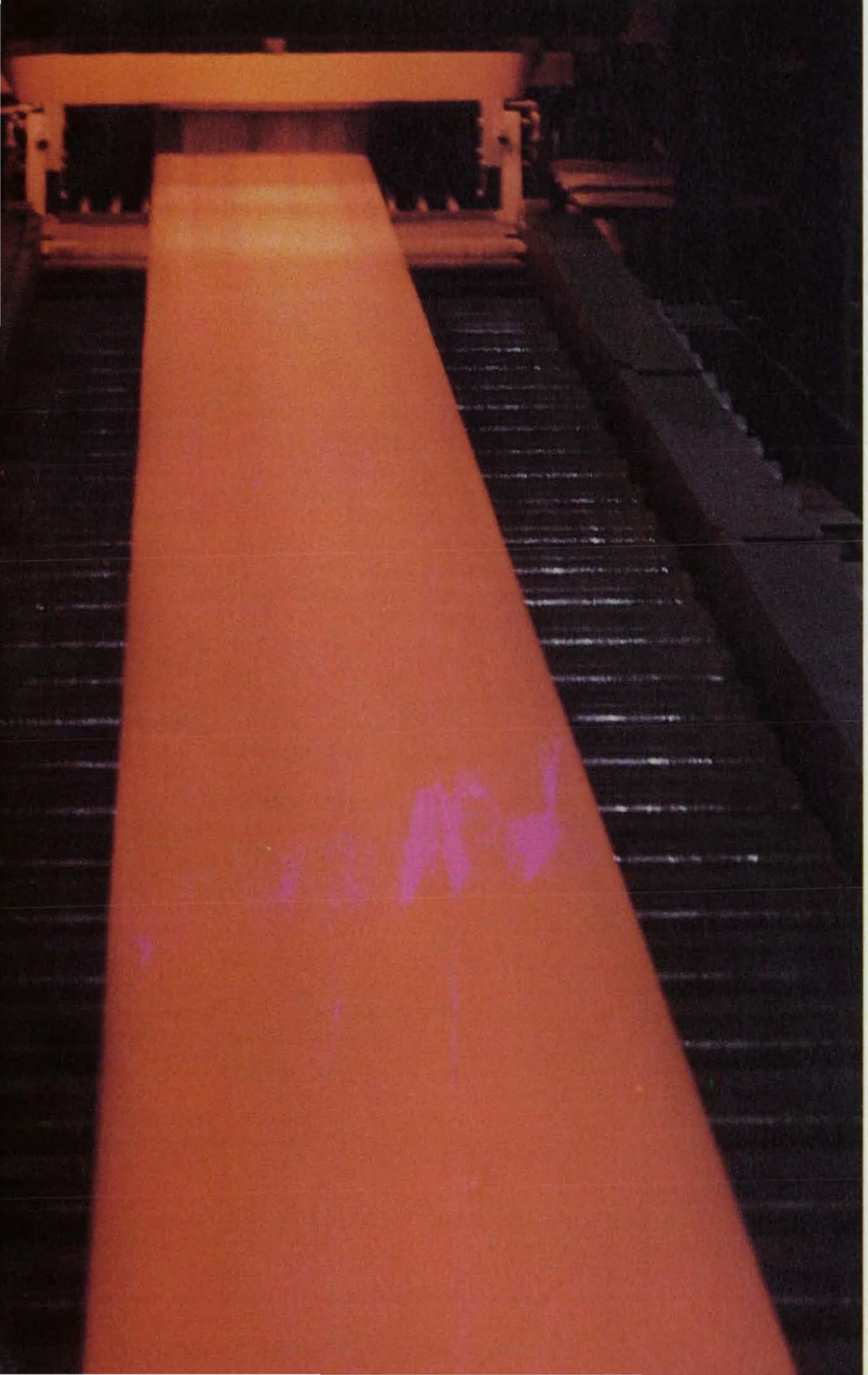

High-performance alloys are increasingly used as sheet and strip, for applications requiring ever-higher quality. Users of heat- and corrosion-resistant alloys want economical sheet/strip sizes, weld-free coils, improved surface quality, more precise section shape, and closer tolerances. Inco Alloys International has taken steps to meet these demands.

A new hot-strip reversing mill, unsurpassed among producers of high-performance alloys, combines with a recently acquired cold-rolling facility to offer you high-quality sheet and strip in thicknesses from .005″ to .250″ and widths from .750″ to 48.″ In addition to close dimensional tolerances, you get a superior surface finish and weld-free lengths in coil weights that can exceed 20,000 lb. And every production step is state-of-the-art, to give you the best product available.

This total in-house production permits strict quality control and traceability of your order from melting to shipment. And with the world's widest selection of high-performance alloys to choose from, you'll find exactly the properties you need. Corrosion resistance, high-temperature strength, superior dimensional stability — whatever it takes to get the job done.

Inco Alloys International also provides the performance and cost-efficiency you demand in a range of other forms such as rod, bar, plate, section, pipe, tubing, wire, and companion welding products. All available through a worldwide sales network including distribution centers located near you.

To find out more, write for a free copy of "High-Quality Superalloy Sheet and Strip." Inco Alloys International, Inc., Huntington, West Virginia 25720. Or, for a quicker reply, FAX us at (304) 526-5441.

INCO ALLOYS INTERNATIONAL

Distributors in the USA: Castle Metals, Metal Goods, Tubesales, and Williams & Co. In Canada: Atlas Alloys and Drummond McCall Inc.

Circle Reader Action No. 569

NASA Tech Briefs

Official Publication of
National Aeronautics and
Space Administration

ABP BPA

NASA Tech Briefs:

Published by .... **Associated Business Publications**
Editor-in-Chief/Publisher .... **Bill Schnirring**
Associate Publisher .... **Frank Nothaft**
Editor .... **Joseph T. Pramberger**
Managing Editor .... **R. J. Laer**
Assistant Editor .... **Theresa M. Detko**
Technical Advisor .... **Dr. Robert E. Waterman**
Production Manager .... **Rita Nothaft**
Traffic Manager .... **James E. Cobb**
Advertising Coordination Manager .... **Maya V.Falek**
Telecommunications Specialist .... **Evelyn Mars**
Reader Service Manager .... **Sylvia Valentin**

Briefs & Supporting Literature:
Provided to National Aeronautics and Space Administration by **International Computers & Telecommunications, Inc.**, NY, NY with assistance from **Logical Technical Services**, NY, NY
Technical/Managing Editor .... **Ted Selinsky**
Art Director .... **Luis Martinez**
Administrator .... **Elizabeth Texeira**
Chief Copy Editor .... **Lorne Bullen**
Staff Writers/Editors .... **Dr. James Boyd, Dr. Larry Grunberger, Dr. Theron Cole, Jordan Randjelovich, George Watson, Oden Browne**
Graphics .... **Vernald Gillman, Charles Sammartano**
Editorial & Production .... **Bill Little, Ivonne Valdes, Frank Ponce, Susan Finelli**

NASA:
NASA Tech Briefs are provided by the National Aeronautics and Space Administration, Technology Utilization Division, Washington, DC:
Administrator .... **Richard H. Truly**
Assistant Administrator for Commercial Programs ..... **James T. Rose**
Deputy Assistant Administrator (Programs) .... **Henry J. Clarks**
Acting Director TU Division (Publications Manager) .... **Leonard A. Ault**
Manager, Technology Utilization Office, NASA Scientific and Technology Information Facility .... **Walter M. Heiland**

Associated Business Publications
41 East 42nd Street, Suite 921, New York, NY 10017-5391
(212) 490-3999 FAX (212) 986-7864
President .... **Bill Schnirring**
Executive Vice President .... **Frank Nothaft**
Vice President .... **Domenic A. Mucchetti**
Operations Manager .... **Rita Nothaft**
Controller .... **Felecia Lahey**

Advertising:
New York Office: (212) 490-3999 FAX (212) 986-7864
Director of Advertising Sales .... **James G. McGarry**
Regional Sales Manager (Mid-Atlantic) .... **Michelle Larsen**
Account Executive .... **Debby Crane** at (201) 967-9838
Account Executive (Midwest, Northwest) .... **Paul Lesher, CBC** at (708) 501-4140
Regional Sales Manager (South-Central) .... **Douglas Shaller** at (212) 490-3999
Account Executives (Eastern MA, NH, ME, RI) .... **Paul Gillespie** at (508) 429-8907; **Bill Doucette** at (508) 429-9861
Account Executives (Western MA, CT, VT) .... **George Watts** or **David Haggett** at (413) 253-9881
Account Executives (Southeast) .... **Newton Collinson** or **Jonathan Kiger** or **Lawrence Mischik** at (404) 939-8391
Account Executives (Calif., AZ, NV, NM) ....
for Area Codes 818/213/805 —**Thomas Stillman**
for Area Codes 408/415/916/209 —**Elizabeth Cooper**
and for Area Codes 619/714 —**Karen Mock** at (213) 372-2744

NTBM-Research Center
Account Supervisor .... **Lourdes Del Valle**

Editorial Notebook

Technology 2000

Since we placed the small announcement about Technology 2000 in the February issue of *NASA Tech Briefs*, the phone has been ringing constantly. One of the most persistent callers has been our Director of Operations, demanding that I write an editorial explaining the show in a little more detail.

Technology 2000 will be the first major national conference and exposition devoted to NASA technology transfer and will be jointly sponsored by NASA, the Technology Utilization Foundation, and *NASA Tech Briefs* Magazine.

The event will be held November 27-28, 1990 at the Washington, DC Hilton Hotel. Scientists, project leaders, and engineering innovators from NASA Headquarters and field centers will present a series of symposia on present and planned NASA R&D programs which will focus on industry involvement and commercial application of emerging technologies evolving from projects such as Mission to Planet Earth, lunar base and Mars mission studies, and advanced communications research.

The need for such a conference is more pressing than ever. U.S. corporate R&D expenditures have steadily dwindled over the years to the point where they no longer keep pace with inflation, and government-sponsored research programs have correspondingly grown in importance as sources for the innovative technologies needed to create new commercial products. NASA field centers and other federal laboratories now account for over 50% of all R&D dollars spent in the U.S. each year. It is important that the transfer of the technology gained through current efforts be as comprehensive and effective as possible.

A recent study by the Chapman Research Group looked at a sample of 259 NASA spinoffs and found that secondary applications of space-based technologies have generated over $22 billion in product sales and business savings. As much technology as NASA's TU Program has transferred to American industry, a vast storehouse of untapped technology and technical knowledge awaits us.

Technology 2000 is designed to help you tap into that storehouse. Attendees will have the opportunity to interact with top NASA/contractor researchers and officials to learn about licensing arrangements, cooperative R&D ventures, and near-term agency needs and contracting opportunities. NASA Industrial Applications Centers will be among the exhibitors, as well as NASA contractors and other high-tech companies with technology available for transfer .

We see Technology 2000 as the first national gathering of the NASA Tech Briefs community, where the authors, researchers, readers, and vendor communities can gather to exchange ideas face to face at the exhibits and the symposia.

For further information on either attending or exhibiting at Technology 2000, write to me or Joe Pramberger, NASA Tech Briefs' Editor, at NASA Tech Briefs, 41 East 42nd St., Suite 921, New York, NY 10017, or call (212) 490-3999.

New Product Ideas

New Product Ideas are just a few of the many innovations described in this issue of *NASA Tech Briefs* and having promising commercial applications. Each is discussed further on the referenced page in the appropriate section in this issue. If you are interested in developing a product from these or other NASA innovations, you can receive further technical information by requesting the TSP referenced at the end of the full-length article or by writing the Technology Utilization Office of the sponsoring NASA center (see page 22). NASA's patent-licensing program to encourage commercial development is described on page 22.

Gallium Arsenide Domino Circuit

An experimental gallium arsenide field-effect-transistor (FET) domino circuit could be replicated in large numbers for use in dynamic-logic systems. The circuit fulfills a need for low-power, fast, dynamic-logic circuits with acceptable noise margins.
(See page 36)

Lightweight, Thermally Conductive Composite Material

A lightweight composite material consisting of an aluminum matrix containing graphite fibers has greater thermal conductivity than that of copper at temperatures from −20 to +140 °C. Per unit weight, the material is approximately 4 times as conductive as pure copper, twice as conductive as pure aluminum, and 2.6 times as conductive as 6061 structural aluminum alloy.
(See page 66)

Automatic Tension Adjuster for Flexible-Shaft Grinder

The flexible shaft of a grinding tool is automatically maintained in tension by air pressure. The probelike tool can be bent to reach hard-to-reach areas for grinding and polishing.
(See page 93)

Pressure-Measuring Diaphragm Transmits Optical Signals

A proposed sapphire diaphragm would allow both optical and pressure measurements in an instrumented research engine or pressure vessel. Strain gauges around the edge of the diaphragm would measure the deflection caused by pressure or vacuum in the vessel, and at the same time, the transparent diaphragm would transmit light for optical measurements.
(See page 76)

This symbol appears next to technical briefs which describe inventions having potential commercial applications as new products. The process for developing a product from a NASA invention is described at the top of this page.

After centuries of practice, mankind perfects engineering calculations: MathCAD.

Announcing MathCAD 2.5: The Dawn of a New Age.

What the historians will call it, only time will tell.

Perhaps the Century of Speed, or the Era of Ease. But whatever the name, this is the age of MathCAD 2.5, the only math package that looks and works the way you think.

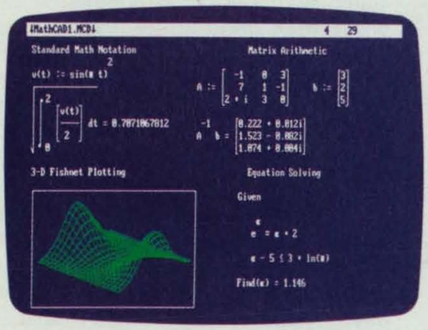

MathCAD 2.5 includes 3-D plotting, HPGL sketch import, and PostScript output.

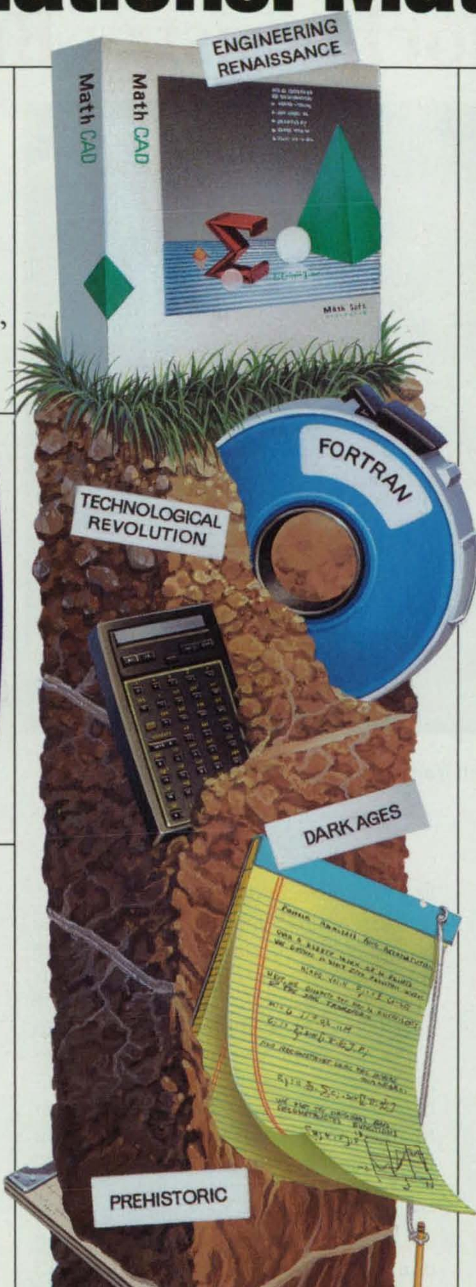

MathCAD is far and away the best-selling math package in the world. Because it lets you perform engineering and scientific calculations in a way that's faster, more natural and less error-prone than the way you're doing them now–whether you're using a scratchpad, calculator, spreadsheet or program that you wrote yourself.

And now we've made the best even better. MathCAD 2.5 is a dramatically improved version that includes three-dimensional plotting, enhanced numerical analysis, and the ability to import HPGL files from most popular CAD programs, including AutoCAD.® And now you can print on PostScript® compatible printers.

And like before, MathCAD's live document interface™ lets you enter equations anywhere on the screen, add text to support your work, and graph the results. Then print your analysis in presentation-quality documents.

It has over 120 commonly used functions built right in, for handling equations and formulas, as well as exponentials, differentials, cubic splines, FFTs and matrices.

No matter what kind of math you do, MathCAD 2.5 has a solution for you. In fact, it's used by over 60,000 engineers and scientists, including electrical, industrial, and mechanical engineers, physicists, biologists, and economists.

But don't take our word for it; just ask the experts. PC Magazine recently described MathCAD as "everything you have ever dreamed of in a mathematical toolbox."

PC MAGAZINE EDITORS' CHOICE
March 14, 1989 issue.
Best of '88
Best of '87

And for Macintosh® users, we present MathCAD 2.0, rewritten to take full advantage of the Macintosh interface. Entering operators and Greek letters into equations is pure simplicity!

Look for MathCAD 2.5 at your local software dealer, or give us a call. For more information, a free demo disk, or upgrade information, dial 1-800-MATHCAD (in MA, 617-577-1017).

Available for IBM® compatibles and Macintosh computers.

MathCAD®

MathSoft, Inc. One Kendall Square, Cambridge, MA 02139

22

U.K.: Adept Scientific 0462-480055; **France:** ISE CEGOS 1-46092768; **Germany:** Softline 07802-4036; **Japan:** CRC 03-665-9768. *PE*

Circle Reader Action No. 682

NASA's Top Inventors:

Marshall Scientist Earns Inventor Of The Year Award For Biochemistry Breakthrough

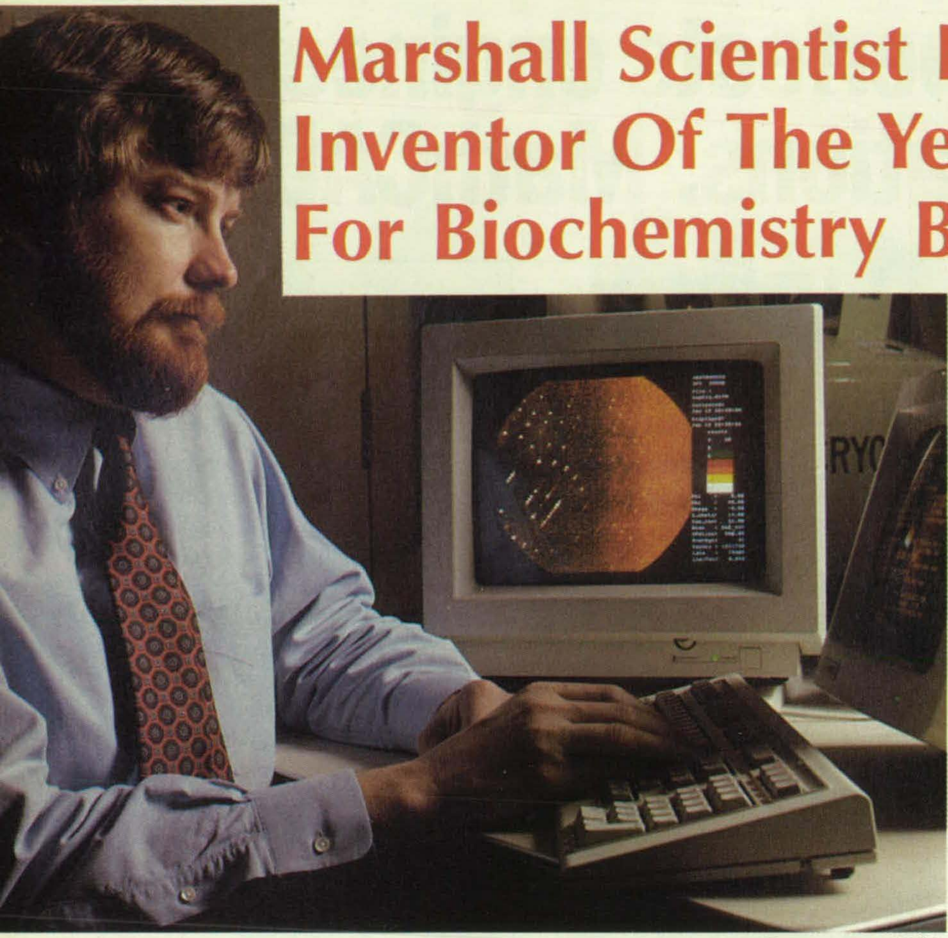

Photo courtesy NASA

Dr. Daniel Carter studies a diffraction pattern from a crystal of human serum albumin.

Dr. Daniel C. Carter, a senior scientist in the Marshall Space Flight Center's Biophysics Branch, has been named NASA's 1990 Inventor of the Year for his pathfinding work in the field of protein crystallography. Carter, 35, has solved the three-dimensional structure of human serum albumin (HSA), the principal protein of the circulatory system. His discovery could lead to major advances in drug design and genetic engineering.

Carter determined the molecule's makeup using a technique called x-ray crystallography, in which protein crystals are placed in an x-ray beam to create diffraction patterns for analysis. By compiling the images from hundreds of diffraction experiments, Carter's research team built a three-dimensional computer model showing the snake-like arrangement of HSA's 585 amino acids.

"This molecule (HSA) has been flowing through the veins of man for millions of years," Carter said. "Now, for the first time, we can see what it looks like and how it operates."

HSA's structure is of great medical importance because the protein binds and transports thousands of endogenous ligands and therapeutic drugs in plasma. Carter has mapped HSA to a resolution of four angstroms, allowing reseachers to pinpoint where calcium, copper, fatty acids, and other molecules attach to the protein. The Marshall group has already identified the binding sites for more than a dozen drug compounds, including aspirin, diazepam, ibuprofen, and AZT, a drug used to stop the spread of the AIDS virus. Explained Carter: "Because of HSA's incredible ability to transport and sequester such a chemically diverse group of molecules, scientists previously thought that binding was random. We have found, however, that the protein's multifunctional binding properties can be explained by only two to three active regions on the molecule."

Knowledge of the binding areas will allow pharmaceutical companies to design new drugs or alter existing drugs so they may be more efficiently carried by HSA through the body. Many existing drugs are ineffective because they bind too tightly to serum albumin and never reach their targets.

Carter has teamed with British chemist Max Perutz, the founding father of macromolecular crystallography, to study the binding modes of drugs designed to treat sickle-cell anemia. "These drugs work great in the test tube but are rendered ineffective by HSA in the body," Carter said. The researchers will look at ways to tailor the molecular structures of the drugs to reduce their affinity for HSA and increase it for the sickle cell hemoglobin.

A possible alternate approach, Carter said, is to develop a "generic" inhibitor molecule that would block serum albumin's active regions during drug therapy. "That way you wouldn't have to custom-design each drug to avoid serum albumin's grasp," he explained.

The Marshall scientist is also collaborating with several biotechnology companies to conduct genetic engineering experiments based on the newfound knowledge of HSA's architecture. One company is exploring site-directed mutagenisis of HSA; another is developing polypeptides one-sixth the size of the parent HSA molecule which offer applications as blood substitutes and as the active components of biosensors and chromatographic matrices. The latter group has produced a synthetic protein and wants to know "how it matches up to the real McCoy," according to Carter. "The 3D structure gives them a model for comparison. They can check, for instance, whether or not the different disulfide bridges are formed properly."

Melding Science And Art

Crystallographers have been trying to solve the structure of serum albumin for nearly a century, but their efforts have been thwarted by problems with crystal size and quality. Carter's success is due primarily to his ability to

(continued on page 20)

The 1990 Award Finalists

NASA's Office of General Counsel, sponsor of the agency's Inventor of the Year competition, selected Marshall nominee Dr. Daniel Carter from a field of six finalists whose inventions were patented and/or commercially available during 1989. The other nominees' innovative work—which includes advances in materials science, signal processing, and spaceflight safety—is highlighted in the following pages.

Goddard Space Flight Center

Dr. Sheng Y. Lee

Invention:
Cellular Thermosetting Fluorodiepoxide Polymers
(page 16)

Langley Research Center

James I. Clemmons (left) and **James F. Meyers**

Invention: Frequency Domain Laser Velocimeter Signal Processor (page 16)

Lewis Research Center

left to right: **Bruce A. Banks**, **Michael J. Mirtich**, and **James S. Sovey**

Invention:
Dual-Ion-Beam Deposition of Diamond-Like Carbon Films
(page 18)

Johnson Space Center

left to right, top row: **Margaret E. Grimaldi, John P. McManamen, Bruce H. Becker, Clarence J. Wesselski** bottom row: **Jon B. Kahn, Edgar O. Castro, Timothy E. Pelischek** absent: **Dr. Winston B. Goodrich**

Invention: The Orbiter Escape Pole (page 18)

Ames Research Center

left to right: **Dr. Salvatore R. Riccitiello, Dr. Ming-Ta S. Hsu,** and **Dr. Timothy S. Chen**

Invention: Boron-Containing Organosilane Polymers
(page 18)

Frequency Domain Laser Velocimeter Signal Processor

James F. Meyers and James I. Clemmons, Jr.
Langley Research Center, Hampton, VA

Langley's nominees collaborated with scientists at the Old Dominion University Research Foundation to create an innovative scheme for processing signals from laser velocimeter systems. Their invention is a "smart" digital instrument that reconfigures itself, based on the input signal characteristics, to achieve highly accurate measurements. It can solve fluid flow problems requiring a low signal-to-noise ratio (SNR), as in flare conditions identified with near surface measurements, or high accuracy, as in laminar flow measurements.

Laser velocimetry is a nonintrusive method for gauging the velocity of micron sized particles embedded in fluids or microscopic flaws in surfaces. The optical system creates an interference fringe pattern using two crossed laser beams. As a particle passes through the fringes, it scatters light from the lighted bands. A portion of this oscillating light is collected by a photomultiplier tube and converted to an electrical signal. This signal — a burst about a microsecond long — contains a chirp whose frequency is directly related to the rate at which the particle passes through the lighted bands.

The Langley invention employs a transient recorder to capture the signal burst and digital signal processing to determine its oscillation frequency. This approach offers an eight-fold increase in measurable signals and a five-fold increase in measurement accuracy over conventional techniques such as burst counters. Further, it reduces the required SNR by a factor of 32, allowing measurements within boundary layers of wind tunnel models.

The signal processor can be incorporated into any standard laser velocimeter system. In addition to benefiting aerodynamics research, the invention permits laser velocimetry to be used in industrial applications requiring precise velocity measurements of moving objects such as strip material and transmission parts. For example, by measuring the velocity of sheet aluminum to determine its length, manufacturers of aluminum cans could save an estimated $100,000 per plant each month.

Under an exclusive licensing agreement, Macrodyne Inc. of Clifton Park, NY is manufacturing a commercial version of this invention called the Model 3100 Frequency Domain Processor. It features a 50 MHz sample rate, providing a 20 MHz bandwidth, with a minimum sensitivity of 50 mV full-scale. Testing at NASA's Ames Research Center in near-wall, boundary layer conditions with low SNR shows the Model 3100 significantly enhances the accuracy of complex flow measurements.

Flow visualization and wind tunnel laser velocimeter measurements of the leading-edge extension (LEX) generated vortex above an F-18 at 25 degrees angle of attack.

Photo courtesy NASA

Cellular Thermosetting Fluoropolymers

Dr. Sheng Y. Lee
Goddard Space Flight Center, Greenbelt, MD

Dr. Lee has developed a process for making fluoropolymer foams with controllable amounts of inert-gas fillings in the foam cells. Unlike thermoplastic fluoropolymers, the thermosetting fluoropolymers do not require foaming additives that leave undesirable residues, and can be formed at relatively low temperatures and pressures. Applications include coatings, electrical insulation, and wire products such as coaxial cables and power lines.

The process involves mixing a fluorodiepoxide and a curing agent, typically an adduct amine, at or near room temperature. After deaeration in a vacuum, the mixture is placed in a chamber, which is then filled with a gas at a pressure of several atmospheres. The filling gas can be air, oxygen, nitrogen, or any of a variety of elements that do not react chemically with the mixture. Experiments have shown that the gas reacts physically with the mixture in a controlled way and can be squeezed into the mixture as long as the fluorine content is at least 30 to 40 percent by weight.

The mixture is allowed to cure partially at room temperature. Once the mixture has gelled, the gas is trapped in the polymer, which is then removed from the pressure chamber and heated to approximately 70°C to complete the cure. By comparison, thermoplastic fluoropolymers must be heated to 240°C or higher and are subjected to pressures approaching 1500 psi.

While the polymer is being cured, the trapped gas causes it to foam by heating. The depth of foaming depends on the type of gas and can be increased by increasing the pressure during the partial curing stage.

The type and amount of gas can be varied to achieve a desired mass density. The material can be foamed to the maximum extent, for example, to reduce the amount of flouropolymers needed and thereby cut costs. A gas filling — possibly sulfur hexafluoride — could be used to enhance the dielectric properties of a foam for electrical insulation; another gas such as oxygen or Freon could be selected to support or retard combustion.

The fluoropolymer resins employed can be any thermosetting fluoropolymer including fluoroepoxies, fluoropolyurethanes, and fluoroacrylates.

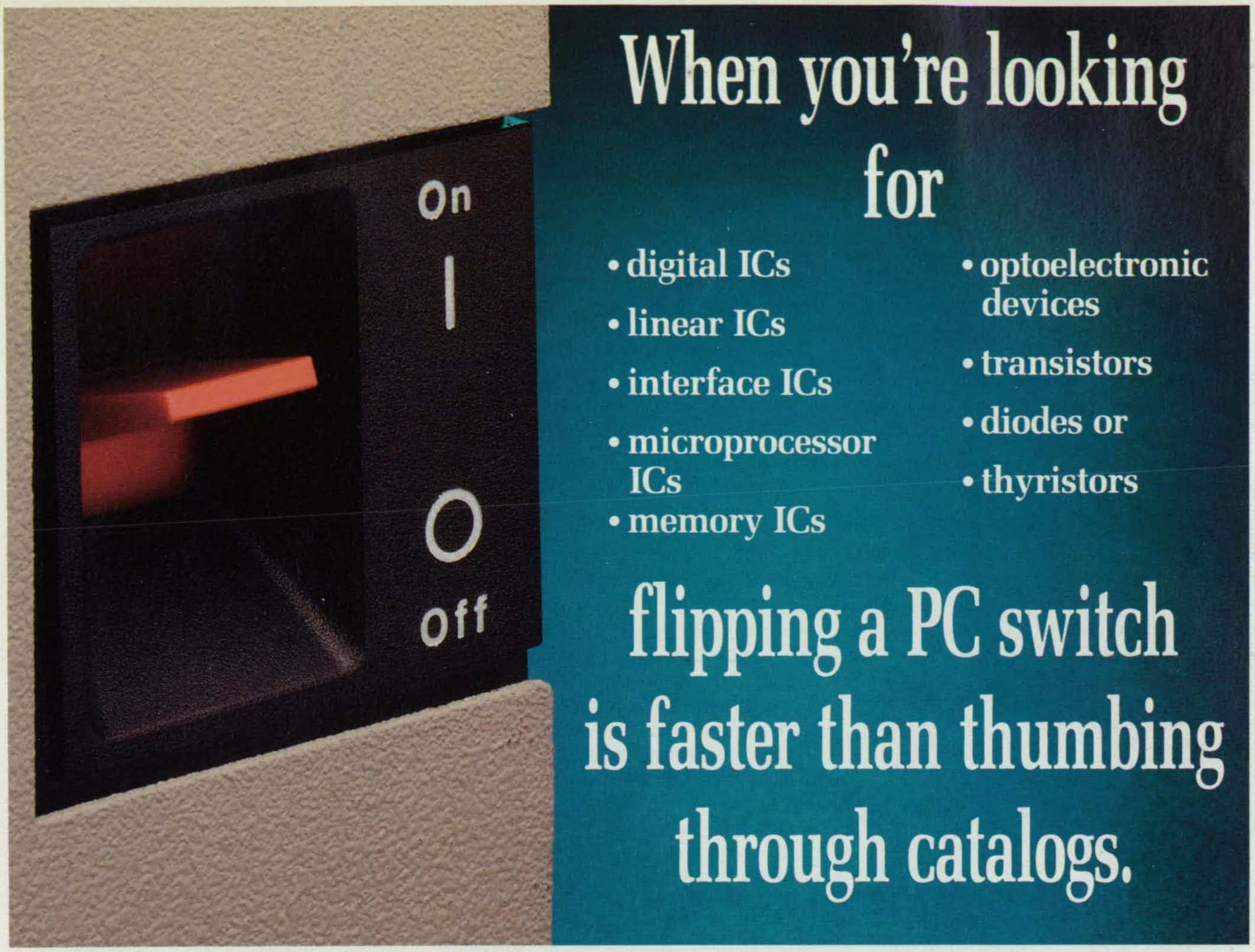

That's why the IC/Discrete Parameter Database is on CD-ROM!

Now do component research a new way. Software for your IBM® AT® compatible and a database on CD-ROM provide fingertip access to over 1.1 million ICs and discrete semiconductors from 1,100 manufacturers.

- Search for active *and* discontinued devices, commercial and mil/high rel.
- Locate devices by component characteristic, IC generic number, manufacturer part number, Mil/883 part number, Mil slash sheet number, NSN or DESC drawing number.
- Access over 272,000 manufacturers' datasheets and 19,000 Mil spec/QPL 38510 and 19500 slash sheets. *Exact* images of the hardcopy version! And, all the text, application notes, mechanical data, outline drawings, packaging and ordering information can be printed in seconds.

All the critical information you need at the flip of a switch!

The results? Time saving searching—and time is money.

Circle Reader Action No. 546

For a free demo diskette return the coupon below or call toll-free:

800-241-7824

In Colorado and outside the U.S.A.: 303-790-0600 ext. 59
Telex: 4322083 IHS UI
Fax: 303-799-4085 (U.S.A.); 303-799-4097 (outside the U.S.A.)

Yes! Please send me a FREE DEMO DISKETTE and more information.

Name ______________________

Dept./Title ______________________

Organization ______________________

Address ______________________

City __________ State __________ Zip __________

Phone ( ) ______________________

Information Handling Services®
15 Inverness Way East; Englewood, Colorado 80150

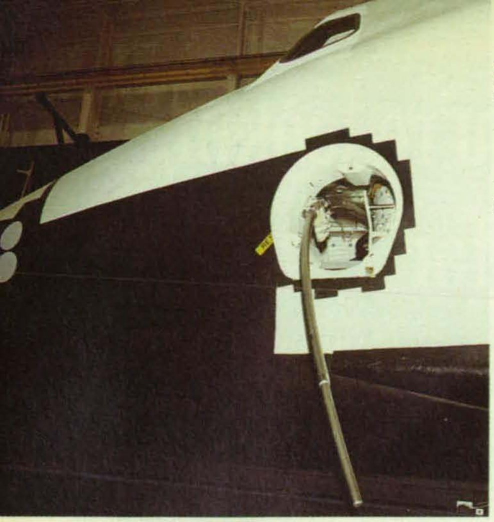

Photo courtesy NASA

In the event of an aborted launch or other mission failure, the Orbiter Escape Pole will enable shuttle astronauts to quickly and safely bail out of the orbiter.

The Orbiter Escape Pole

Dr. Winston B. Goodrich, Clarence J. Wesselski, Timothy E. Pelischek, Bruce H. Becker, Jon B. Kahn, Margaret E. Grimaldi, John P. McManamen, and Edgar O. Castro
Johnson Space Center, Houston, TX

In the wake of the space shuttle Challenger accident, NASA sought to provide shuttle astronauts with an emergency escape capability. The escape system NASA selected features a curved telescoping pole that allows crew members to bail out of the orbiter without danger of hitting a wing or other structure. The lightweight aluminum and steel pole is simple to operate and safer than alternative propulsive modes of crew expulsion. It enables eight astronauts to bail out in less than two minutes.

The escape pole will only be used in the event of an aborted launch or other emergency situation in which the orbiter cannot reach a runway and must be ditched. Once the shuttle is brought into a controlled, gliding flight mode, the cabin is depressurized and the side hatch pyrotechnically jettisoned. A crew member then activates the pole's automatic extension system, which extends the pole out, down, and rearward from the hatch opening. Crew members attach their parachute harnesses to a magazine-fed, roller loop lanyard connected to the pole, egress the hatch, slide down the pole, and descend to a safe landing.

The pole housing attaches to the orbiter's middeck ceiling and is 126.75 inches long. The primary extension is 112.54 inches (arched length) and the end extension is 32.65 inches. For launch and landing, the unextended pole is oriented toward the closed crew hatch. During on-orbit operations, it is repositioned toward the middeck lockers and stowed on the ceiling so that it does not interfere with crew activities in the middeck area.

At the beginning of deployment, a kicker-spring mechanism pushes the main pole out of the housing, guided by a bearing block. An arrester assembly stops the pole as it reaches the limit of its movement, absorbing its kinetic energy. Then a second spring pushes the end extension outward. A locking device prevents the extension from retracting once it has been deployed. If the kicker spring mechanism fails, a redundant manual system can be used to deploy the pole.

Johnson Center engineers designed and developed the escape pole in time for Discovery's "return to flight" mission in September 1988, and it has been carried on each subsequent mission.

Boron-Containing Organosilane Polymers

Dr. Salvatore R. Riccitiello, Dr. Ming-Ta S. Hsu, and Dr. Timothy S. Chen
Ames Research Center, Moffett Field, CA

This research team garnered Ames' nomination by developing a new, improved way to make high-performance ceramic materials. They have successfully synthesized boron-silicon polymers which yield non-oxide, high-temperature silicon borides, silicon carbide, and Si-B-C ceramics upon pyrolysis.

Non-oxide ceramics are exceptionally hard materials that resist creep and thermal shock and have a low coefficient of thermal expansion. Fabricating these materials into usable shapes is difficult, however, and requires sintering their powders at 1500°C or higher, often under extreme pressure. Polymer pyrolysis is an emerging alternate method that promises improved ceramics and expanded applications for new ceramics. One advantage of polymer processing is that parts are formed without using additives or binding agents.

The Ames group synthesized several polymers with boron-silicon bonds in their backbones through the coupling reaction of boron halides or organoboron halides with halosilanes in an aprotic solvent. Black ceramic materials were produced from the polymers upon thermal degradation at temperatures above 1000°C, with a ceramic yield of up to 70%. The ceramics are stable in air to 1100°C with little weight gain or loss. They consist of a mixture of silicon carbide, silicon borides, and amorphous Si-B-C, with small amounts of silica and free silicon.

Further studies show that these polymers can be melt-spun to green fiber with a 30-80μm diameter. The new Si-C-B fibers are similar in tensile strength to NICALON silicon carbide at room temperature. Preliminary data indicates, however, that at 1200°C the tensile strengths of Si-B-C are higher than at room temperature. In contrast, NICALON fibers lose strength above 1150°C.

Deposition Of Diamond-Like Carbon Films

Bruce A. Banks, Michael J. Mirtich, and James S. Sovey
Lewis Research Center, Cleveland, OH

A unique dual ion beam system developed by these Lewis scientists enables low-temperature deposition of diamond-like carbon coatings on plastics, quartz, silicon, metals, and a variety of other materials. The patented process can be used to coat relatively large objects and produces films with high electrical resistivity, extreme hardness and clarity, and chemical inertness — making them well-suited for optics and electronics applications.

The carbon thin-film is deposited on the substrate surface by exposing the surface to an argon ion beam containing a hydrocarbon, typically methane. The ion beam's current density is kept low during initial deposition of the film, then increased to full power. At the same time, a second ion beam with a higher energy level is directed towards the substrate surface. The added energy improves the mobility of the condensing atoms and removes lesser bound atoms.

NASA has licensed this technology to Air Products and Chemicals, Inc. of Allentown, PA. The company is currently using the deposition process to create scratch-resistant coatings for watch crystals, plastic sunglass lenses, and eyeglass lenses.

Full commitment. By the numbers.

MIL-C-38999, series I, II, III, IV. The choice you need in qualified connectors. The commitment you need from your supplier.

The MATRIX MIL-C-38999 line from AMP is the first to be qualified to series I, II, III, and IV—and the first to give you a meaningful selection for today's all-encompassing design environment.

Start with the features you'd expect with the freedom to choose from *any* series. Cover basics with high density and reliable, scoop-proof mating. Move up and save space, and weight. Move again to cover applications in extreme environments. Move again when you need outstanding vibration resistance.

And the full MATRIX line from AMP offers even more.

- Filtered/surge-protected versions.
- Hermetically sealed versions.
- Versions with firewall inserts.
- Aluminum, stainless steel, and composite shell versions.

Plus our full commitment to support and delivery performance.

For details on the MATRIX MIL-C-38999 line, call us at 1-800-522-6752. Or write: AMP Aerospace and Government Systems Sector, Harrisburg, PA 17105-3608.

THIS IS AMP TODAY. **AMP**

Circle Reader Action No. 657

Dual beam ion source for deposition of films with diamond-like properties

Other applications include insulating gates for field effect transistors, integral coatings for solar cells or laser windows, and protective coatings for metals.

For information on licensing or sublicensing any of these inventions, contact the patent counsel at the NASA field center that sponsored the research (see page 22).

Photo courtesy NASA

NASA's Inventor Of The Year

(continued from page 14)

grow large (0.5 to 1.0 mm), highly-ordered crystals that are easily reproduced and strong enough to withstand analysis. "Protein crystal growth is as much an art as a science, " said Carter, who holds a PhD in x-ray crystallography from the University of Pittsburgh. "The crystals are extremely delicate and it takes a lot of trial and error to obtain a good crystal form."

Carter said he has performed "tens of thousands" of protein crystallography experiments since joining the Marshall Center's Space Science Laboratory in 1985. "Perseverance is a crystallographer's greatest asset," he said with a smile. "You often work for years before you get a breakthrough, so you have to be willing to hang in there."

As a co-investigator in NASA's crystal growth experiments aboard the space shuttle, Carter is currently studying the effects of microgravity on the growth of HSA. He hopes to use especially pure space-grown crystals to develop a three-angstrom image of the protein's structure. "When we get to three angstroms resolution," he said, "we'll be able see the chemistry of the individual binding sites — how Mother Nature arrived at these multifunctional binding pockets."

Carter likens his work to that of an astronomer "peering into the unknown" in seach of new discoveries. "Our telescopes are x-ray diffraction machines and computers," he said. "Astronomers look at outer space and we look at inner space — the basic mechanisms of life."

By winning NASA's Inventor of the Year Award, Carter automatically qualifies as the agency's nominee for the National Inventor of the Year competition sponsored by the Intellectual Property Owners Inc., a Washington, DC group that lobbies for stricter laws to protect patents, trademarks, and copyrights. The winner — to be chosen from approximately 100 industry and government nominees nationwide — will be announced in May. ❑

For more on Dr. Carter's work, see NASA Tech Briefs *Vol. 13, Num. 9.*

Computer model shows the electron density in one of serum albumin's six bundles of intertwining amino acids.

Illustration courtesy NASA

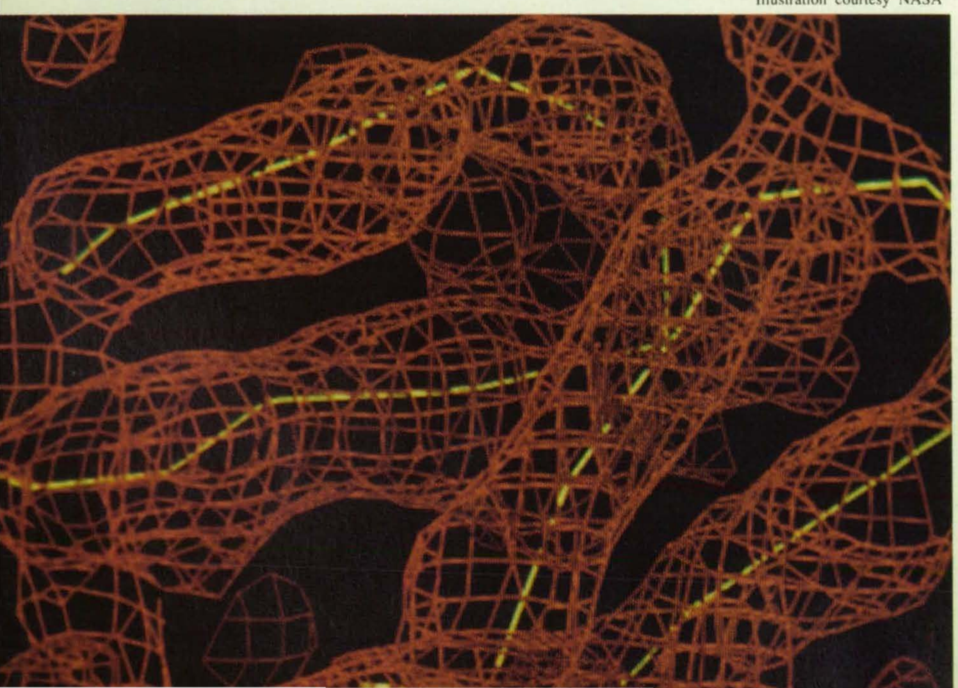

HOW YOU CAN BENEFIT FROM NASA's TECHNOLOGY UTILIZATION SERVICES

If you're a regular reader of TECH BRIEFS, then you're already making use of one of the low- and no-cost services provided by NASA's Technology Utilization (TU) Network. But a TECH BRIEFS subscription represents only a fraction of the technical information and applications/engineering services offered by the TU Network as a whole. In fact, when all of the components of NASA's Technology Utilization Network are considered, TECH BRIEFS represents the proverbial tip of the iceberg.

We've outlined below NASA's TU Network—named the participants, described their services, and listed the individuals you can contact for more information relating to your specific needs. We encourage you to make use of the information, access, and applications services offered by NASA's Technology Utilization Network.

How You Can Utilize **NASA's Industrial Applications Centers**—A nationwide network offering a broad range of technical services, including computerized access to over 100 million documents worldwide.

You can contact NASA's network of Industrial Applications Centers (IACs) for assistance in solving a specific technical problem or meeting your information needs. The "user friendly" IACs are staffed by technology transfer experts who provide computerized information retrieval from one of the world's largest banks of technical data. Nearly 500 computerized data bases, ranging from NASA's own data base to Chemical Abstracts and INSPEC, are accessible through the ten IACs located throughout the nation. The IACs also offer technical consultation services and/or linkage with other experts in the field. You can obtain more information about these services by calling or writing the nearest IAC. User fees are charged for IAC information services.

Aerospace Research Applications Center (ARAC)
Indianapolis Center for Advanced Research
611 N. Capitol Avenue
Indianapolis, IN 46204
Dr. F. Timothy Janis, Director
(317) 262-5036

Central Industrial Applications Center/NASA (CIAC)
Rural Enterprises, Inc.
P. O. Box 1335
Durant, OK 74702
Dr. Dickie Deel, Director
(405) 924-5094

Science and Technology Research Center (STRC)
Post Office Box 12235
Research Triangle Park, NC 27709-2235
H.L. (Lynn) Reese, Director
(919) 549-0671

NASA Industrial Applications Ctr. 823 William Pitt Union
University of Pittsburgh
Pittsburgh, PA 15260
Dr. Paul A. McWilliams, Exec. Director
(412) 648-7000

NASA/Southern Technology Applications Center
Box 24
Progress Ctr., One Progress Blvd.
Alachua, FL 32615
J. Ronald Thornton, Director
(904) 462-3913
(800) 354-4832 (FL only)
(800) 225-0308 (toll-free US)

NASA/UK Technology Applications Program
University of Kentucky
109 Kinkead Hall
Lexington, KY 40506-0057
William R. Strong, Director
(606) 257-6322

NERAC, Inc.
One Technology Drive
Tolland, CT 06084
Dr. Daniel U. Wilde, President
(203) 872-7000

Technology Application Center (TAC)
University of New Mexico
Albuquerque, NM 87131
Dr. Stanley A. Morain, Director
(505) 277-3622

NASA Industrial Applications Center
University of Southern California Research Annex
3716 South Hope Street
Los Angeles, CA 90007-4344
Robert Stark, Director
(213) 743-6132
(800) 642-2872 (CA only)
(800) 872-7477 (toll-free US)

NASA/SU Industrial Applications Center
Southern University Department of Computer Science
P. O. Box 9737
Baton Rouge, LA 70813-9737
Dr. John Hubbell, Director
(504) 771-6272

If you represent a public sector organization with a particular need, you can contact NASA's Application Team for technology matching and problem solving assistance. Staffed by professional engineers from a variety of disciplines, the Application Team works with public sector organizations to identify and solve critical problems with existing NASA technology. **Technology Application Team, Research Triangle Institute, P. O. Box 12194, Research Triangle Park, NC 27709. *Doris Rouse, Director,* (919) 541-6980**

How You Can Access Technology Transfer Services At NASA Field Centers: **Technology Utilization Officers & Patent Counsels**—Each NASA Field Center has a Technology Utilization Officer (TUO) and a Patent Counsel to facilitate technology transfer between NASA and the private sector.

If you need further information about new technologies presented in *NASA Tech Briefs,* request the Technical Support Package (TSP). If a TSP is not available, you can contact the Technology Utilization Officer at the NASA Field Center that sponsored the research. He can arrange for assistance in applying the technology by putting you in touch with the people who developed it. If you want information about the patent status of a technology or are interested in licensing a NASA invention, contact the Patent Counsel at the NASA Field Center that sponsored the research. Refer to the NASA reference number at the end of the Tech Brief.

Ames Research Ctr.
Technology Utilization Officer: Laurance Milov
Mail Code 223-3
Moffett Field, CA 94035
(415) 694-4044
Patent Counsel: Darrell G. Brekke
Mail Code 200-11
Moffett Field, CA 94035
(415) 694-5104

Lewis Research Center
Technology Utilization Officer: Anthony F. Ratajczak (acting)
Mail Stop 7-3
21000 Brookpark Road
Cleveland, OH 44135
(216) 433-5568
Patent Counsel: Gene E. Shook
Mail Code LE-LAW
21000 Brookpark Road
Cleveland, OH 44135
(216) 433-5753

John C. Stennis Space Center
Technology Utilization Officer: Robert M. Barlow
Code HA-32
Stennis Space Center, MS 39529
(601) 688-1929

John F. Kennedy Space Center
Technology Utilization Officer: Thomas M. Hammond
Mail Stop PT-PMO-A
Kennedy Space Center, FL 32899
(407) 867-3017
Patent Counsel: James O. Harrell
Mail Code PT-PAT
Kennedy Space Center, FL 32899
(407) 867-2544

Langley Research Ctr.
Technology Utilization Officer: John Samos
Mail Stop 139A
Hampton, VA 23665
(804) 864-2484
Patent Counsel: George F. Helfrich
Mail Code 279
Hampton, VA 23665
(804) 864-3523

Goddard Space Flight Center
Technology Utilization Officer: Donald S. Friedman
Mail Code 702.1
Greenbelt, MD 20771
(301) 286-6242
Patent Counsel: R. Dennis Marchant
Mail Code 204
Greenbelt, MD 20771
(301) 286-7351

Jet Propulsion Lab.
NASA Resident Office
Technology Utilization Officer: Gordon S. Chapman
Mail Stop 180-801
4800 Oak Grove Drive
Pasadena, CA 91109
(818) 354-4849
Patent Counsel: Paul F. McCaul
Mail Code 180-801
4800 Oak Grove Drive
Pasadena, CA 91109
(818) 354-2734
Technology Utilization Mgr. for JPL: Dr. Norman L. Chalfin
Mail Stop 156-211
4800 Oak Grove Drive
Pasadena, CA 91109
(818) 354-2240

George C. Marshall Space Flight Center
Technology Utilization Officer: Ismail Akbay
Code AT01
Marshall Space Flight Center, AL 35812
(205) 544-2223
Fax (205) 544-3151
Patent Counsel: Bill Sheehan
Mail Code CC01
Marshall Space Flight Center, AL 35812
(205) 544-0021

Lyndon B. Johnson Space Center
Technology Utilization Officer: Dean C. Glenn
Mail Code IC-4
Houston, TX 77058
(713) 483-3809
Patent Counsel: Edward K. Fein
Mail Code AL3
Houston, TX 77058
(713) 483-4871

NASA Headquarters
Technology Utilization Officer: Leonard A. Ault
Code CU
Washington, DC 20546
(202) 453-8377
Assistant General Counsel for Patent Matters: Robert F. Kempf, Code GP
Washington, DC 20546
(202) 453-2424

A Shortcut To Software: **COSMIC®**—For software developed with NASA funding, contact COSMIC, NASA's Computer Software Management and Information Center. New and updated programs are announced in the Computer Programs section. COSMIC publishes an annual software catalog. For more information call or write: **COSMIC®** 382 East Broad Street, Athens, GA 30602 *John A. Gibson, Dir.,* (404) 542-3265

If You Have a Question . . . **NASA Scientific & Technical Information Facility** can answer questions about NASA's Technology Utilization Network and its services and documents. The STI staff supplies documents and provides referrals. Call, write or use the feedback card in this issue to contact: **NASA Scientific and Technical Information Facility,** Technology Utilization Office, P.O. Box 8757, Baltimore, MD 21240-0757. *Walter M. Heiland, Manager,* (301) 859-5300, Ext. 242, 243

Electronic Components and Circuits

Hardware, Techniques, and Processes

26 Wideband Microstrip Antenna-Feeding Array
28 Ge/Si Integrated Circuit for Infrared Imaging
32 Field-Induced-Gap Infrared Detectors
33 An Optimal Design for Steerable Dish Antenna With BWG
34 Tunable-Quantum-Well Infrared Detector
36 Gallium Arsenide Domino Circuit
38 32-GHz Wideband Maser Amplifier
40 Epoxies Bond Waveguides to Flanges

Wideband Microstrip Antenna-Feeding Array

Special impedance-matching probes help to reduce feed complexity.

NASA's Jet Propulsion Laboratory, Pasadena, California

A lightweight array of microstrip antenna elements is designed to transmit and to illuminate a reflector antenna with circularly polarized radiation at 1,545 to 1,550 MHz and to receive circularly polarized radiation at 1,646 to 1,660 MHz. The array is a cluster of seven subarrays (see Figure 1), each of which contains four linearly-polarized microstrip radiating elements arranged at 90° intervals of orientation and of phase at the feed points. The array is intended to be part of a larger overlapping-cluster array that will generate multiple contiguous beams.

The subarrays are made from honeycomb-supported microstrip substrates 0.5 in. (12.7 mm) thick. This thickness — about 0.07 wavelength at the operating frequencies — is unusually large for a microstrip radiator and is needed to achieve the required bandwidth of 7.5 percent. The radiating patches of each subarray are fed by a strip-line four-way hybrid power divider that includes delay lines to obtain the 0°, 90°, 180°, and 270° phases at the feed points. The six outer subarrays are fed at an amplitude 13 dB below that of the central subarray to obtain the proper edge taper for low side lobes.

Because the substrate is relatively thick, it generates relatively-large surface waves, which give rise to undesired coupling between the subarrays. This coupling can give rise to asymmetry in the components of the radiation field and degrade the circular polarization. Metallic baffles 1 in. (2.5 cm) tall are therefore installed between the subarrays to block out most of the surface waves. Within each subarray, the orientation and phase relationships among the radiating patches suppress most of the effects of the surface waves.

Normally, impedance-matching circuit

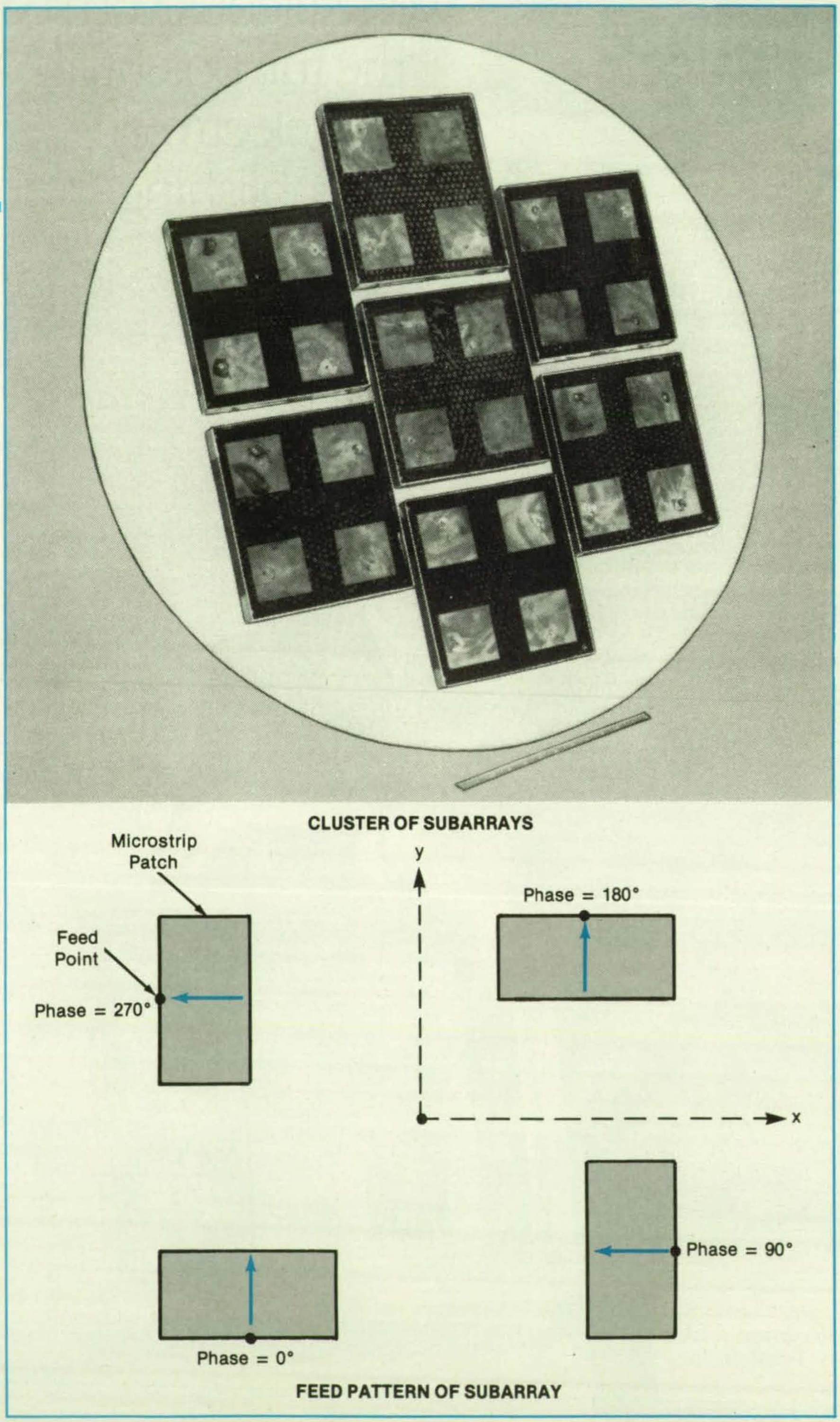

Figure 1. The **Microstrip Array** is a cluster of 7 subarrays containing a total of 28 microstrip patches. The array produces a circularly polarized beam with suitable edge taper to illuminate a reflector antenna.


THE WAVE OF THE FUTURE
Rise above any waveform measurement challenge with the new Nicolet System 500.
It's the most powerful and flexible digital waveform acquisition system available. With more channels. More speed. More memory. Greater resolution. And in the optimum configuration, starting as low as $1,645 per channel.
Available in portable or rack mount, this premier *turnkey* system features:
Independent digitizer boards with maximum sampling rates of up to 10 MS/s.
Multichannel flexibility. Whether it's two or 200 channels, the 500 can handle it.
Local processing. Lightning-fast on board calculation capabilities save you time.
And . . . *Instant start-up.* The System 500 is ready to start working almost as soon as it's out of the box. Send now for free brochure.
Nicolet
INSTRUMENTS OF DISCOVERY
Nicolet Test Instruments Division
5225 Verona Road, Madison, WI 53711-4495, 608/273-5008 or 800/356-3090
Circle Reader Action No. 696

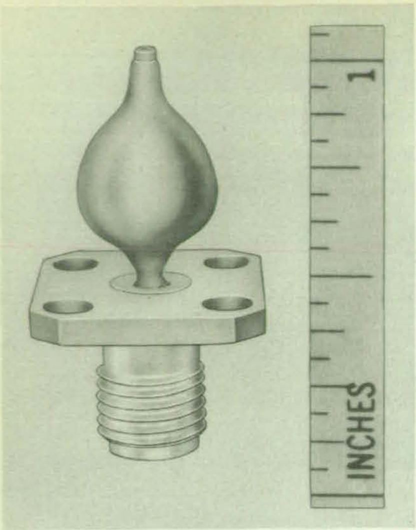

sections would be added to the power-dividing circuits to tune out the inductances at the feed points. However, these sections increase the size and complexity of the circuits and introduce additional losses. Therefore, for simplicity, the impedances are matched at each feed point by a teardrop-shaped probe (see Figure 2). The teardrop shape introduces the capacitance needed to cancel the effect of the undesired inductance.

Figure 2. The **Teardrop-Shaped Feed Probe** provides a gradual change of field from a coaxial transmission line into the microstrip substrate. The shape is not critical.

The array achieves an axial ratio of 0.8 dB (0 dB indicates pure circular polarization) at the peak of the radiation pattern, and the voltage standing-wave ratio remains below 1.5 across the required 7.5-percent frequency band. A bandwidth of 10 to 15 percent should be achievable by use of a thicker substrate and a similar design.

This work was done by John Huang of Caltech for **NASA's Jet Propulsion Laboratory**. *For further information, Circle 41 on the TSP Request Card.*

Inquiries concerning rights for the commercial use of this invention should be addressed to the Patent Counsel, NASA Resident Office-JPL [see page 22]. Refer to NPO-17548

Ge/Si Integrated Circuit for Infrared Imaging

Photodetectors would be deposited on signal-processing circuitry at the focal plane.

NASA's Jet Propulsion Laboratory, Pasadena, California

A proposed integrated circuit would consist of a focal-plane array of metal/germanium Schottky-barrier photodetectors on the same chip with silicon-based circuits that would process the signals from the photodetectors (see figure). Because the heights of Schottky barriers on germanium are much lower than on silicon, the germanium-based detectors can operate at strategically important longer wavelengths — typically 8 to 12 μm — whereas silicon detectors are limited to the range of 3 to 5 μm. At shorter wavelengths, the germanium detectors would exhibit higher quantum efficiencies.

First, the signal-processing circuitry would be made by standard silicon-fabrication techniques. Bare areas of silicon would be left where the photodetectors were to be placed. The silicon wafer would be cleaned, then placed in an ultra-high-vacuum chamber for the molecular-beam epitaxial deposition of germanium. Growth at low temperature, which is a principal feature of molecular-beam epitaxy, is necessary to avoid degradation of the circuitry on the wafer.

After the deposition of the germanium, a layer of metal would be deposited directly on the germanium without breaking the vacuum. (The maintenance of the vacuum helps prevent the incorporation of impurities at the metal/germanium interface. Such impurities could dominate the properties of the Schottky barrier.) The properties of the Schottky barrier may be further improved by reacting the metal into the germanium to form a metal germanide. The wafer would then be removed from the chamber, and the detector pattern and connections to the silicon circuitry would be formed by standard low-temperature processing techniques. The combination of the described techniques should result in high-resolution infrared-imaging circuits of superior performance.

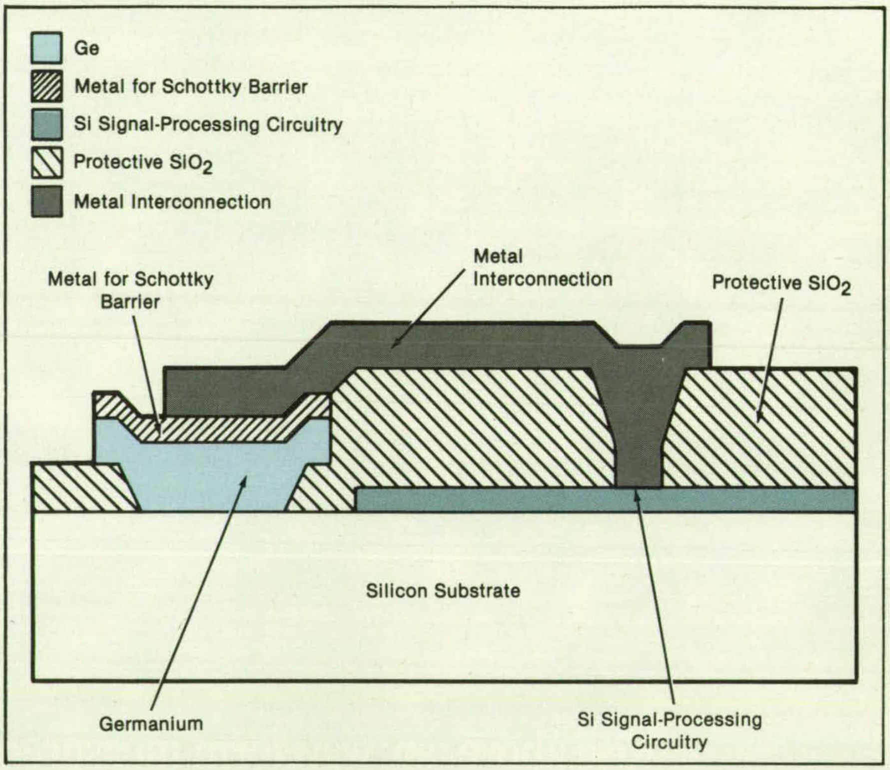

Metal/Germanium Schottky-Barrier Photodetectors like this one would be made compatible with the underlying silicon-based circuitry by growing the germanium epitaxially on silicon circuit wafers. The metal could be deposited in an ultrahigh vacuum immediately after the growth of the germanium.

This work was done by Robert W. Fathauer of Caltech for **NASA's Jet Propulsion Laboratory**. *For further information, Circle 54 on the TSP Request Card.*

In accordance with Public Law 96-517, the contractor has elected to retain title to this invention. Inquiries concerning rights for its commercial use should be addressed to

Edward Ansell
Director of Patents and Licensing
Mail Stop 301-6
California Institute of Technology
1201 East California Boulevard
Pasadena, CA 91125

Refer to NPO-17397, volume and number of this NASA Tech Briefs *issue, and the page number.*

FLUKE

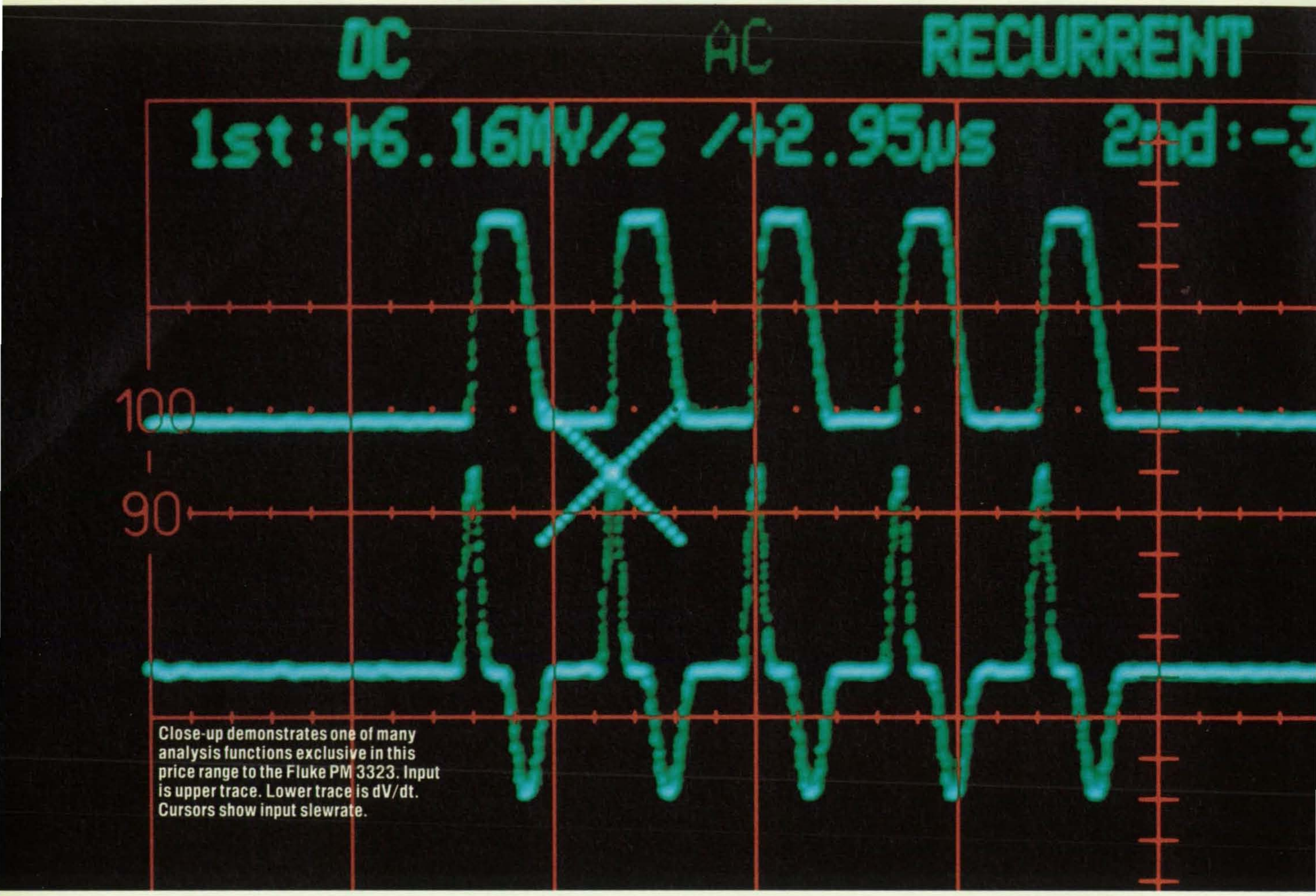

Close-up demonstrates one of many analysis functions exclusive in this price range to the Fluke PM 3323. Input is upper trace. Lower trace is dV/dt. Cursors show input slewrate.

Here's the picture Tek® &

For the full picture, true high performance DSOs must provide superior signal capturing, exceptional analytical power, plus automation. The Fluke PM 3323 does. The competition doesn't.

Digital Storage Oscilloscopes promise great advantages over analog scopes.

But fulfilling that promise means carefully choosing the best DSO performance for your budget.

With the PM 3323 you get all the acquisition and analytical power you need to extract a wealth of information from your signals.

Try getting the information pictured above with the Tek 2440 or HP 54502A, and you'd need them both. Plus, the PM 3323 can give you all this performance within your current automated test environment.

Signal Acquisition.

Before you can analyze signals you have to capture them. Here the PM 3323 stands alone. You get a wide 300 MHz bandwidth for capturing repetitive signals. You get 500 MS/s real-time sampling for single-shot events, even to a fast 50 MHz.*

For even the fastest transient signals, you get 2 ns horizontal resolution, a 1.17 ns risetime, and a 3 ns glitch capture function.

Added features including automatic dc offset and digital delay let you really zero in on the signal you want. All with precise 10 bit vertical resolution and easy-to-use AUTOSET.

*At 10 samples per period.

Signal Analysis.

With the processing power of 2 AT-type computers, the PM 3323 lets you analyze signals, not just look at them.

Going far beyond amplitude and time measurements like RMS, Rise/Fall time, and frequency, the PM 3323 provides advanced functions such as integrate for area, differen-

A L L I A N C E   I N   T E S T   &   M E A S U R E M E N T

PHILIPS

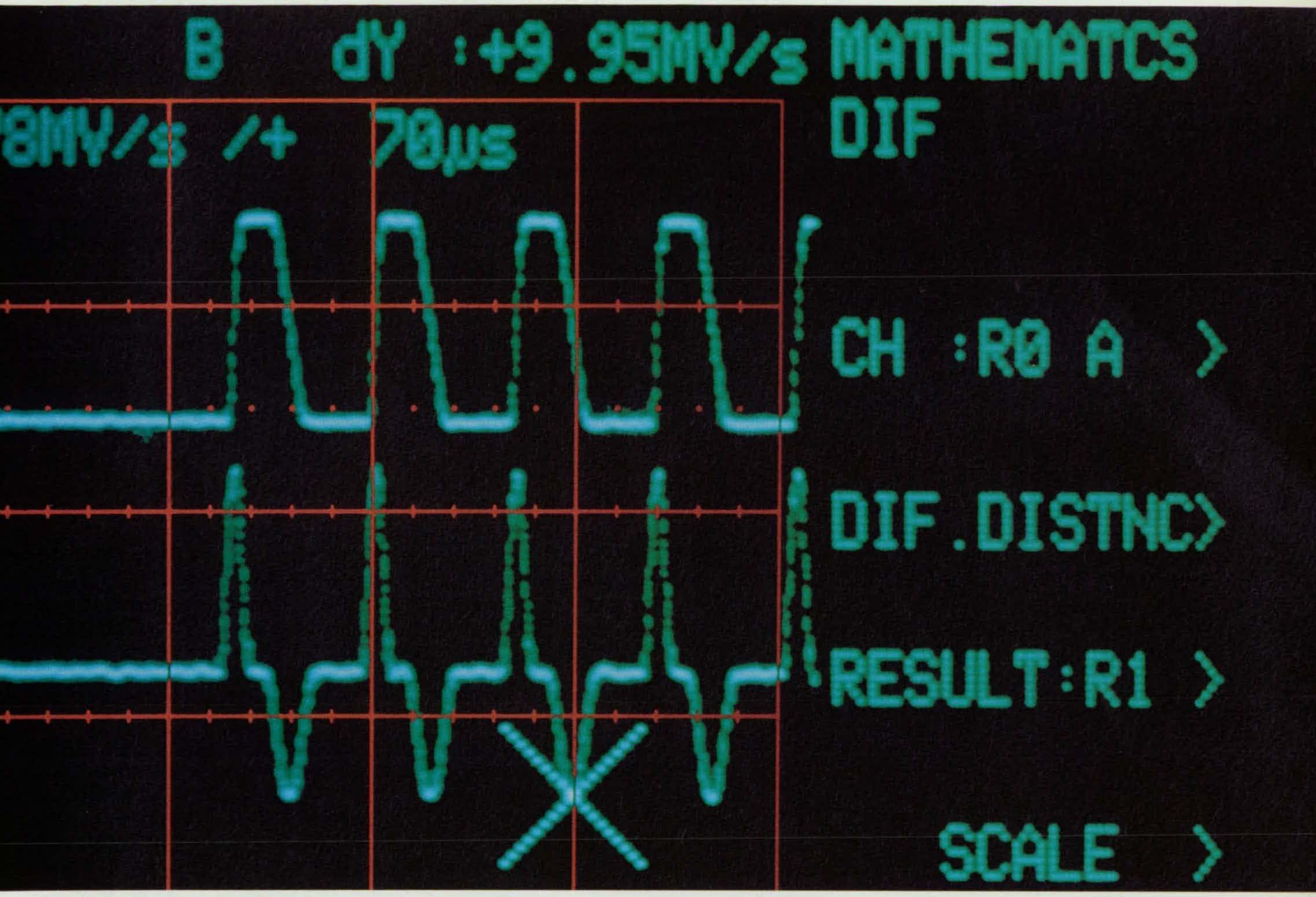

HP® don't want you to see.

tiate for slewrate, calculate amplitude probability, even FFTs to show frequency domain. And there's no need for an external computer.

Plus, memory sufficient for 251 front panel setups makes automation easy.

See the difference. Only from Fluke.

At only $7,750, the PM 3323 is just one of the talented DSOs from Fluke offering superior specs for unparalleled performance and value.

See them all, including our medium frequency combination digital/analog scopes which make the transition from analog to digital easier than ever, by sending for our free video titled "DSOs With a Difference: Chapter II." Just fill out and mail the postage paid card provided, or call **1-800-44-FLUKE, ext. 77.**

Features	Fluke PM 3323	Tek® 2440	HP® 54502A
Speed	300 MHz 500 MS/s	300 MHz 500 MS/s	100 MHz real time, 400 MHz repetitive 400 MS/s
Vertical Resolution	10 bits	8 bits	6 bits
Glitch Capture	Yes	Yes	No
Stop/Save on Difference	Yes	Yes	No
Analysis Functions (Int., Diff., Hist., Filter, FFT)	Yes	No	No
Math Functions (add, subtract, multiply, divide)	Yes	Multiply only	Yes
Measurement Functions (RMS, Freq., etc.)	Yes	Yes	Yes

FLUKE

Circle Reader Action No. 668

Field-Induced-Gap Infrared Detectors

Semimetals would become semiconductors under applied magnetic fields.

NASA's Jet Propulsion Laboratory, Pasadena, California

Tunable detectors of infrared radiation would be made by applying magnetic fields to semimetals, according to a proposal. The new detectors would require less cooling equipment because they would operate at temperatures somewhat higher than the liquid-helium temperatures required by extrinsic-semiconductor detectors. The magnetic fields for the new detectors would be provided by electromagnets based on the recently-discovered high-transition-temperature superconducting materials.

The detector material has to be a semiconductor, in which a photon is absorbed by exciting an electron/hole pair across the gap E_g of forbidden energies between the valence and conduction energy bands. In a semimetal of the gray-tin type [for example, α-Sn, HgTe, HgSe, and $Hg_{1-x}Cd_xTe$ (where $0 \leqslant x \leqslant 0.15$)], the bottom of the conduction band touches the top of the valence band; that is, $E_g = 0$. However, when a magnetic field is applied, additional valence and conduction subbands are formed, and E_g rises above zero (see Figure 1). In effect, the semimetal becomes an intrinsic semiconductor, in which E_g increases with increasing applied magnetic field.

E_g is the minimum photon energy that can be absorbed by the material, and the corresponding wavelength λ_c, called the cutoff wavelength, is the maximum detectable wavelength. Thus, in principle, small magnetic fields could enable detection in the far infrared or even at submillimeter wavelengths. For example, in a magnetic-flux density of 10 T, the λ_c of HgTe would be about 80 μm.

E_g and λ_c can also be adjusted via the composition of the material. For example, in $Hg_{1-x}Cd_xTe$, E_g increases with x; in an applied magnetic field of 10 T, an alloy of x 0.15 has a λ_c of 20 μm.

The magnetic- and compositional-tuning effects can be combined to obtain a two-absorber detector that has a narrow passband. By variation of the applied magnetic field, the passband would be swept through the spectrum of interest.

In one version of such a detector (left side of Figure 2), both absorbers would be made of $Hg_{1-x}Cd_xTe$ (with $x = 0.15$), but a slightly-higher magnetic field B would be applied to the outer absorber. The outer absorber would act as a blocking filter, preventing most photons of wavelength shorter than its λ_c from reaching the inner absorber. On the other hand, the inner absorber would detect only those photons of wavelength shorter than its λ_c, which

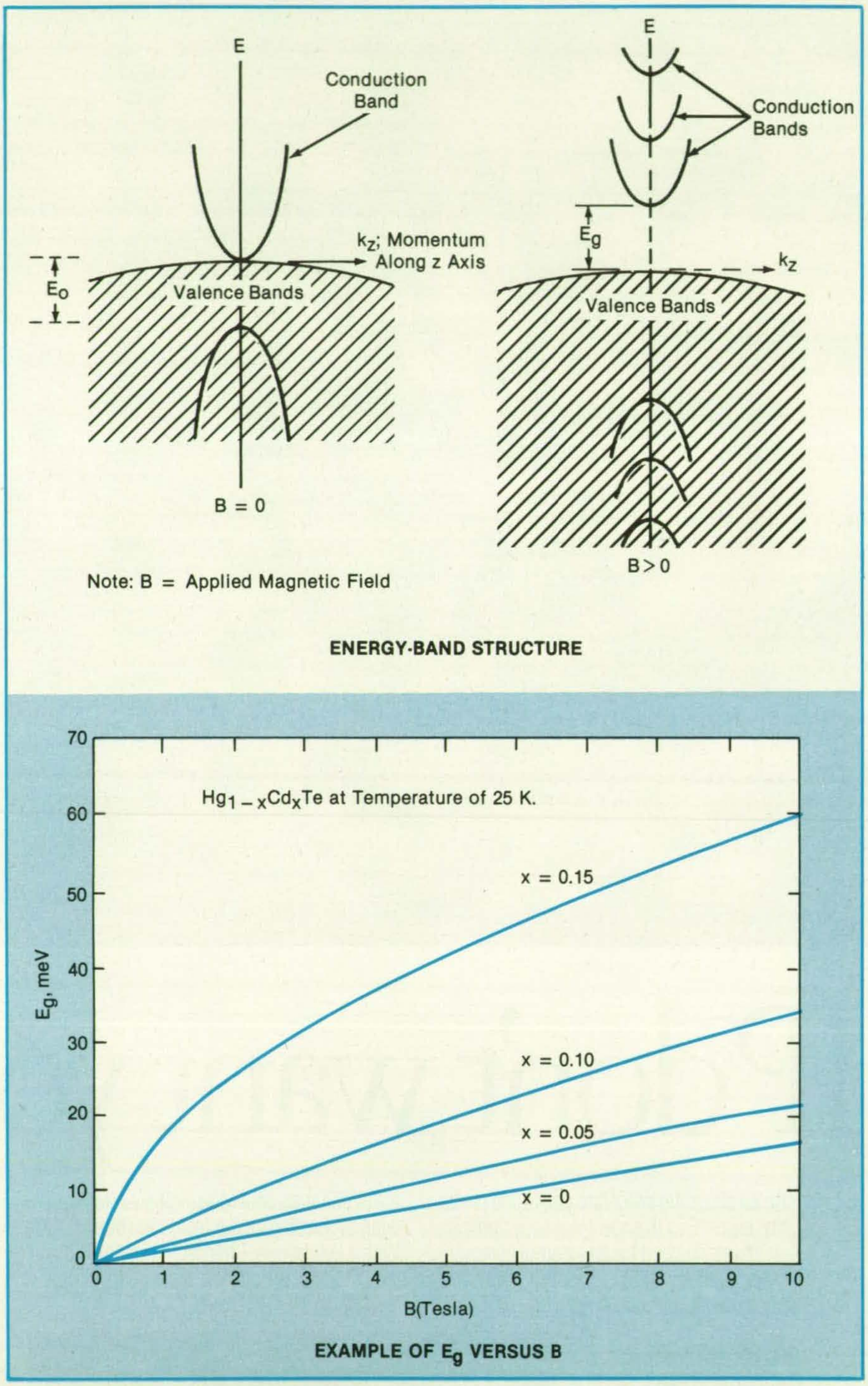

Figure 1. The **Extrema of the Valence and Conduction Bands** at the center of the Brillouin zone in a semimetal of the gray-tin type touch at zero magnetic field. When a magnetic field is applied, the extrema move apart, creating a gap, E_g, of energies that are forbidden to electrons.

would be slightly greater than the other λ_c. Thus, the tunable passband would be the wavelength interval between the λ_c's of the two absorbers. In the second version (right side of Figure 2), the magnetic field would be equally intense in both absorbers, and the λ_c's of the two absorbers would be made different by a slight difference in the composition.

This work was done by C. Thomas Elliott of Caltech for **NASA's Jet Propulsion Laboratory**. *For further information, Circle 20 on the TSP Request Card.*

Inquiries concerning rights for the commercial use of this invention should be addressed to the Patent Counsel, NASA Resident Office-JPL [see page 22]. Refer to NPO-17526

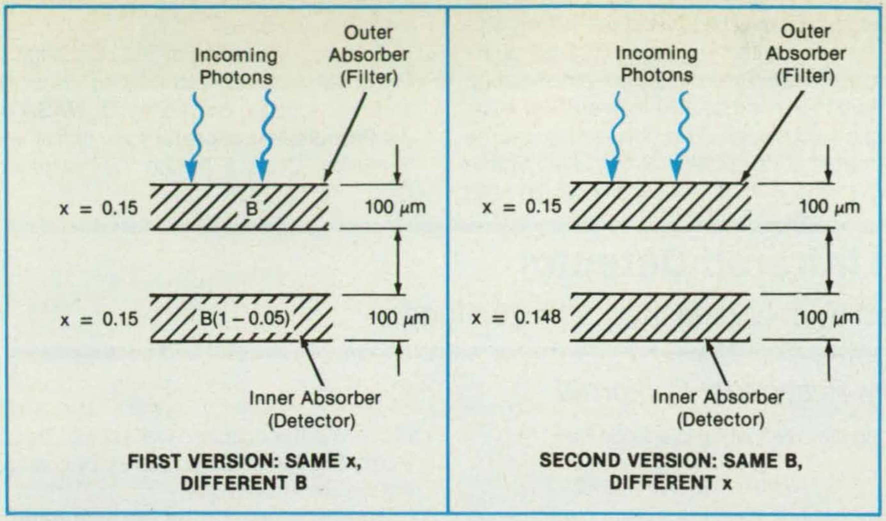

Figure 2. **$Hg_{1-x}Cd_xTe$ Tunable Infrared Detectors** of the new type would combine compositional and magnetic tuning.

An Optimal Design for Steerable Dish Antenna With BWG

Advanced features and modular design promise high performance.

NASA's Jet Propulsion Laboratory, Pasadena, California

A new design has been proposed for the highly-efficient 34-m-diameter millimeter-wavelength antennas of NASA's Deep Space Network. The design incorporates an axial beam waveguide, BWG, (see figure) and an improved structure to maintain the shape and alignment of the reflecting surfaces. The engineering concepts involved in this design can be adapted to the design of other large, steerable antennas for telecommunications, radio astronomy, and military uses.

The essence of the design problem was the derivation of an optimum configuration for the 34-m antenna structure for which a new center-fed beam waveguide system could be introduced. Contributing to the difficulty in design was the necessity to adopt the 34-m antenna envelope and subsystem structural components for economical reasons. The general approach to the conceptual construction of the structure was to modularize the overall system so that critical constraint conditions pertaining to microwave optics and structural performance could be satisfied.

The paraboloidal reflecting dish is supported by an octagonal truss structure, which in turn is supported by a "cross-box" truss substructure where the elevation wheel (the large gear that tilts the antenna) is attached. The main reflector, cross-box, and octagonal truss were optimized to accommodate the beam waveguide and satisfy many other design constraints, including the following:

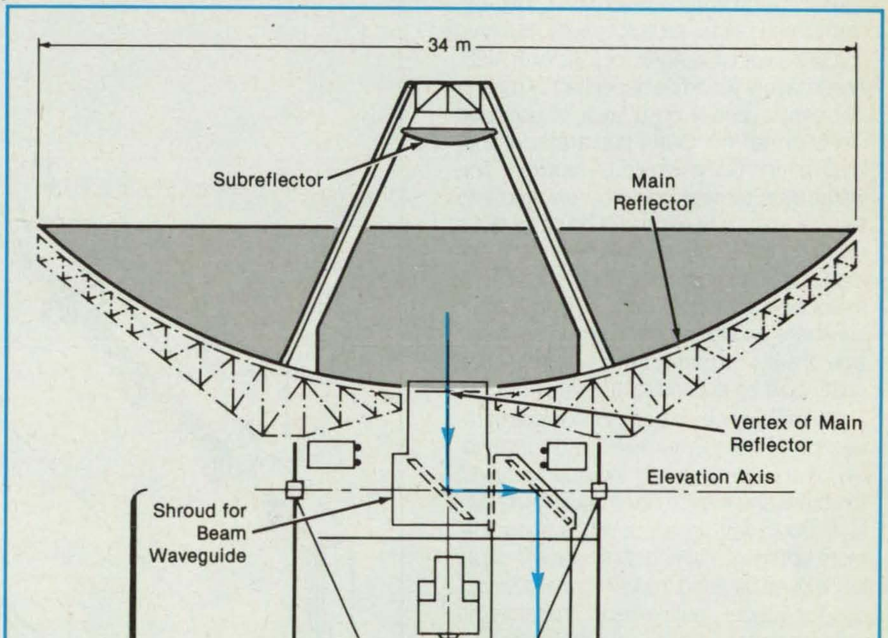

The **Beam Waveguide** is routed through the alidade and reflector structures.

- Maximum allowable root-mean-square (rms) distortion of the reflecting surface due to worst-case gravitational and wind loads;
- Maximum allowable aiming error under worst-case wind load;
- Maximum allowable weight of the tipping structure;
- Elevation range sufficient for intended operations;

- Upper and lower bounds on sizes of structural members;
- Maximum allowable stresses in structural members; and
- Survivability at the zenith position in a high wind.

According to computer simulations, the loss in gain at X-band due to gravitational loading in an antenna of the new design should be only half that of the existing version. The antenna should exhibit adequate microwave performance at frequencies up to 90 GHz and be able to operate at multiple frequencies. The new design can be retrofitted to existing NASA Deep Space Network 34-m antennas, or it can be used as the basis to build large ground-based steerable antennas.

This work was done by K. L. Chuang of PRC's Aerospace Technologies Division and F. L. Lansing of Caltech for **NASA's Jet Propulsion Laboratory**. *For further information, Circle 5 on the TSP Request Card. NPO-17429*

Tunable-Quantum-Well Infrared Detector

The wavelength would be adjusted by changing the applied voltage.

NASA's Jet Propulsion Laboratory, Pasadena, California

A proposed detector of infrared photons would be based on photon-assisted, resonant quantum-mechanical tunneling between adjacent energy wells in its semiconductor structure. The wavelength of maximum sensitivity (that is, of the resonance) would depend on the electric field in the device, which would be controlled via the applied voltage.

The device would contain alternating layers of different semiconductors that would form a double-quantum-well electron-energy structure. For example, (In, Ga)As could be alternated with GaAs, (Al, Ga)As with GaAs, (In,Ga)As with (In,Al)As, (In,Ga)As with (Ga,Al)As, or InAs with AlSb. These layers would be deposited by molecular-beam epitaxy on a layer of undoped GaAs on an n^+ GaAs substrate. A final layer of n^+ GaAs would be applied. The wafer thus formed could be cleaved into several units, and each unit could be divided along its length to form the picture elements of a line detector (see Figure 1). A metal contact would be added to the n^+ substrate and to the n^+ layer on the other side of each element, and an antireflection coat could be applied to the cleaved edge.

The differences among the indices of refraction of the quantum-well and surrounding layers are such that the quantum-well structure and the n^+ GaAs layer to the surface could act as an optical waveguide. More optimum waveguide structures could be devised by using thicker layers of low index for optical confinement. Therefore, in operation, the infrared light incident upon the cleaved edge would be channeled along the quantum-well structure. The portion of this light polarized with its electric field perpendicular to the quantum-well surfaces would interact with the charge carriers in the device.

A quantum-well structure that favors photon-assisted, resonant tunneling is illustrated schematically in Figure 2. The thickness, *a*, of the quantum wells would be chosen so that each well would contain only the energy levels E_1 and E_2. The structure would also be designed to put E_2 near the top of the well so that most photoexcited electrons could escape from the well instead of relaxing to E_1, in which level they would be temporarily trapped. The condition for resonance is approximately

$$h\nu = E_2 - E_1 - eFb$$

where h is Planck's constant, ν is the frequency of the photon, e is the electron charge, b is the thickness of the first two energy barriers, and F is the applied electric field in the quantum-well region. Thus, the device can be tuned merely by changing the applied voltage.

The thickness of the barriers determines the probability of tunneling, which can be increased or decreased to increase or decrease the probability of absorption of

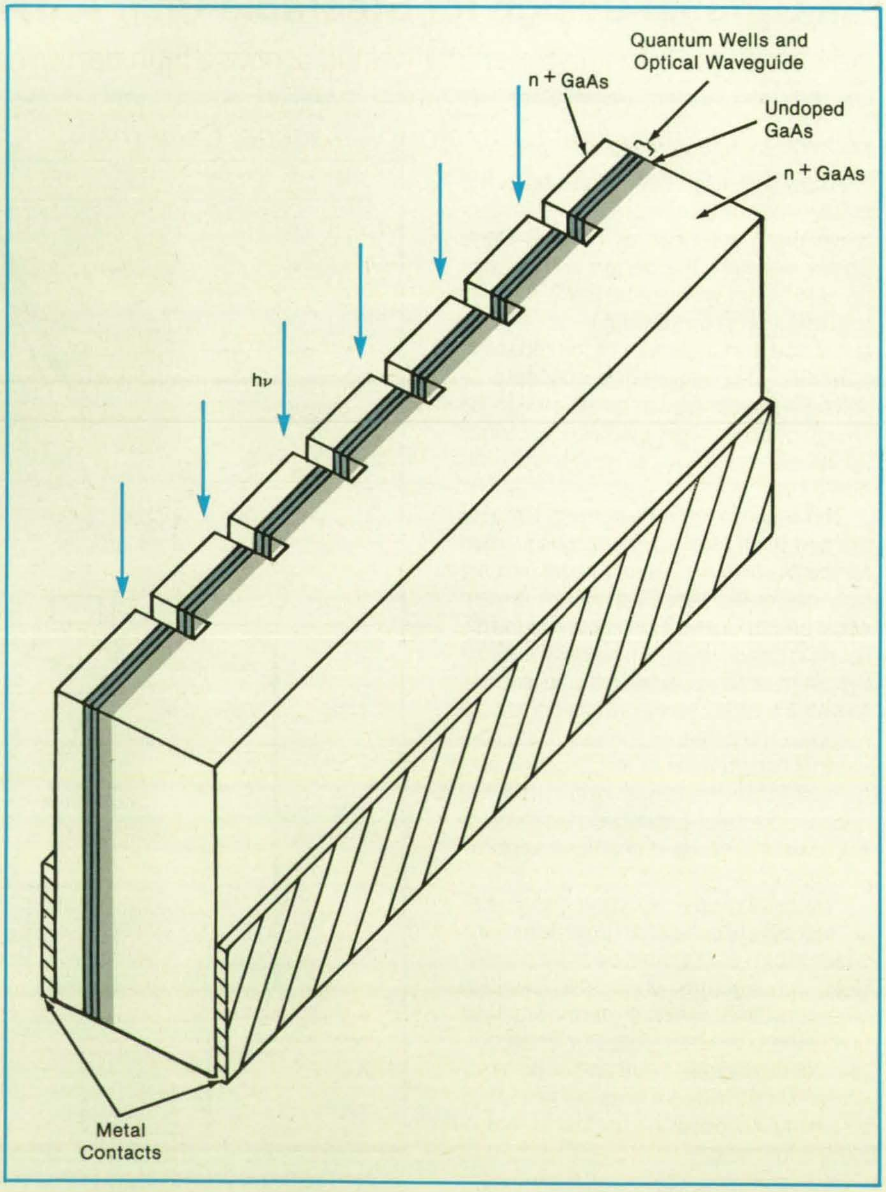

Figure 1. **Tunable-Quantum-Well Detectors** made on a single chip would constitute a line imager. Many such devices could be stacked to form a two-dimensional imaging device. Signal-processing circuitry could be integrated into the chip at its lower end.

a photon and, consequently, the absorption distance along the optical waveguide. For example, if the probability of tunneling were set at 10^{-3}, the absorption distance would be of the order of millimeters. The third barrier would be made somewhat thicker to block dark tunneling from the ground state (corresponding to E_1) of the normally-empty second well into the continuum of energy states beyond this barrier.

This work was done by Joseph Maserjian of Caltech for **NASA's Jet Propulsion Laboratory**. *For further information, Circle 123 on the TSP Request Card.*

In accordance with Public Law 96-517, the contractor has elected to retain title to this invention. Inquiries concerning rights for its commercial use should be addressed to

Edward Ansell
Director of Patents and Licensing
Mail Stop 301-6
California Institute of Technology
1201 East California Boulevard
Pasadena, CA 91125

Refer to NPO-17361, volume and number of this NASA Tech Briefs *issue, and the page number.*

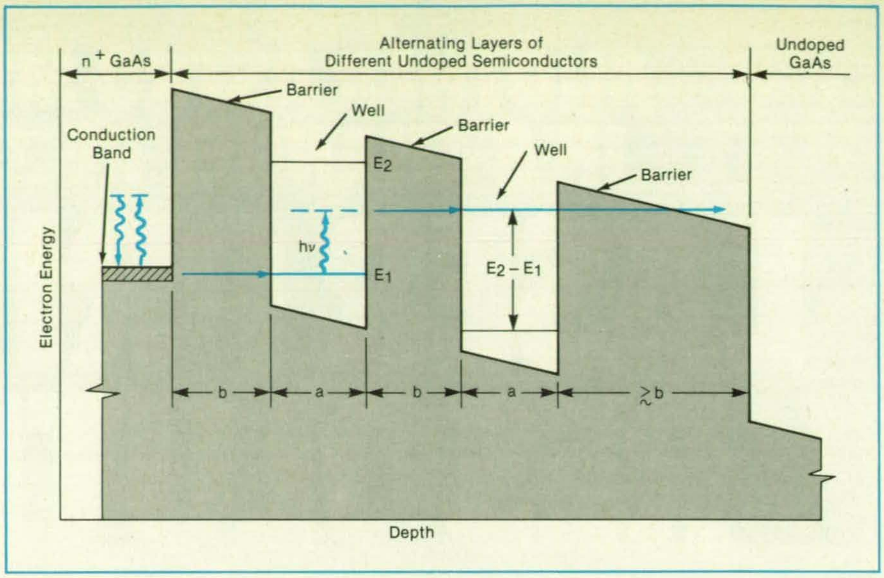

Figure 2. The **Potential Barriers and Wells** (with respect to electron energies) are produced by alternating layers of different semiconductor materials. The steepness of the slope is proportional to the applied electric field. The electric field and the thicknesses and heights of the barriers are selected to favor photon-assisted, resonant quantum-mechanical tunneling at the chosen photon frequency.

Gallium Arsenide Domino Circuit

Advantages include reduced power and high speed.

NASA's Jet Propulsion Laboratory, Pasadena, California

An experimental gallium arsenide field-effect-transistor (FET) domino circuit could be replicated in large numbers for use in dynamic-logic systems. The name of the circuit denotes the mode of operation, in which logic signals propagate from each stage to the next when successive stages are operated at slightly staggered clock cycles, in a manner reminiscent of dominoes falling in a row. The circuit fulfills a need for low-power, fast, dynamic logic circuits with acceptable noise margins.

The building block of the GaAs domino circuit includes an input substage that executes the input combinational logic. In the example of the figure, this substage consists of a clocked inverter Q_5 in series with an AND gate of one to four inputs ($Q_{1\sim4}$). When the clock signal goes high, the gate capacitance of Q_6 at node *A* is precharged through Q_5, causing Q_6 to predischarge *C*. The high clock signal also causes Q_8 to conduct strongly, bringing the output voltage, v_{out}, down to the drain-supply voltage V_{ss}. This prepares the circuit for the transfer of information from the preceding stage to the following stage during the subsequent low-clock-signal half cycle.

The operation of the circuit depends on a peculiarity of GaAs FET's: a slightly-negative gate-to-source voltage is required to cut off conduction. When the clock signal goes low, Q_5 is cut off. If any input is low, then the charge stored in the gate capaci-

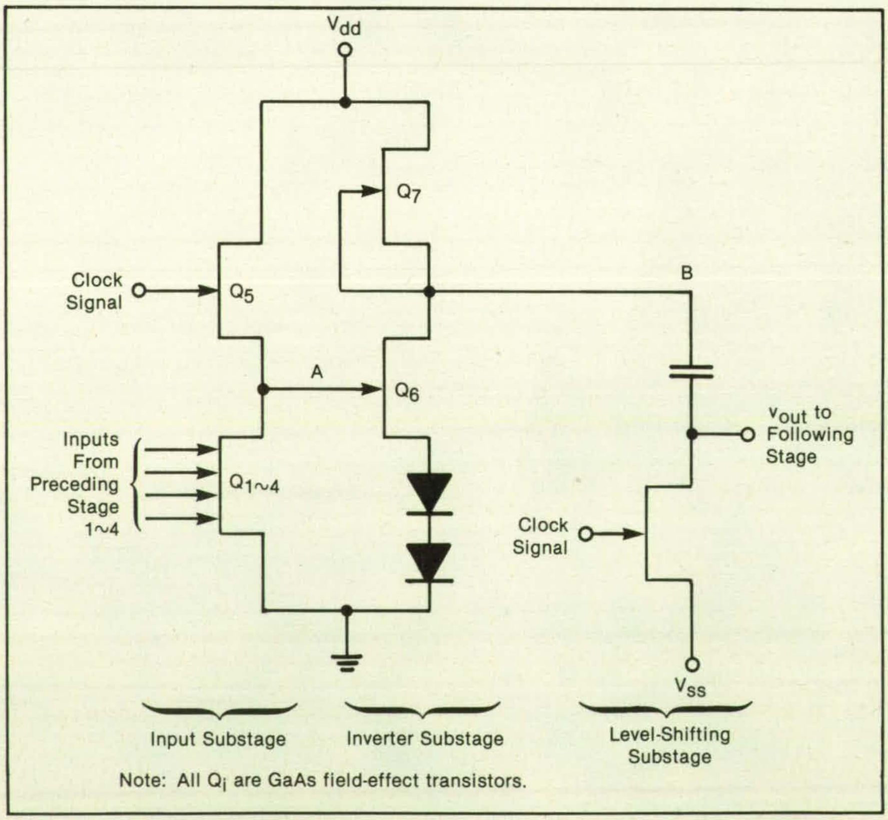

The **Building Block of the Domino Circuit** includes input, inverter, and level-shifting substages. The combinational logic is executed in the input substage. During the low half of the clock cycle, the result of the logic operation is transmitted to the following stage.

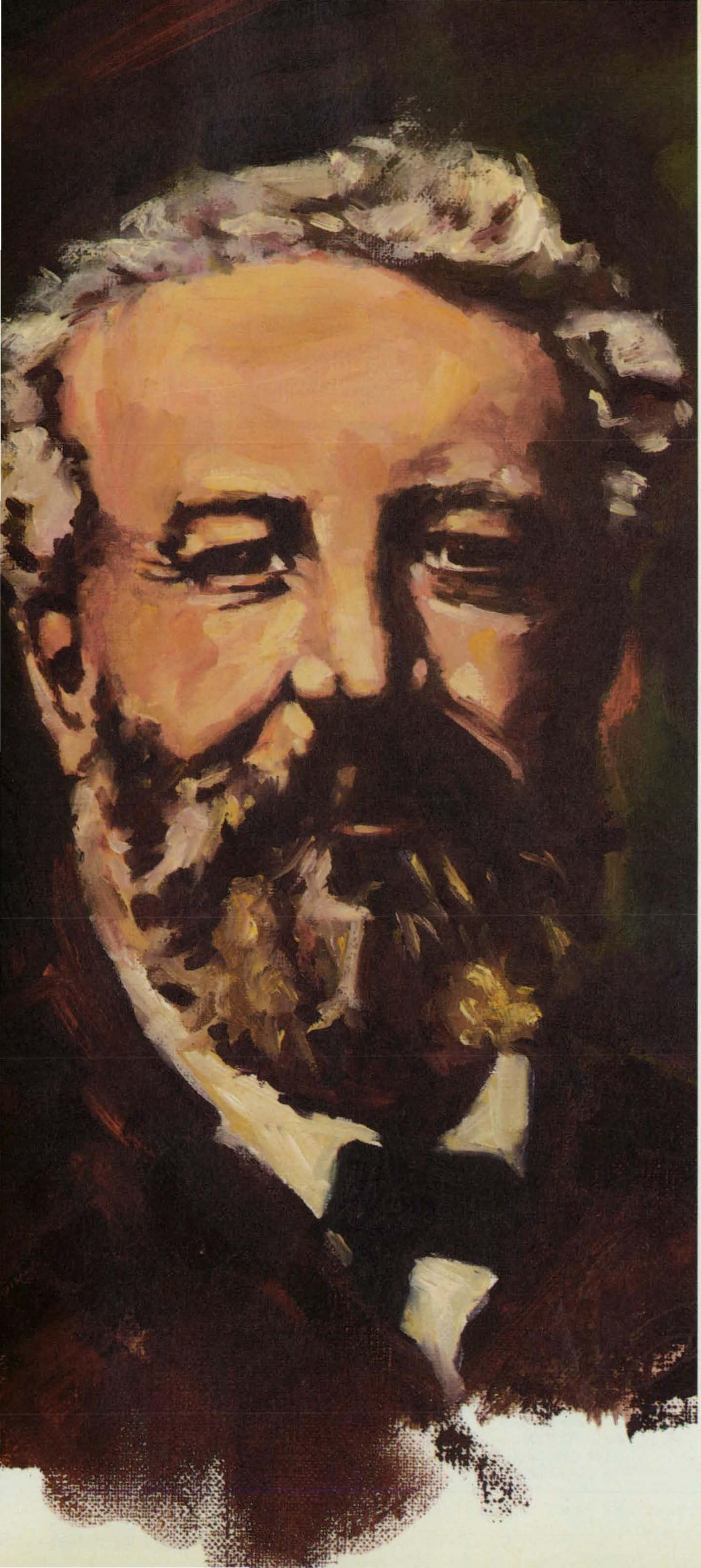

tance at node *A* maintains Q_6 above or near a gate-to-source voltage of zero, causing Q_6 to continue to conduct, thereby keeping *C* discharged and the output low. The advantage of this arrangement is that the low gate-to-source voltage keeps the gate leakage low.

If all the inputs are high, the gate capacitance of Q_6 is discharged through $Q_{1\sim4}$, bringing node *A* down to ground voltage. The diodes in series with Q_6 supply enough negative bias to the gate of Q_6 so that when node *A* is thus grounded, conduction in Q_6 is nearly cut off. This causes the voltage at node *B* to rise toward the drain-supply voltage V_{dd}. Because the low clock signal also cuts off Q_8 (provided that V_{ss} is somewhat above ground), the rise in voltage at *B* is transmitted through *C* to the output.

The required value of *C* depends on the required swing in output voltage, the capacitances of the interconnections, and the fanout because the charge stored in *C* is shared by the load capacitances. In a circuit that has very long interconnections or a large fanout, a static source follower is preferable to a coupling capacitor.

This work was done by Long Yang and Stephen I. Long of the University of California for **NASA's Jet Propulsion Laboratory**. *For further information, Circle 42 on the TSP Request Card.*

This invention is owned by NASA, and a patent application has been filed. Inquiries concerning nonexclusive or exclusive license for its commercial development should be addressed to the Patent Counsel, NASA Resident Office-JPL [see page 22]. Refer to NPO-17417.

32-GHz Wideband Maser Amplifier

Features include low input equivalent noise temperature and 400-MHz bandwidth.

NASA's Jet Propulsion Laboratory, Pasadena, California

A high-gain, wideband, microwave amplifier is based on ruby cooled by liquid helium. The amplifier is particularly useful for the detection of weak microwave signals in radio astronomy and communications.

The amplifier includes eight ruby stages and is of the reflected-wave design (see Figure 1), which was chosen to achieve low noise and wide bandwidth about a center frequency of about 32 GHz. Low noise is made possible by the absence of a comb-type slow-wave structure. The bandwidth requirement is satisfied by using a large volume of ruby (about 60 cm in total length) and subjecting it to a magnetic field with a large gradient. The number of stages is dictated by the requirements for nearly constant gain across the operating-frequency band, ease of fabrication of the ruby bars, and good noise performance across the band.

The tuning range, limited by the frequency response of the Y-junction circulators that connect the ruby stages, is 29 to 34 GHz. However, at present, pump-power requirements dictate the use of fixed-tuned impact-avalanche-and-transit-time (IMPATT) diode oscillators, effectively making the

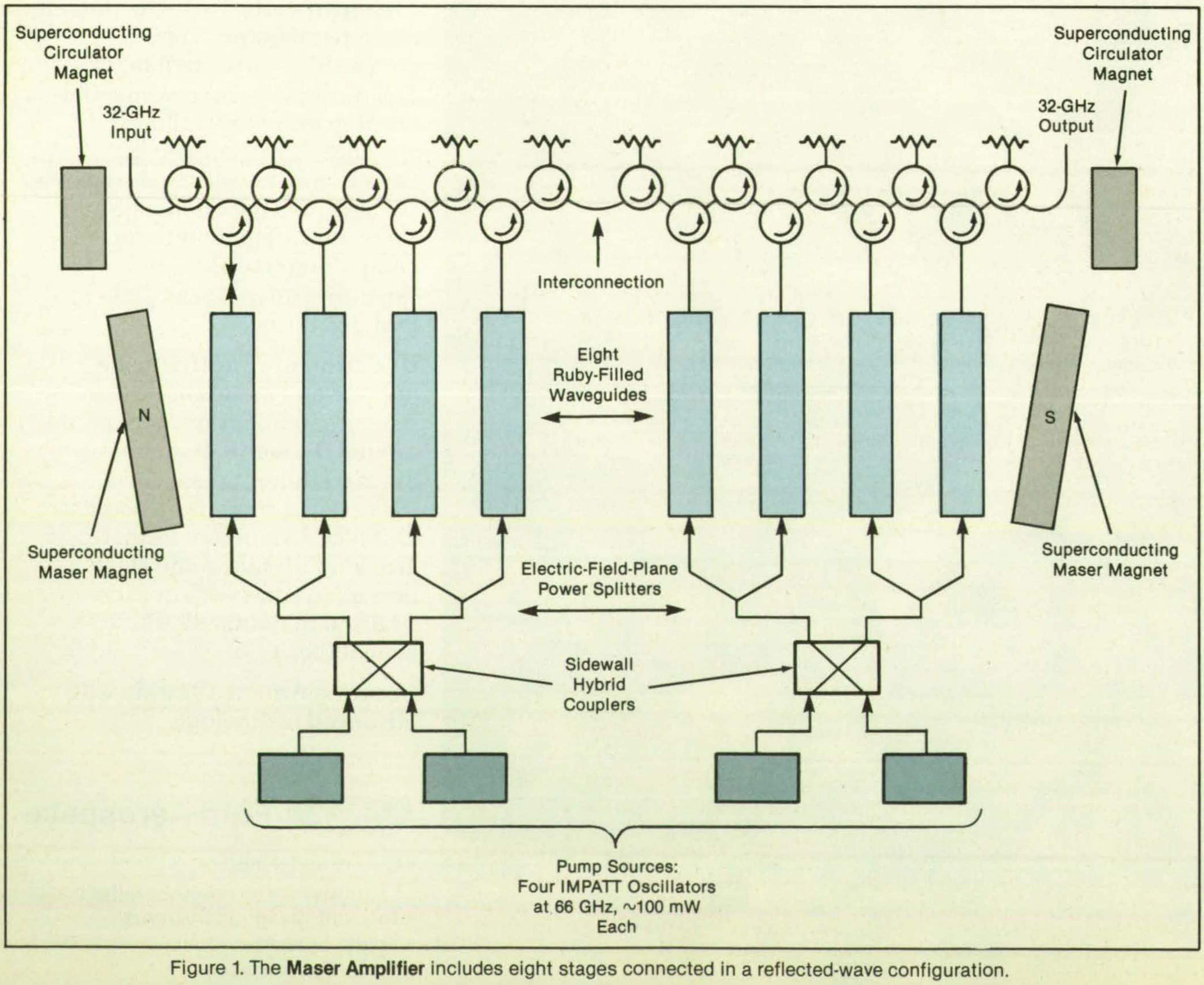

Figure 1. The **Maser Amplifier** includes eight stages connected in a reflected-wave configuration.

NUPRO packless valves for exacting service

All metal seals give you leak-tight performance under extreme conditions involving:

- Corrosive, toxic, radioactive, pyrophoric, expensive and other fluids demanding safe containment
- High purity requirements
- Temperatures from cryogenics to 1500°F (816°C)
- Pressures from high vacuum to 3500 psi (24,100 kPa)

SWAGELOK® — TM Crawford Fitting Company
CAJON® VCO® & VCR® — TMs Cajon Company
MONEL — TM Huntington Alloys
Various NUPRO products are subjects of patent or patents pending applications

NUPRO bellows and diaphragm sealed valves also offer these benefits to meet your design and performance needs:

- Sizes from 1/8" to 1" and 6mm to 18mm
- Choice of end connections — SWAGELOK Tube Fitting, tube extensions, weld, NPT, ISO Tapered, CAJON VCO® & VCR® zero clearance fittings
- Materials include 316 stainless steel, Monel & brass
- Large range of flow capacities
- Non-rotating stem tips improve cycle life
- Bottom and panel mounting
- Air actuated models with choice of Normally Open, Normally Closed and Double Acting actuators
- 100% helium leak tested at the factory

When you need valve performance beyond the limits of conventional packed valves, select from these NUPRO lines. They're available from local stocks. **Nupro Company, 4800 East 345th St., Willoughby, OH 44094**

NUPRO®
A SWAGELOK® COMPANY

Circle Reader Action No. 378

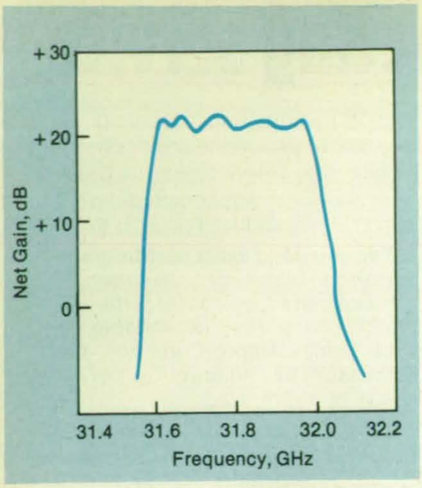

Figure 2. The **Gain vs. Frequency** of the maser amplifier is fairly flat at about 21 dB across a frequency band ~400 MHz wide, centered on 31.8 GHz.

amplifier a fixed-frequency device.

The design is basically an extension of previous reflected-wave masers built for the frequency range of 18 to 26 GHz. The ruby bars are housed in copper waveguide structures equipped with channels for the liquid helium. A single-coil "racetrack" superconducting magnet provides the ~12-kG magnetic field required to bias the ruby. The ferrites in the circulators are biased simultaneously by a separate superconducting magnet.

Four IMPATT oscillators with a total output power of 400 mW are required. Because the IMPATT output powers can differ considerably from unit to unit, the outputs are combined and redivided in sidewall hybrid couplers, then split again with electric-field-plane power splitters.

Figure 2 shows the performance of the amplifier at a liquid-helium temperature of 4.6 K. The net gain within the frequency band of 31.8 ± 0.2 GHz is about 21 dB and varies no more than ~1 dB with frequency, the exact variation depending on the middle frequency.

This work was done by J. S. Shell and D. E. Neff of Caltech for **NASA's Jet Propulsion Laboratory**. *For further information, Circle 146 on the TSP Request Card.*
NPO-17558

Epoxies Bond Waveguides to Flanges

Each waveguide/flange joint is made with a conductive adhesive and a structural adhesive.

NASA's Jet Propulsion Laboratory, Pasadena, California

Strong, electrically conductive joints can be made between waveguides and waveguide-end flanges by slight modifications of the conventional flange structures and the use of both structural and conductive adhesives. The new two-adhesive joints overcome many of the disadvantages of dip-brazed joints, including damage caused by the heat of the brazing process, corrosion of joints by brazing salts retained in them, cracks in joints, weakening of the waveguide material, and limitation to the use of aluminum alloys, which are the only ones that can be dip-brazed.

The inside of the flange is machined wider than the waveguide to provide a gap of 0.005 to 0.015 in. (0.13 to 0.38 mm) for the structural adhesive. In the version shown in the figure, the inner edge of the flange at the end of the waveguide is beveled approximately 0.050 by 0.050 in. (1.3 by 1.3 mm). The flange is placed on the end of the waveguide, and the gap, but not the bevel, is filled with the structural adhesive — typically an epoxy with a consistency like that of putty. If necessary, the bevel can be filled with a temporary masking material to keep the structural adhesive out of the bevel. In some cases, it may be preferable to put the conductive adhesive in the bevel first.

The conductive adhesive is typically an epoxy that contains at least 50 weight percent of particles of silver. The main requirements are that the conductivity of the adhesive be suitable for the transmission of microwaves and that the bevel be large enough so that the heat generated by the microwaves does not damage the conductive joint. Of course, both the structural and conductive adhesives must be suitable for the environment in which the waveguide is to be used.

This work was done by Jay D. Bloom of Harris Corp. for **NASA's Jet Propulsion Laboratory**. *For further information, Circle 30 on the TSP Request Card.*

Title to this invention has been waived under the provisions of the National Aeronautics and Space Act [42 U.S.C. 2457(f)], to the Harris Corp. Inquiries concerning licenses for its commercial development should be addressed to

Harris Corporation
Government Aerospace Systems Div.
P.O. Box 9400
Melbourne, FL 32902

Refer to NPO-17497, volume and number of this NASA Tech Briefs *issue, and the page number.*

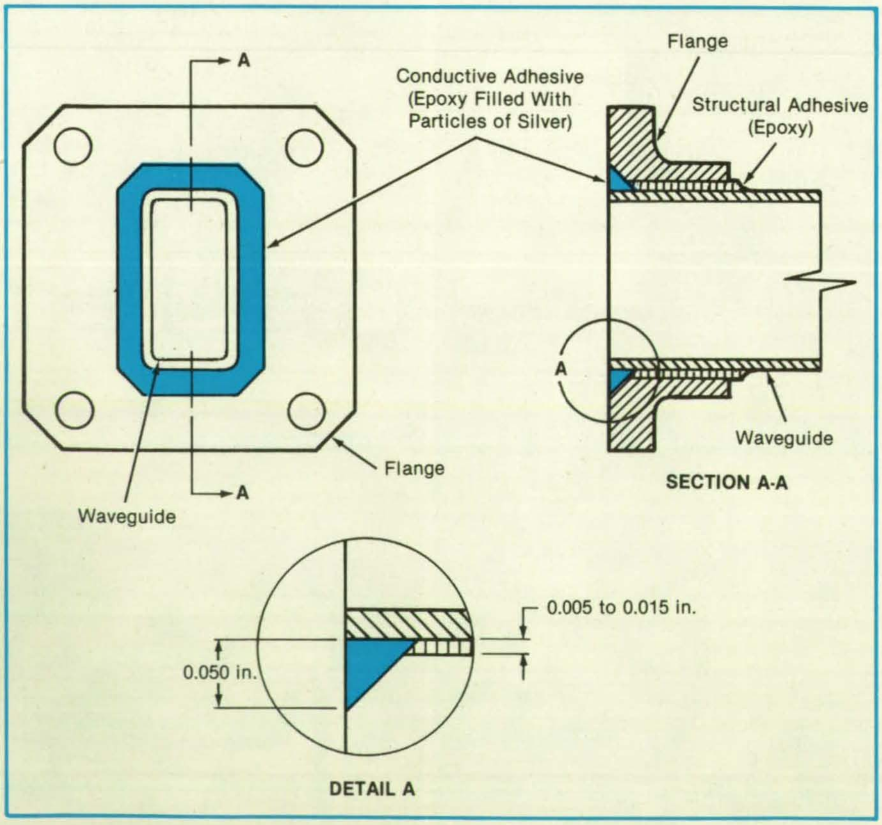

The **Flange Is Machined Slightly Oversize and Beveled** to accommodate structural and conductive adhesives.

Electronic Systems

Hardware, Techniques, and Processes
42 Disturbance-Accomodating Controller Would Aim Antenna
44 Digital Demodulator for Advanced Receiver
48 Peripheral Equipment Interchanges Bytes of Data
50 Concept for Generation of Long Pseudorandom Sequences
52 High-Resolution Imaging Spectrometer
52 Balanced-Bridge Feedback Control of Motor
54 Programmable Direct-Memory-Access Controller

Computer Programs
68 Analyzing Optical Communication Links

Disturbance-Accommodating Controller Would Aim Antenna

Existing methods of control are combined to suppress systematic errors.

NASA's Jet Propulsion Laboratory, Pasadena, California

A proposed system for aiming a large paraboloidal-dish antenna is based on the theory of disturbance-accommodating control. The new concept of control incorporates features from previously developed concepts to suppress systematic errors caused by misalignment of the antenna, sensor noise, and random thermal and wind disturbances.

Errors in the aiming of antennas in pointing and tracking are typically functions of static and dynamic factors. Mechanical misalignments of sensors or inaccuracies in the predictions can be considered as static factors, whereas dynamic factors would include wind, thermal, and gravitational loading. The approach here is to cancel the static errors for precise pointing of the antenna by treating the systematic misalignment errors, as well as the servocommands, as disturbances to the controlled system.

Aiming can be improved through a sequence of modifications solely in existing software. Current algorithms can be enhanced to provide simultaneously servotracking and correction of the systematic errors as well as stabilization of beams in the presence of random disturbance torques. For a given antenna, servodrive, feed, and distortion of the surface, a software package could be developed to optimize the performance to achieve, adapt-

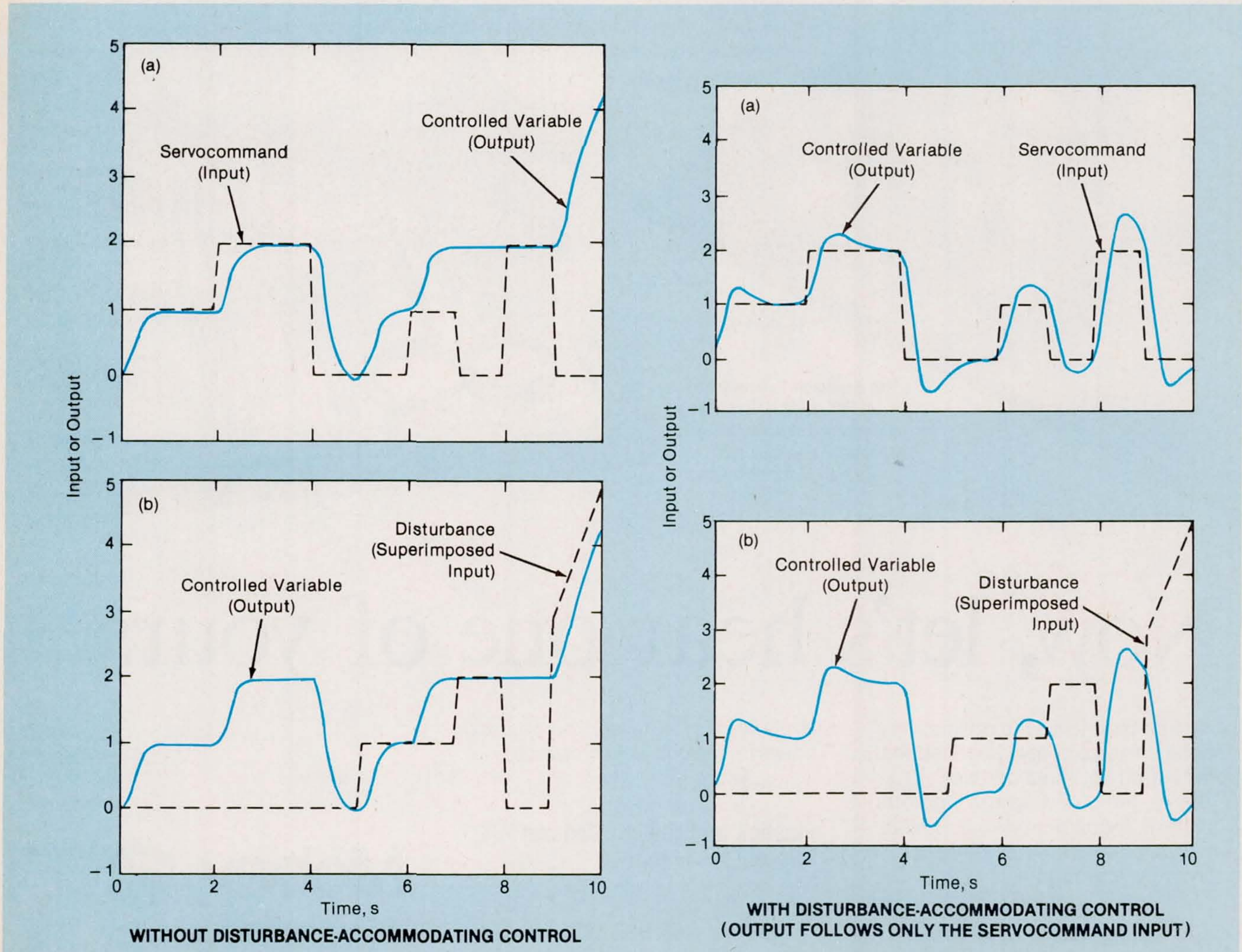

The **Servocommand Responses** of a single-variable system with discrete-time digital control were simulated numerically. The disturbance in the output is clearly suppressed when disturbance-accommodating control is included.

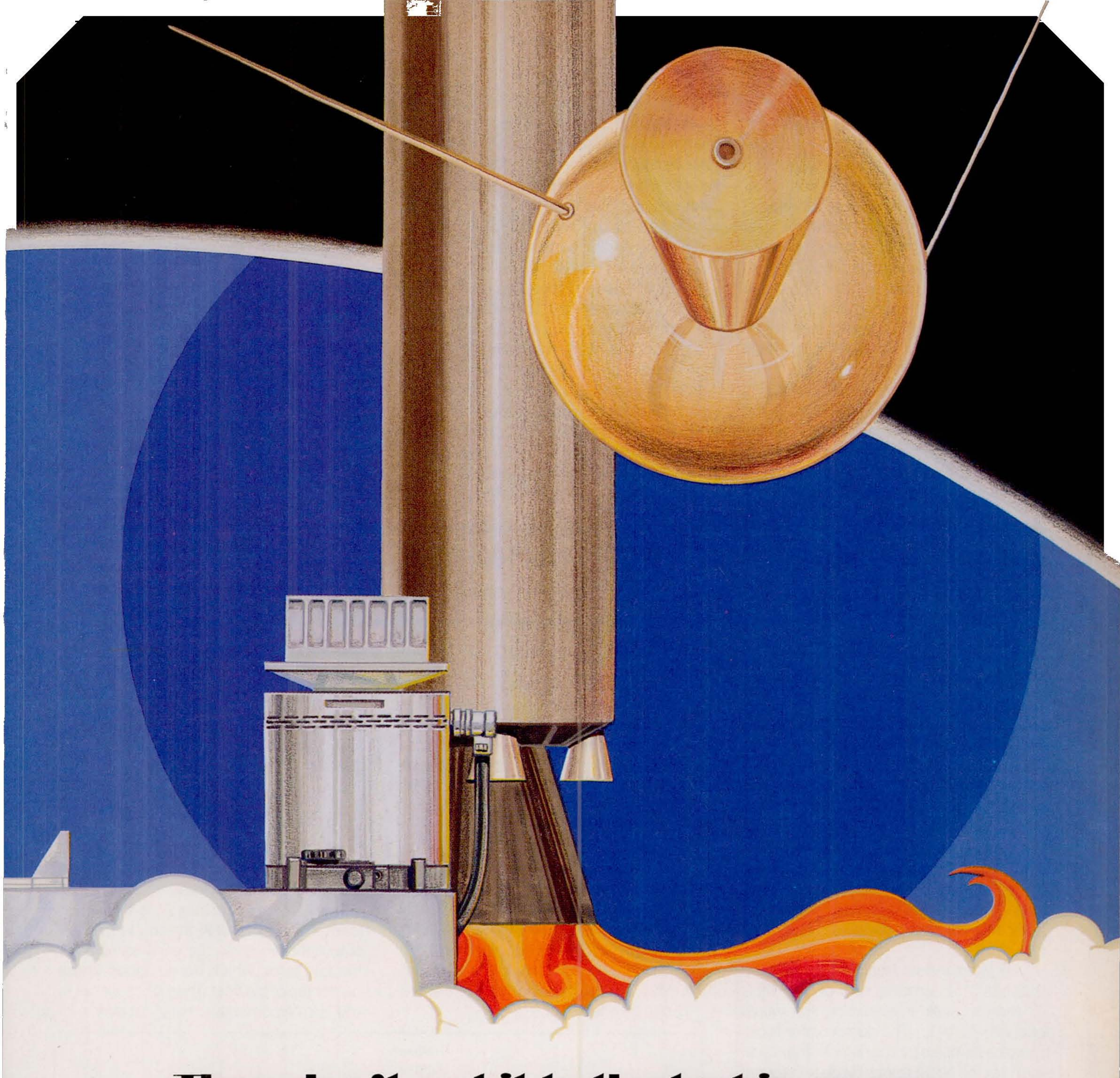

ively, the maximum antenna gain for a prescribed direction vector with a "smart" controller.

A typical antenna controller includes an analog velocity-control loop and a position-control loop closed through a digital computer. The algorithms for the control of position are either proportional-integral (PI) or state feedback control algorithms. The PI control involves the application of gains to the position error and the integral of position error. The weighted sum of these signals is the commanded rate for the velocity-control loop. This type of control system results in zero steady-state error when the input is a ramp signal.

The more sophisticated method utilizing state feedback allows specification of the eigenvalues of the closed position-control loop. The initial disadvantage of state feedback is the requirement that all the states of the system be available for the feedback control. The technique of estimation of the state has circumvented this problem, providing the controller with an estimate for each of the unmeasurable or uncertain state signals. The feedback gains are selected to yield the designer's selected eigenvalues to achieve the desired performance of the system.

In the proposed disturbance-accommodating controller, another vector would be estimated simultaneously with the estimation of the state vector. This other vector would represent the disturbance state, which could then be used in determining a more-complete control strategy.

The disturbance-accommodating controller is designed to synthesize and reject the waveformlike disturbances that are encountered in practice in tracking systems for antennas. The disturbances can be mathematically modeled according to a priori data by determination of the corresponding differential equation and, hence, the representation of the state of the waveform-structured noise.

The results of a computer simulation show that the disturbance-accommodating controller can cancel systematic errors, while simultaneously allowing an optimal-control policy to regulate the system (see figure). The disturbance-accommodating controller is easy to implement along with the existing servocontrol. Such practical issues as the order of the mathematical model, computation time, and storage requirements offer no expected challenges in the design of microprocessor-based controllers.

This work was done by L. L. Gresham, F. L. Lansing, and C. N. Guiar of Caltech for **NASA's Jet Propulsion Laboratory**. *For further information, Circle 84 on the TSP Request Card.*
NPO-17631

Digital Demodulator for Advanced Receiver

Complexity and cost are reduced by a new design for half-band filters.

NASA's Jet Propulsion Laboratory, Pasadena, California

A digital demodulator has been designed for use in the reception of phase- and amplitude-modulated digital signals of bandwidths up to 15 MHz on microwave carriers. The system performs coherent demodulation in phase and in quadrature with the carrier locked in phase to an intermediate frequency of 10 MHz. In statistical simulations and in tests of a "breadboard" version, the demodulator exhibited the expected high performance at low signal-to-noise ratios. The design is suitable for fabrication in very-large-scale integrated circuitry.

The intermediate frequency is digitized to 8 bits at a sampling rate of 39.6 MHz (chosen to avoid interference that would occur at 40 MHz). The demodulator multiplies the samples by cosine and sine waveforms at the 10-MHz intermediate frequency, thereby generating the in-phase and quadrature baseband signals, plus the sum-frequency components (see Figure 1).

The principal innovative feature of the demodulator is the design of the half-band digital low-pass filters that remove the sum-frequency components. In concept, this kind of filter is a special case of the class of low-pass finite-impulse-response (FIR) filters of order N. The half-band concept was chosen partly because almost half of the N filter coefficients are zero, and consequently, the number of multiplications and additions required is only half that of an arbitrary linear-phase digital filter. This reduces the required complexity of the circuitry, particularly when decimation by 2 is used.

Other considerations that favor this selection include the following:

- The width of the stopband equals the width of the passband. This is ideal for the elimination of sum frequencies that cause complex heterodyning, because the sum-frequency components have the same bandwidth as that of the difference-frequency components to be passed.
- The peak deviations of the ripples in the passband and the stopband are equal. As a result, the signal-to-noise ratio due to the passband ripple is about the same as that due to the sum-frequency noise aliased into the passband after decimation by 2.
- When a decimation factor of 2 is employed, the processing rate is also reduced by a factor of 2.

Figure 2 illustrates a simplified architecture for the Nth (N odd) order half-band finite-impulse-response filter. The output y_n of the filter at the nth sampling interval is given by

$$y_n = \sum_{j=-[(N-1)/2]}^{j=[(N-1)/2]} h_j x_{n-j} + x_n$$

where j is odd and x_k denotes the input at the kth sampling interval.

In this expression for y_n with even n (decimation factor of 2), the only term in the output that involves the even samples is the last term, which corresponds to the center tap of the filter. Thus, it is possible to reduce the computation of y_n for even n in-

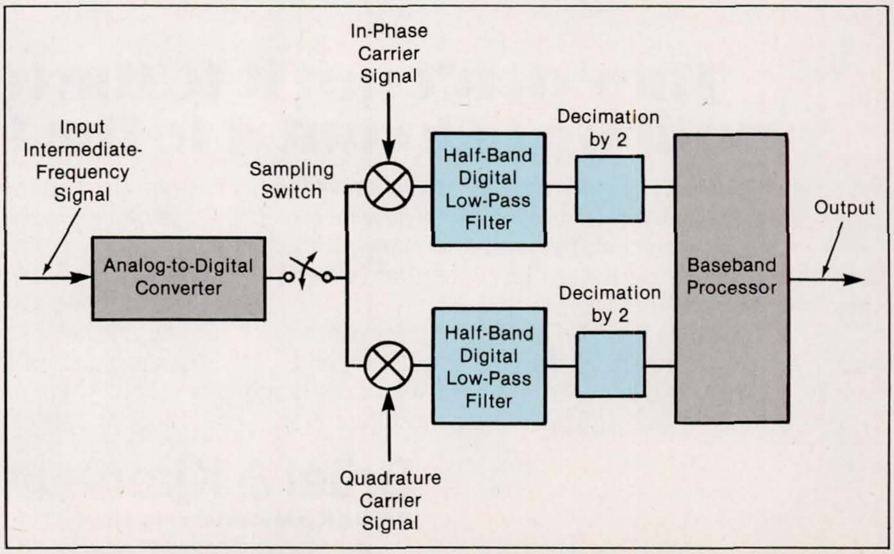

Figure 1. The **Digital Demodulator** performs coherent demodulation on the in-phase and quadrature components.

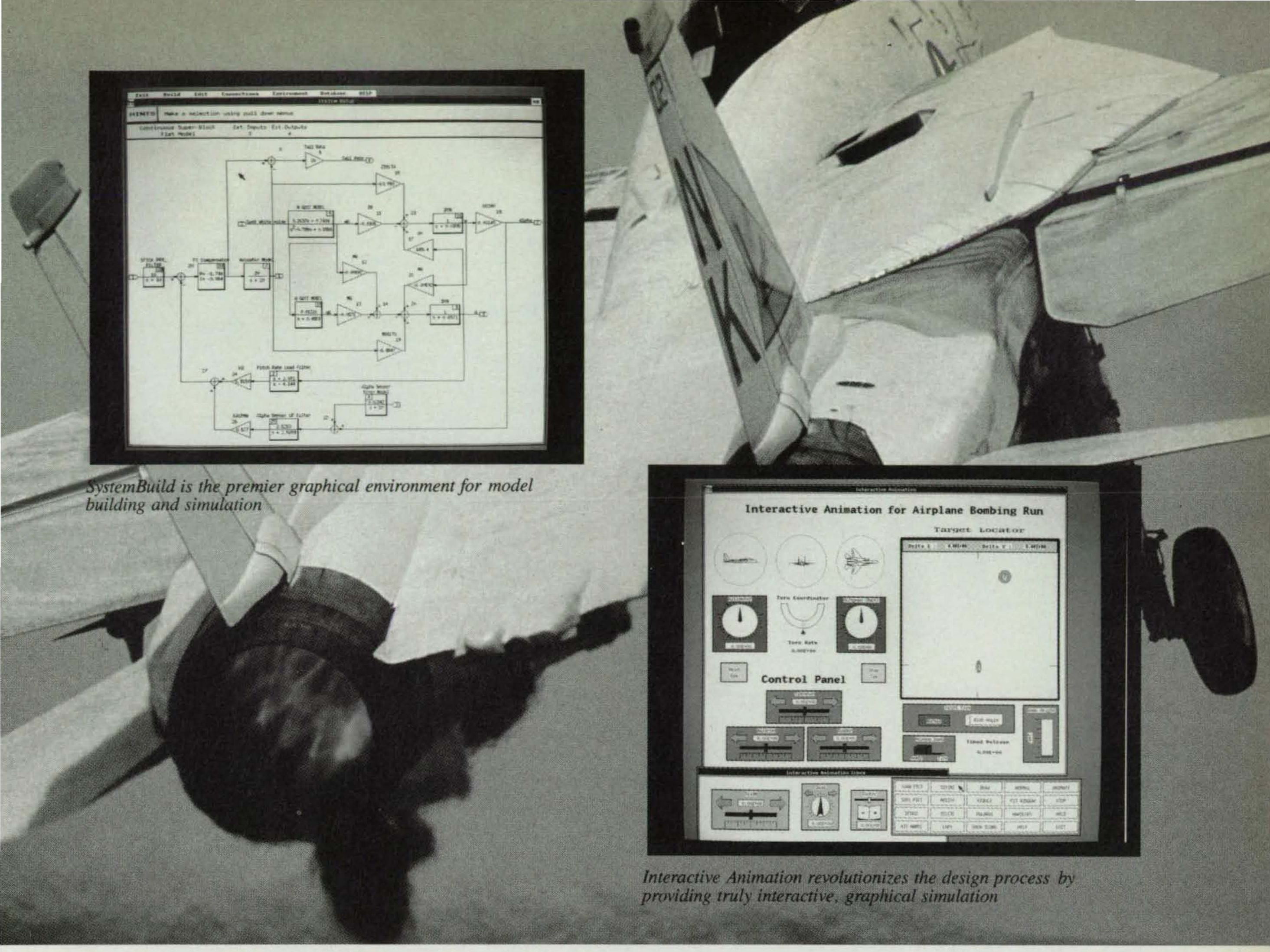

SystemBuild is the premier graphical environment for model building and simulation

Interactive Animation revolutionizes the design process by providing truly interactive, graphical simulation

TAKE CONTROL WITH MATRIXx.

Only one family of products offers a streamlined software environment for each phase of control system development — the ISI Product Family. For aerospace, automotive, computer peripherals, industrial control, and material processing.

Build a complex graphical system model. Analyze the system and design a controller. Run real-time animated simulations. Plot the results. Refine the design. Generate real-time Fortran, C, or Ada code. Download it into a target processor. Run it in real-time. All with one family of software products.

- Solve arithmetic and engineering problems without programming in Fortran or C.
- Design multivariable engine controllers faster.
- Optimize controllers for nonlinear robotics applications.
- Model and simulate complicated nonlinear braking systems for antilock brake control.
- Create innovative satellite attitude controllers using the latest robust design techniques.
- Simulate aircraft and missile guidance systems before expensive hardware testing.
- Prototype systems in hours — not months.

Analysis and Design
MATRIX$_X$®:
- Engineering and mathematical analysis
- Programming
- Comprehensive 2- and 3-D graphics

Expansion Modules:
- Control Design
- Robust Control
- Optimization
- Digital Signal Processing
- System Identification

Modeling and Simulation
System Build™:
- Mouse-driven graphical modeling
- Nonlinear, hybrid, multi-rate, and event-driven simulation
- 75+ engineering blocks
- 6 integration algorithms

Expansion Modules:
- Interactive Animation
- Remote Simulation
- Simulation Accelerator
- Automatic Documentation
- Project Database

Real-Time Code Generation
AutoCode™:
- Automatic Code Generation in Ada, C, or Fortran

Implementation and Testing
AC-100™:
- Real-time multi-processor system
- "Hardware-in-the-loop" control

MATRIXx is the least expensive engineering analysis product available today — from $595 for PCs and $4000 for workstations.

Engineering professionals worldwide continue to rely on ISI's products to streamline control system design. Now it's your turn. **Call 408-980-1500** for information, a complete set of Data Sheets, or the phone number of your nearest sales representative.

integrated systems inc.

2500 Mission College Blvd.
Santa Clara, California 95054
Tel: (408) 980-1500
Fax: #408-980-0400

DESIGN • SIMULATION • CODE GENERATION • IMPLEMENTATION

Circle Reader Action No. 557

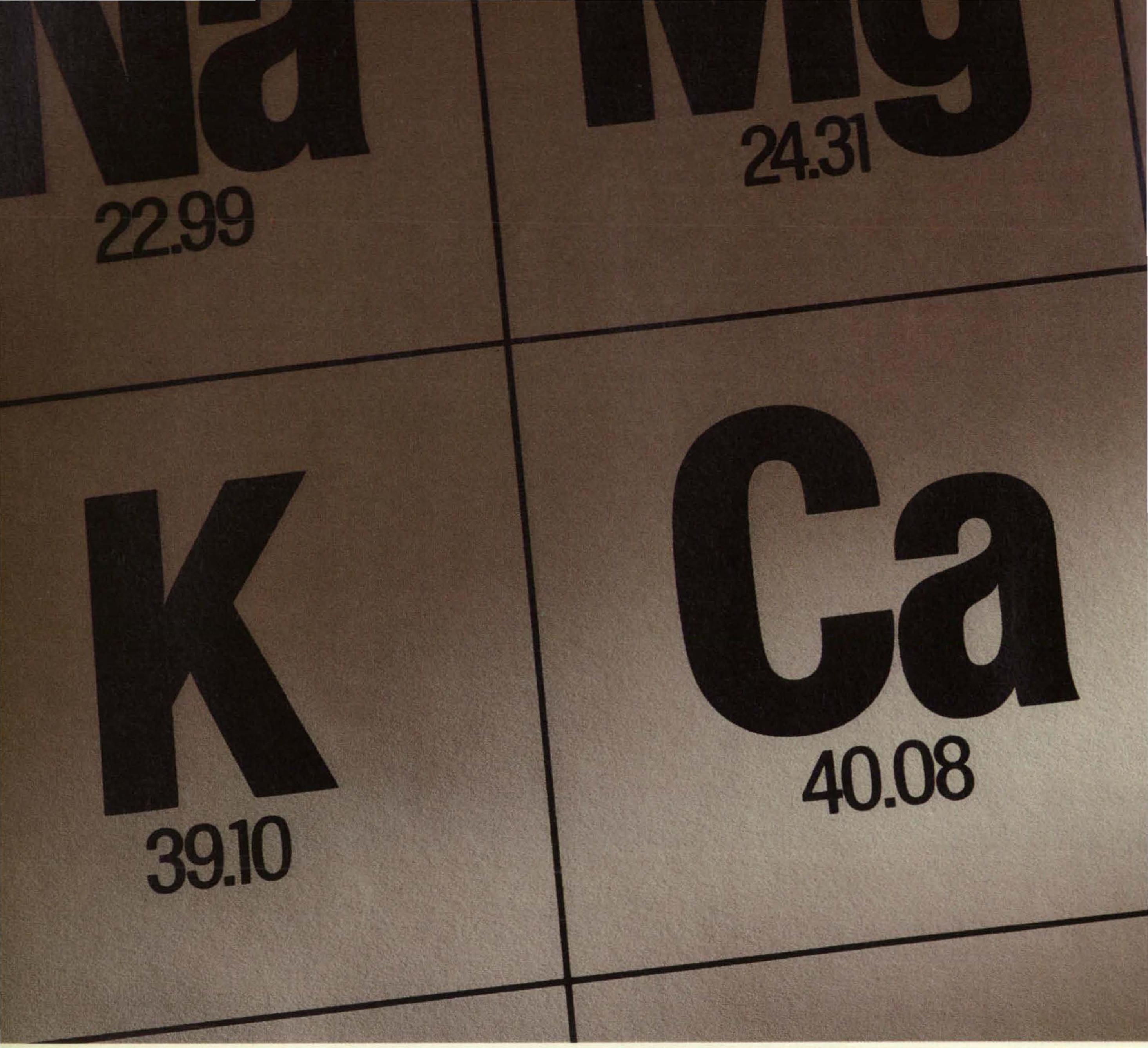

A basic element in any solution is IBM.

It's IBM scientific computing for chemistry: unbeatable combinations of products, applications, service and support that can help chemists in virtually any discipline work more productively.

IBM's chemistry solutions offer a wide range of system choices with the diverse applications, powerful graphics capabilities and development tools chemists need to improve information quality and reduce job turnaround time.

These versatile IBM solutions provide powerful support at every step of the process: instrument data acquisition and control, laboratory information systems, access to

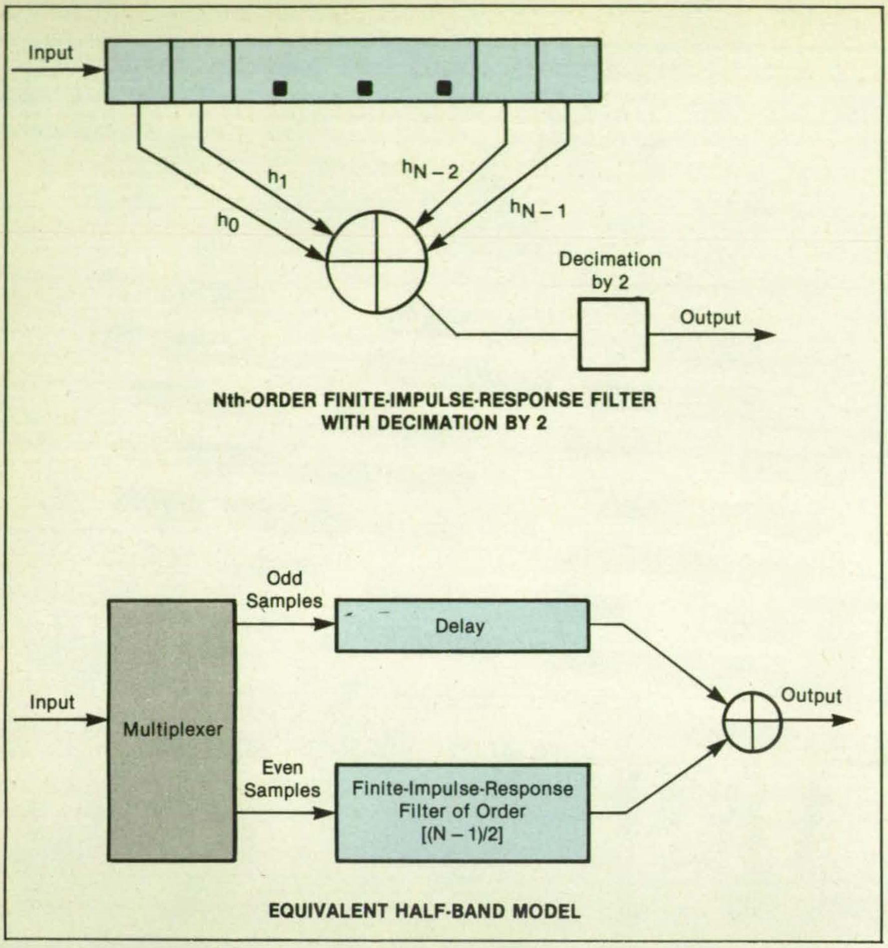

Figure 2. The **Half-Band Digital Low-Pass Filters** of Figure 1 are a special case of *N*th-order finite-impulse-response filters suitable for decimation by 2.

to a lower-order (half) filtering and an addition operation. First, the input is demultiplexed into odd and even samples. The odd samples are filtered by an $[(N+1)/2]$-tap finite-impulse-response filter. The output of the filter is summed with the delayed even sample. The simplicity of this architecture is evident in the comparison with structure of the general fast-impulse-response filter. The length of the delay (in sampling periods) in the simplified model is $(N+1)/2 + \tau$, where τ is the pipeline delay through the fast-impulse-response filter.

This structure has the important additional advantage that the filter operates at half the input frequency. Thus, the components can be slower than those of a general finite-impulse-response filter. This helps to reduce the cost. It also enables building the filter to operate at twice the speed of available multipliers or FIR filter circuits. Furthermore, it is also possible to take advantage of the symmetry of the coefficients of the fast-impulse-response filter to reduce the number of multiplications by another factor of 2.

This work was done by Ramin Sadr and William J. Hurd of Caltech for **NASA's Jet Propulsion Laboratory**. *For further information, Circle 46 on the TSP Request Card.*

Inquiries concerning rights for the commercial use of this invention should be addressed to the Patent Counsel, NASA Resident Office-JPL [see page 22]. Refer to NPO-17628

Peripheral Equipment Interchanges Bytes of Data

A pair of circuit boards relieves a central processing unit of this task.

Marshall Space Flight Center, Alabama

A method for the conversion of data formats between incompatible computers reduces conversion time by 80 percent. The method transposes the high and low bytes of a word so that data from computer A match the storage format of computer B.

In the application for which the method was developed, data are acquired from test firings of rocket engines; in a typical test, about 40 data files of 16,000 blocks apiece are processed. Previously, the central processing unit of computer A (a Digital Equipment Corp. VAX 11/750) was used to convert the data and took about 10 min to convert each file. Therefore, the total conversion time was 400 min.

In the new method, a file can be converted in only 2 min. This is fast enough to enable the data to be recorded on magnetic tape while they are being acquired. The 40 files can be converted in only 80 min. Computer B (a Perkin-Elmer system) can then use the tape directly.

In the new method, two interface circuit boards convert the data. Such boards are ordinarily used for communication between computers. In the format-conversion application, the cable connecting the boards is modified so that the high-8-bit and low-8-bit data lines are interchanged (see figure), with the result that the data words are in the proper format for computer B.

The byte-swapped data flow from computer A over a local-area network (Ethernet) to a host computer (a MicroVAX II), which sends the data to a 6,200-bit-per-in. (2.44-kilobit-per-cm) tape drive for recording. The recorded data can then be transferred to computer B for further processing.

This work was done by Robert B. Aguilar of Rockwell International Corp. for **Marshall Space Flight Center**. *No further documentation is available.*
MFS-29478

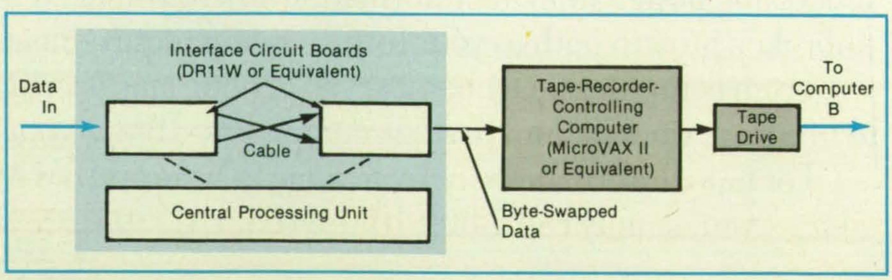

A **Pair of Interface Boards** reverses positions of high and low bytes of data. The boards are housed in computer A. Another computer feeds the converted data to a tape recorder. The tape can be transferred subsequently to computer B.


ENGINEERING...
Online on
STN International®

Concept for Generation of Long Pseudorandom Sequences

A VLSI design would be based on exponentiation in a finite field.

NASA's Jet Propulsion Laboratory, Pasadena, California

A conceptual very-large-scale integrated (VLSI) digital circuit would perform exponentiation in a finite field. An algorithm that generates unusually long sequences of pseudorandom numbers would be executed by a digital processor that includes such circuits. The new concepts are particularly advantageous for such applications as spread-spectrum communications, cryptography, and the generation of ranging codes, synthetic noise, and test data, where it is usually desirable to make pseudorandom sequences as long as possible.

A previously-developed modular VLSI multiple-tap pseudorandom-sequence generator is composed of n stages of shift register and generates a periodic sequence with period $2^n - 1$. The sequence produced by that circuit is believed to have a maximum length for linear algorithms of n stages. Like the maximal-length shift register, the new system requires n shift registers, but it also requires exponentiation in finite fields and yields a much longer period. Although the new sequences may not have flat spectra as do the sequences generated by the maximum-length shift register, the increase of the period is very desirable in some applications.

The first problem is to calculate the exponential $\beta = \alpha^N$, where α is in the finite field $GF(2^m)$ and $1 \leqslant N \leqslant 2^m - 1$. The solution is obtained by successive multiplications according to a recursive algorithm executed by the combination of a cyclic-shift circuit, a parallel-type Massey-Omura multiplier, and a control-logic circuit (see figure).

It can be shown that if A_o is a primitive element in $GF(2^m)$, and if $\{E_k\}$ is a sequence of $2^n - 1$ distinct numbers (where $n \leqslant m$), which are less than 2^n, then the sequence of exponentials $A_k = A_0^{E_k}$ in $GF(2^m)$ represents a sequence of pseudorandom numbers that repeats with a period of $2^n - 1$. A random-number sequence can also be generated from

$$A_k = A_0^{p^{s}\prod_{i=1}^{t} E_i}$$

where $p = (2^n - 1)!\bmod(2^m - 1)$, $k = s(2^n - 1) + t$, and $n < m$. If $2^m - 1$ is a Mersenne prime, then the period of $\{A_k\}$ is increased to $(2^n - 1)r$, where r is an integer that satisfies several other criteria. In general, this period is much greater than that of a sequence generated by a maximal-length shift register of an equivalent number of stages. For example, with $m = 19$ and $n = 17$, the period is 34,359,345,153, which is 262,143 times the period 131,071 generated by a 17-stage shift register.

This work was done by C. C. Wang of Caltech for **NASA's Jet Propulsion Laboratory**. *For further information, Circle 141 on the TSP Request Card.*

This invention is owned by NASA, and a patent application has been filed. Inquiries concerning nonexclusive or exclusive license for its commercial development should be addressed to the Patent Counsel, NASA Resident Office-JPL [see page 22]. Refer to NPO-17241.

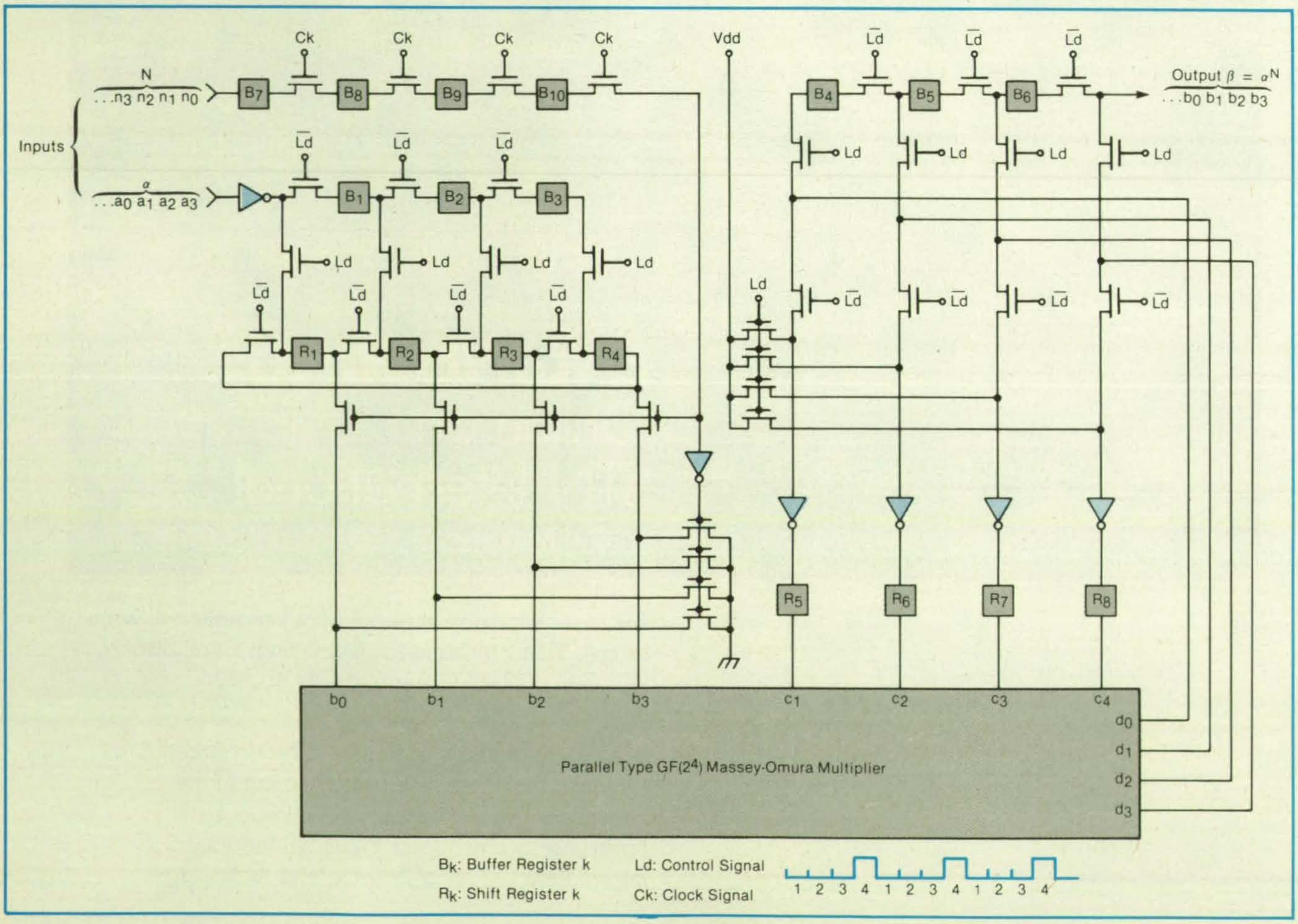

This **Circuit Computes Exponentials $\beta = \alpha^N$** in the finite field $GF(2^4)$, where N ranges from 1 to 15. The circuit operates in a "pipeline" manner: each computation requires four clock cycles, during which the bits of the previously computed β are shifted out and the bits of the following α are fed in.

One thing NASA and modern medicine have in common: Seikosha video printers.

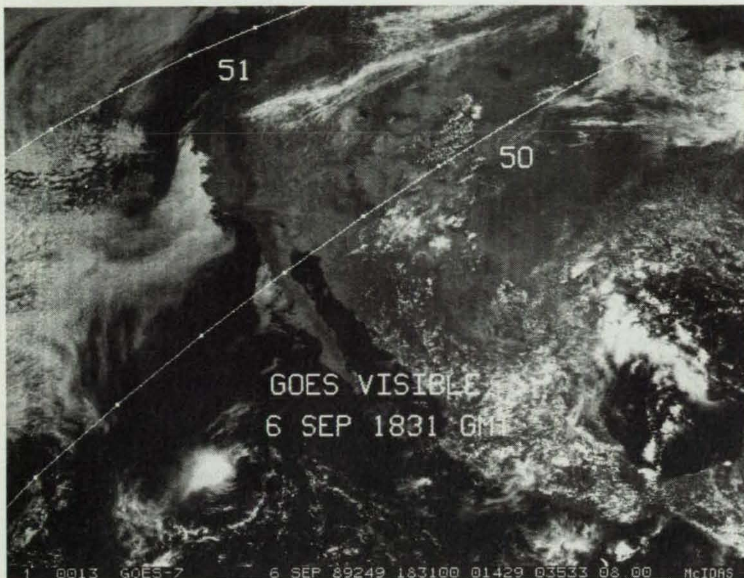

The high-resolution Seikosha VP-3500.

It was Seikosha, a Seiko Group company, that invented the first video printer in 1979.

And it was Seikosha that understood the importance of making a video printer with a line rate high enough for applications ranging from MRI to electron microscopy to industrial QC/QA.

The hard copy images NASA produced on the VP-3500 from geostationary satellite transmissions were used by the last four Space Shuttle crews.

Our 1280-line, multi-format video printer can make things perfectly clear.

The bottom line for any application is picture quality. And the VP-3500's bottom line is very impressive.

The Seikosha VP-3500 gives you 1280 x 1240 resolution with full 64-tone gray-scale prints from any video source: NTSC, PAL, SECAM and RS-170. Plus you can choose multi-format prints.

Let us introduce you to the video printer with the resolution good enough for modern medicine and NASA.

For a demonstration, or additional information on the Seikosha VP-3500, call 1 800-338-2609 or 1 201-327-7227.

SEIKOSHA

A SEIKO GROUP COMPANY

Serious printers for serious business.

Circle Reader Action No. 462

High-Resolution Imaging Spectrometer

Earth resources will be observed in greater detail.

NASA's Jet Propulsion Laboratory, Pasadena, California

The High-Resolution Imaging Spectrometer, undergoing development for use in NASA's Earth Observing System, will measure the reflectance of the Earth's surface in visible and near-infrared wavelengths. From an orbit around the Earth, this instrument will scan the surface of the Earth in 200 wavelength bands simultaneously. It will produce images that will enable the identification of minerals in rocks and soils, important algal pigments in oceans and inland waters, changes in spectra associated with the biochemistry of plant canopies, compositions of atmospheric aerosols, the sizes of grains in snow, and the contamination of snow by impurities that absorb visible light.

From an orbital altitude of 700 km, the instrument will observe a swath 24 km wide with a spatial resolution of 30 m. The instrument will cover the wavelength range of 0.4 to 2.5 μm in spectral bands 10 nm wide. In each picture element, the brightness in each wavelength band (see figure) will be quantized to 12 bits, with a dynamic range suitable for such bright targets as snow.

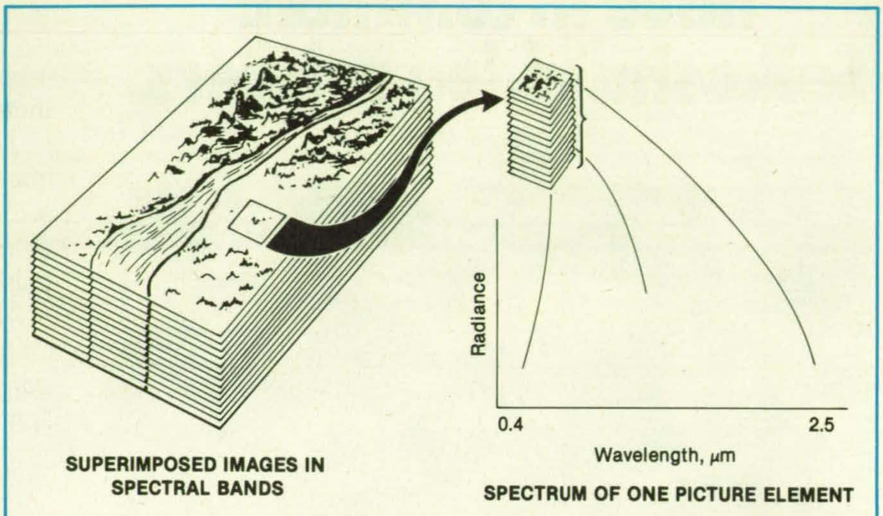

Images Taken Simultaneously in Many Wavelength Bands will be inherently registered with each other. The radiances measured in the wavelength bands in each picture element yield a spectrum for that element that can be used to identify the materials at the surface of the Earth.

The capabilities for aiming the instrument, coordinated with the parameters of the orbit, must satisfy requirements for frequency of repetition of measurements at a given location. In some cases, these requirements are affected by such factors as lighting, visibility (e.g., presence or absence of clouds), and the presence or absence of vegetation. The chosen across-track pointing capability of ±24° enables 3 or 4 repetitions for a site at the Equator and 4 to 5 repetitions for a site at 40° north or south latitude during one 16-day orbital revisit period. An along-track pointing capability of +60°/−30° is provided for measurements of the bidirectional reflectance-distribution functions of surfaces, to remove the effects of atmospheric attenuation, and to implement image-motion compensation to increase the signal-to-noise ratios for dark targets.

As now envisioned, the instrument will be a broadband, "pushbroom," double-pass Schmidt spectrometer containing silicon and hybrid mercury-cadmium-telluride area-array detectors. Incident radiation passing through a slit at the front of the foreoptics will be collimated, separated into two bands, dispersed, and reimaged onto separate detector arrays: silicon for visible and near-infrared wavelengths to 1 μm, and HgCdTe for longer infrared wavelengths to 2.5 μm. Signal-to-noise ratios are expected to range from 50 to 200 in most regions of the spectrum. The mass of the instrument is projected at an upper limit of 987 kg; several modifications of the design may reduce the mass.

The data-processing and -transmitting subsystem of the instrument will provide flexibility in the number of bits and number of bands transmitted, within constraints imposed by the available data rate. Possible modes in which data can be edited include transmission of some (instead of all) available spectral bands, encoding of 8 or 10 bits per band (rather than 12), averaging of adjacent picture elements, and use of a narrower swath. The output data will be augmented with satellite ephemeris data and made available as geocode data that depict various radiometric properties (or properties inferred from radiometry) of the Earth.

This work was done by Jeff Dozier of Caltech and Alexander F. H. Goetz of the University of Colorado for **NASA's Jet Propulsion Laboratory**. *For further information, Circle 83 on the TSP Request Card. NPO-17624*

Balanced-Bridge Feedback Control of Motor

Sensitivity to variations in electrical and mechanical characteristics would be reduced.

NASA's Jet Propulsion Laboratory, Pasadena, California

A proposed control system for a motor-driven rotary actuator would include three nested feedback loops, which, when properly designed, would be decoupled from each other. The system is intended to increase the accuracy of control by mitigating such degrading effects as vibrations and variations in the electrical and mechanical characteristics of the structure to be rotated. The system lends itself to the optimization of performance via the independent optimization of each of the three loops.

The conceptual system includes outer, actuator, and driver feedback loops, configured so that the actuator is a subsystem, and the driver is a subsystem of the actuator (see figure). The torque τ exerted by the motor on the structure is sensed and used as a component of actuator feedback. The angular speed $\dot{\theta}_m$ of the motor shaft relative to the stator and the angular speed $\dot{\theta}$ of the structure in the inertial space are also sensed and used in the actuator and outer feedback loops, respectively.

Current and voltage feedback in the

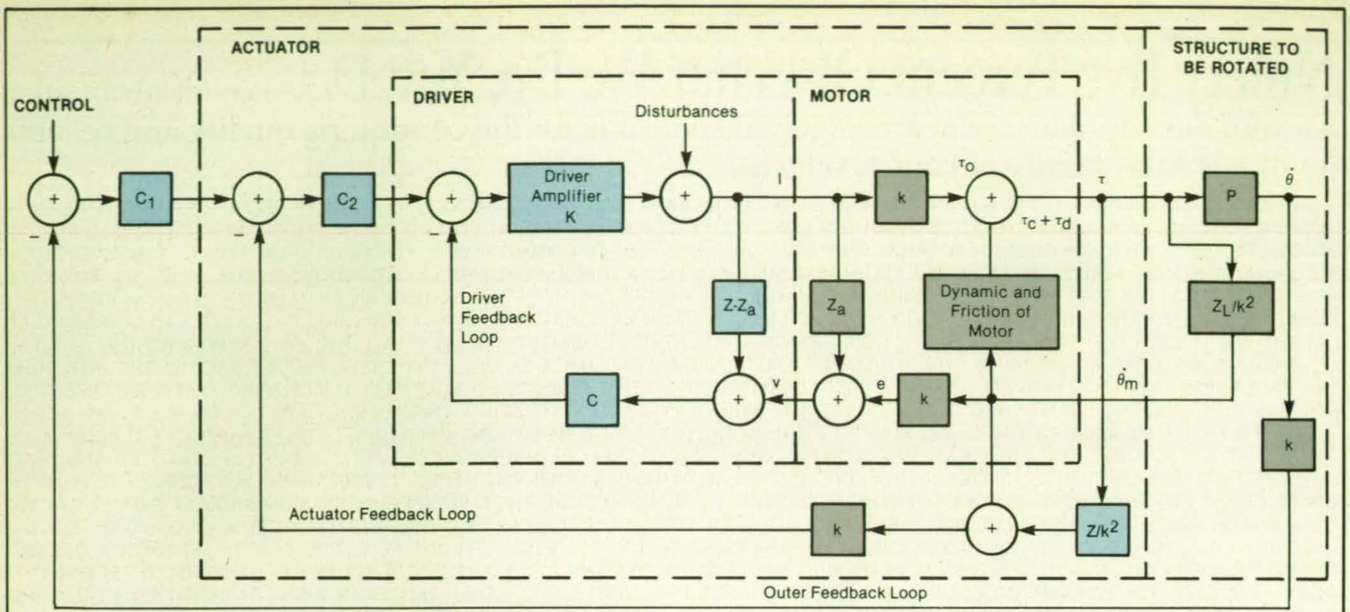

Notes:
1. C_1 and C_2 represent compensators and their transfer functions.
2. K represents the driver amplifier and its transconductance.
3. Z_a = the electrical resistance of the motor winding.
4. τ_o = kI, where I = the motor current and τ_o = the rotor/stator interaction torque.
5. e = the back electromotive force of the motor.
6. V = the voltage applied to the motor.
7. c = a constant transfer coefficient ≈ 0.01.
8. Z_L/k^2 = the driving point function of the structure, expressed as a mechanical impedance loading the motor.
9. τ_c = cogging and frictional torque.
10. τ_d = component of torque due to nonideal dynamics of the motor.
11. Z-Z_a = the output impedance of the driver amplifier.
12. P = the transfer function of the structure to be rotated.
13. Other terms are defined in the text.

The **Feedback Control System** includes three nested loops that can be optimized independently of each other to reduce the susceptibility of the overall system to vibrations in the structure and variations of mechanical and electrical characteristics.

driver loop are chosen to be proportional correspondingly to the torque and $\dot{\theta}_m$ feedback in the actuator loop to obtain a "balanced-bridge" configuration This makes it possible to reduce the sensitivity of the overall closed-loop system to variations in the characteristics of the structure by transferring the effects of uncertainty in the structure from the actuator loop to the driver loop. As a consequence, the gain of the actuator loop can be increased without adversely affecting its stability, thereby reducing significantly the effects of the disturbances that originate in the actuator. Also, the margins of stability of the actuator loop are relatively independent of the characteristics of the structure.

The balanced-bridge configuration also reduces the effects of friction in the motor on the stability of the outer feedback loop. Consequently, the feedback gain of this loop can also be increased to reduce the effects of disturbances that originate there. The flexibility in the choice of the output impedance of the driver can be exploited to improve the overall performance and to reduce further the sensitivity of the outer loop to variations in the parameters of the structure.

This work was done by Boris J. Lurie of Caltech for **NASA's Jet Propulsion Laboratory**. *For further information, Circle 103 on the TSP Request Card.*

This invention is owned by NASA, and a patent application has been filed. Inquiries concerning nonexclusive or exclusive license for its commercial development should be addressed to the Patent Counsel, NASA's Resident Office-JPL [see page 22]. Refer to NPO-17430.

Programmable Direct-Memory-Access Controller

Features include autonomy and the ability to perform functions normally reserved for a CPU.

NASA's Jet Propulsion Laboratory, Pasadena, California

A proposed programmable direct-memory-access controller (DMAC) would operate with computer systems of the 32000 series, which have 32-bit data buses and use addresses of 24 (or potentially 32) bits. The controller could function with or without the help of a central processing unit (CPU) and would start itself. It would include such advanced features as the ability to compare two blocks of memory for equality and to search a block of memory for a specific value. The controller would be made as a single very-large-scale integrated-circuit chip.

The figure shows basic structure of a computer system with a DMAC. The bus includes separate control (C), address (A), and data (D) lines. The CPU and DMAC act as coprocessors; both are capable of driving all bus signals. One or the other (or neither) is the bus master at any time. The CPU is the overall system master. The DMAC requests the bus by asserting HOLD. The CPU releases the bus and asserts HOLDA (hold acknowledge) to the DMAC. The DMAC executes its task and relinquishes HOLD when finished; the CPU resumes its processing. When the DMAC is the bus master, it must generate control signals like those generated by the CPU.

The DMAC has four identical, independent channels. A priority controller resolves conflicts arising from simultaneous requests for access to the bus. Channel priorities are programmed, not hard wired.

Each channel has a pair of "handshake"

Operation	Number of Addresses	Width of Data (in Bits)
Transfer From Memory to Memory	2	16
Transfer Between Memory and Memory-Mapped Input/Output	2	16
Comparison of Blocks of Memory	2	16
Transfer Between Memory and Nonaddressed Input/Output	1	16,32
Copy Value to Memory	1	16
Search Memory for Value	1	16
Generate a Check Sum	1	16

These **Operations Would Be Performed** on data by the programmable DMAC.

GLOBAL REGISTERS

NAME	CONTENTS
Control	Data Size, Channel Priorities
SYSBAR	Bus Access Register for the Chip
ISR	Interrupt Status Register

CHANNEL REGISTERS

NAME	CONTENTS
Command	Bit Fields Defining the Operation
Count	Repeat Count for the Operation
PTR1-MS	High Half of Address Pointer 1
PTR1-LS	Low Half of Access Pointer 1
PTR2-MS	High Half of Address Pointer 2
PTR2-LS	Low Half of Address Pointer 2
SAR-MS	High Half of Sequence Address
SAR-LS	Low Half of Sequency Address
CSR	Channel-Status Register
BAR	Bit Fields Controlling Bus Access
ACC	General Data Values
ITC	Iteration Counter
STOPC	State/Opcode Values

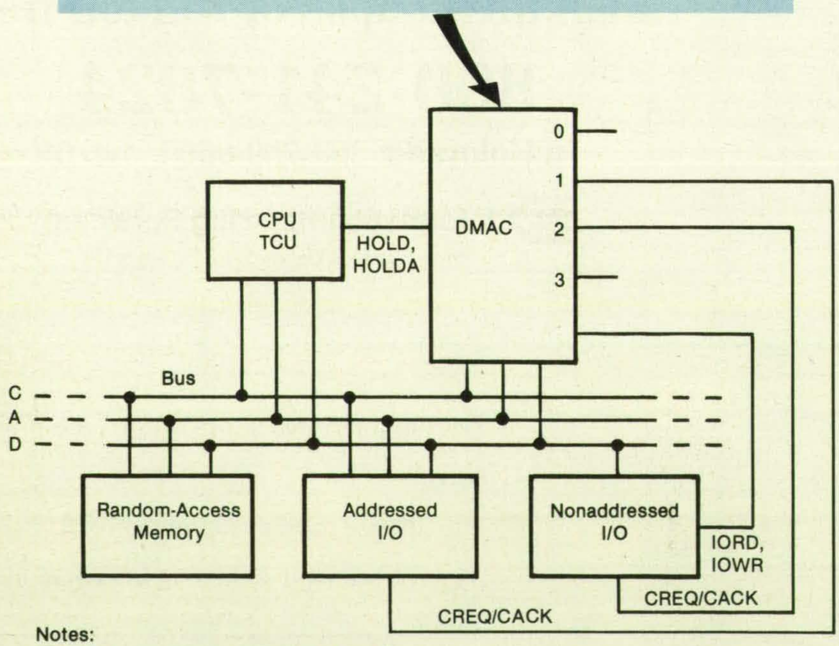

Notes:
1. "TCU" means "timing-and-control unit."
2. "IORD" means "reading input/output device."
3. "IOWR" means "write to input/output device."
4. Other definitions are given in the text.

The **Programmable DMAC** would share control of the computer data bus with the CPU. The program for the DMAC would be contained in its global and channel registers.

lines, CREQ and CACK. If the channel drives an input/output (I/O) device, these lines are connected to it. The device asserts CREQ when it needs service; the channel asserts CACK when the device is allowed access to the bus. In a memory-only DMA process, the handshake lines are not used; the channel decides when to request the bus, using the autorequest mechanism.

The DMAC supports 32-bit data buses by providing the four bus-enabling signals BE0 through BE3. The DMAC data lines are connected to the low 16 bits (two lowest bytes) of the data bus. In a 32-bit system, external logic must be used to multiplex the high and low halves of a data word onto the data lines of the DMAC for transfer of 32-bit data in two 16-bit pieces.

Addresses are incremented or decremented between successive operations by a programmed value in the range −7 to +7 (including zero for constant address values). Addresses can thus be manipulated in a general manner. The available classes of operations on data are shown in the table.

The DMAC consists of a global area and four individual channel areas. Each area has a set of registers, as shown in the detail in the upper part of the figure. All registers are 16 bits wide; 32-bit address values are implemented as register pairs.

The DMAC has two modes of operation: passive and active. In the passive mode, it acts as a memory-mapped I/O device, with an address for each register. For the sake of testability, all registers are both readable and writable. In the active mode, the DMAC acts as bus master for tasks that have been programmed into it.

Although the DMAC can be programmed in the passive mode by writing appropriate values to the registers, it is preferable to program it in the active mode by means of command records placed in memory by the CPU. Certain registers are then written in the passive mode to initialize and start it.

This work was done by David F. Hendry of Caltech for **NASA's Jet Propulsion Laboratory**. *For further information, Circle 88 on the TSP Request Card.*

In accordance with Public Law 96-517, the contractor has elected to retain title to this invention. Inquiries concerning rights for its commercial use should be addressed to

Edward Ansell
Director of Patents and Licensing
Mail Stop 301-6
California Institute of Technology
1201 East California Boulevard
Pasadena, CA 91125

Refer to NPO-17341, volume and number of this NASA Tech Briefs *issue, and the page number.*

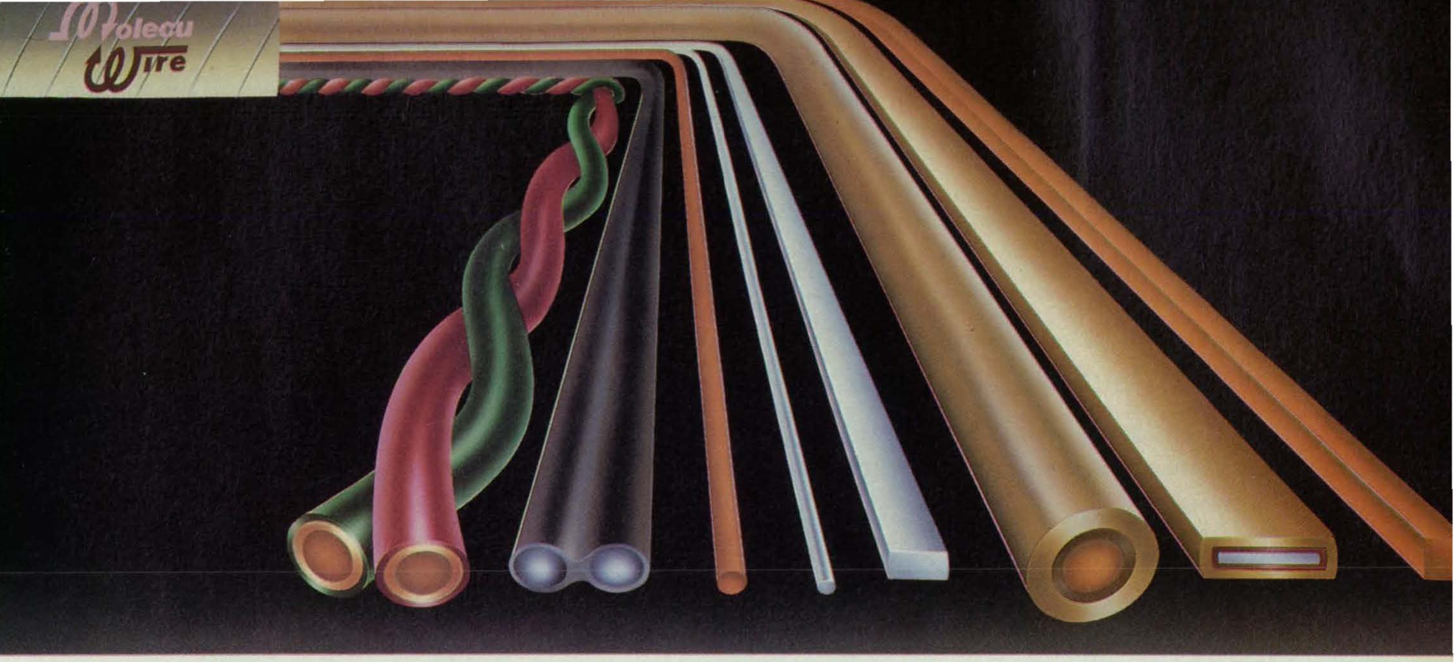

Physical Sciences

Hardware, Techniques, and Processes

58 Doppler-Shifted Raman Spectroscopy Measures Flows

62 Lignin Sensor Based on Flash-Pyrolysis Mass Spectrometry

63 Diagnosis of a Pressure-Modulator-Radiometer Cell

64 Calculating Irradiance for Photosynthesis in the Ocean

Books and Reports

65 Terrestrial-Imaging Spectroscopy

Doppler-Shifted Raman Spectroscopy Measures Flows

Nonintrusive, accurate wind-tunnel measurements are obtained without seeding the flows.

Langley Research Center, Hampton, Virginia

A technique for measuring the velocity, static pressure, and translational temperature of flowing molecules by use of stimulated Raman spectroscopy has been demonstrated in a supersonic wind tunnel at NASA Langley Research Center. These critical aerodynamic quantities were measured simultaneously by this nonintrusive technique, without the need to seed the flow.

A specially designed retrometer was employed to reduce the sensitivity of the system to vibrations. This feature also enabled simultaneous measurements of both the forward- and backward-scattered Raman lines. Analysis of the profiles and relative shifts of these lines renders a single data point for velocity, pressure, and temperature. In the initial demonstration of the technique in the free-stream flow and behind the shock layer of a simple model, mach-number data showed good agreement with the values set aerodynamically.

The extension of the technique to the hypersonic flow regime was also investigated, and simulated spectra for the free-stream flow in several operating hypersonic facilities were generated. These spectra show the viability of the technique and its limitations at very low densities. In particular, it was found that the peaking of the shape of the forward-scattered spectral line with decreasing pressure just compensates for the decrease in density, so that the peak inverse Raman spectroscopy signal in forward scattering remains constant.

The spectral width of the laser beam, however, represents a limiting factor for resolution of the peak in the shape of the forward-scattering line and sets a lower limit on the determination of pressure from the width of the forward-scattering line. Thus, as the density is reduced, the pressure ceases to be measurable, although the forward/backward scheme retains the capability for measuring velocity and temperature.

The simulated spectra were calculated for the ideal conditions of (1) maximum theoretical gain or loss, (2) the shot-noise limit, and (3) a single pulse. To date, only 10 percent of the theoretical gain has been obtained, and limitations are imposed by laser noise. However, with improvements in experimental technique, the shot-noise limit should be achieved, and about 50 percent of the theoretical gain should be attained. The signal-to-noise ratio can therefore be improved in the shot-noise limit by increasing the probe power. In addition, signal averaging can also be employed to increase the signal-to-noise ratio, depending on response-time limitations.

This work proves the viability of and establishes the accuracy of nonintrusive measurements of velocity, temperature, and pressure in a wind tunnel. This capability is very valuable in aerodynamic testing and should prove useful in a wide variety of laboratory, industrial, and engineering applications.

This work was done by Reginald J. Exton, Mervin E. Hillard, Jr., Walter R. Lempert, Peter F. Covell, and David S. Miller of **Langley Research Center**. *For further information, Circle 55 on the TSP Request Card.* *LAR-14133*

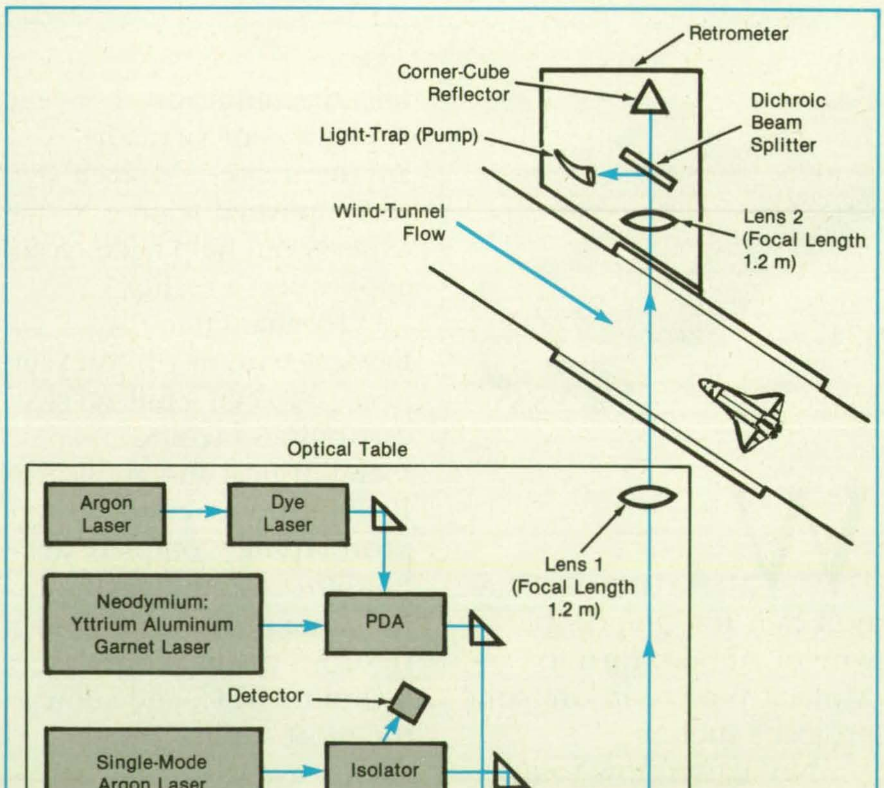

The **Optical Equipment for Vibration-Free Raman Doppler Velocimetry** in a wind tunnel includes a specially designed retrometer that reduces the sensitivity of the system to vibrations.

SPECIFY INCO SPECIALTY POWDERS FOR WIDE RANGE OF ELECTRONIC APPLICATIONS

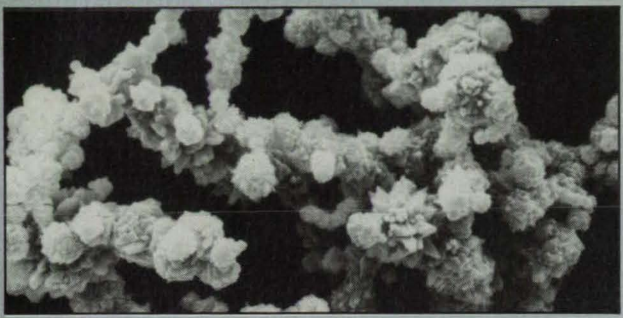

Inco Type T 287 Filamentary Powder, particle size (FSSS) 2.6-3.3 microns, apparent density 0.75-0.95 g/cc, relative surface resistivity 0.30 ohms per square (□).

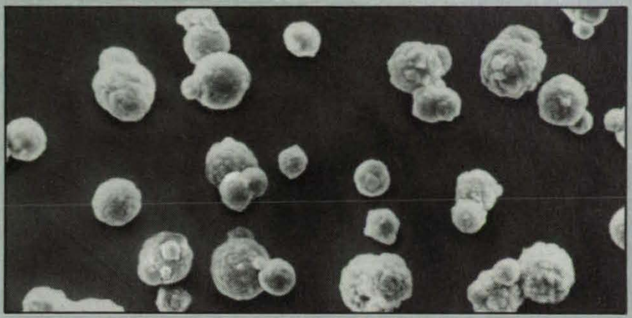

Novamet Silver Coated Nickel Spheres, 15% Ag, 2.5 g/cc apparent density, particle size 10 microns, screen mesh 99%-250, surface resistivity 0.03 Ω/□.

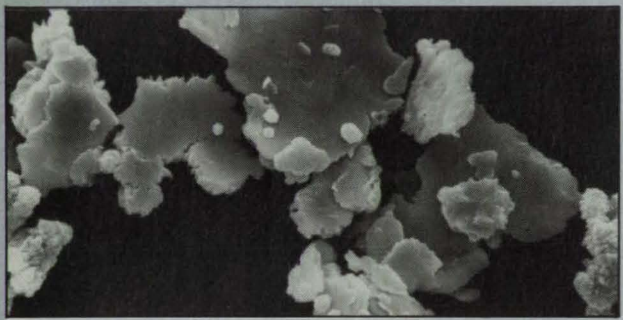

Novamet HCA-1 Flake, screen mesh 98% minus 400, apparent density 0.90 g/cc, thickness 1.0-1.1 microns, surface resistivity 0.25 Ω/□.

Novamet Nickel Coated Graphite, 60% fully encapsulated Ni, apparent density 1.6 g/cc, particle size (FSSS) 100 microns, screen mesh 63% −150/+250, surface resistivity 0.3 Ω/□.

Inco Specialty Powder Products now has a wide range of nickel and coated powders with exceptional conductive and magnetic properties. These properties make them ideal for a spectrum of electronic applications such as conducting film technology, coatings, adhesives, gaskets and EMI shielding.

EXTENSIVE PRODUCT RANGE

The development of computer processed control coupled with the continuous powder production improvements enables us to meet your most stringent powder specifications for electronic applications.

In addition to the products pictured above, INCO SPP has available the following high performance powder products. Novamet Conductive Nickel Spheres, particle size (FSSS) 8-9 microns, apparent density 3.2-3.5 g/cc, surface resistivity 1.0 ohms per square. Novamet 525 Conductive Nickel Pigment, screen mesh 100% minus 400, particle size 3.2 microns, 0.65 BET surface area m^2/g, surface resistivity 0.35 ohms per square. Silver Coated Nickel Flake, 15% Ag, 2.6 g/cc apparent density, particle size (FSSS) 15 microns, screen mesh 99% minus 200, surface resistivity 0.04 ohms per square.

Magnetic ferrites and surge arrestor applications also use our specialized range of nickel oxides. High Purity Black Nickel Oxide, 77.2% Ni, BET 75 (m^2/g) particle size (FSSS) 5.2 microns, minus 325 mesh 99% plus. Green Nickel Oxide, 78.5% Ni, BET 3 (m^2/g) particle size 1.6 microns, −325 mesh 100%.

Inco Specialty Powder Products is your unique source for custom fitting high performance powders into electronic applications. Our customer focused, worldwide marketing service group is ready to help you with your current and future needs.

For more information write INCO Specialty Powder Products, Dept. 1-90, Park 80 West-Plaza Two, Saddle Brook, NJ 07662

INCO SPP

Park 80 West-Plaza Two, Saddle Brook, NJ 07662
Shin-Muromachi Building, 4-3 Nihonbashi-Muromachi 2-Chome, Chuo-ku, Tokyo 103 Japan
1-3 Grosvenor Place, London SW1X7EA England
15/Fl Wilson House, 19-27 Wyndham Street Central, Hong Kong

Circle Reader Action No. 452

Lignin Sensor Based on Flash-Pyrolysis Mass Spectrometry

New instrument speedily evaluates lignin content of wood products.

NASA's Jet Propulsion Laboratory, Pasadena, California

The new lignin sensor takes only a few minutes to measure the lignin content of a specimen of wood, pulp, paper, or similar material. In contrast, the standard chemical method takes more than 30 minutes. The new sensor can be helpful in controlling digestors in paper mills to maintain the required lignin content, and also in bleaching plants, where good control of bleaching becomes possible if a quick determination of lignin content can be made.

The apparatus (see Figure 1) is based on rapid pyrolysis of a sample in a reducing atmosphere of hydrogen, followed by a determination of the mass spectra of the products evolved. An inert atmosphere of helium can also be used. The pyrolysis is followed by continuous dilution by hydrogen. This process produces a reproducible profile in time for all gaseous products. The ion currents are measured over an interval of time and integrated to define appropriate ratios of selected mass peaks or groups of peaks.

The specimen is placed in a platinum cup in the pyrolizer. A flow of nonoxidizing carrier gas (preferably hydrogen, though helium can be used) at a pressure of 2 psi (14 kPa) is set up in the pyrolysis chamber. When the air has been swept out, the cup is heated to a temperature of preferably 550 °C for 1.5 s by passing electric current through a stainless-steel ribbon on which the cup is mounted. The products pass through a capillary tube and enter the ion trap detector (mass spectrometer) for quantitative analysis.

An instantaneous sample spectrum of pine wood pulp of Kappa number 84.9 is shown in Figure 2 (a), where the mass spectral lines from the decomposition of cellulose occur at 127 and 145 daltons. Other peaks at 137, 157, 165, ect., are due to products from lignin. The integrated ion currents from peaks from 135 to 139 and all peaks from 148 to 188 are divided by the total ion current from all peaks from 120 to 250 to obtain a ratio called Q. This quantity is proportional to the lignin content of the test sample.

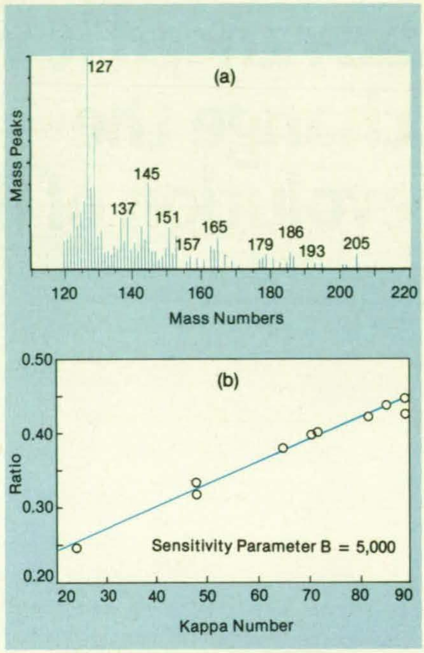

Figure 2. The **Sample Spectrum and a Plot** show the results obtained from the lignin sensor. Pine wood pulp of Kappa number 84.9 shows a spectrum in (a) with components characteristic of lignin at 137, 151, 163, and 179 at pyrolysis temperature of 562°C. A plot of Q ratio as a function of Kappa number shows a linear relationship in (b) for several air dried pulps.

In Figure 2 (b) a plot of Q versus Kappa number is shown. Data were obtained from samples of pulp from a mill for which Kappa numbers were measured by the standard chemical method. It is seen that Q is linearly related to the Kappa number or lignin content. Laboratory tests using samples of wood as well as many types of pulp showed that Q is linear over the whole range of Klason lignin from 0 to 0.3.

Dry samples of pulp have silvers of darkwood that, if included in the sample, produce higher variability than that seen in the chemical method, which uses much bigger samples. However, wet samples can be chosen sliver-free, and these yield Q ratios with variability comparable to that achieved in the standard chemical method.

This work was done by Eug Y. Kwack, Daniel D. Lawson, and Parthasarathy Shakkottai of Caltech for **NASA's Jet Propulsion Laboratory**. *For further information, Circle 124 on the TSP Request Card.*
NPO-17592

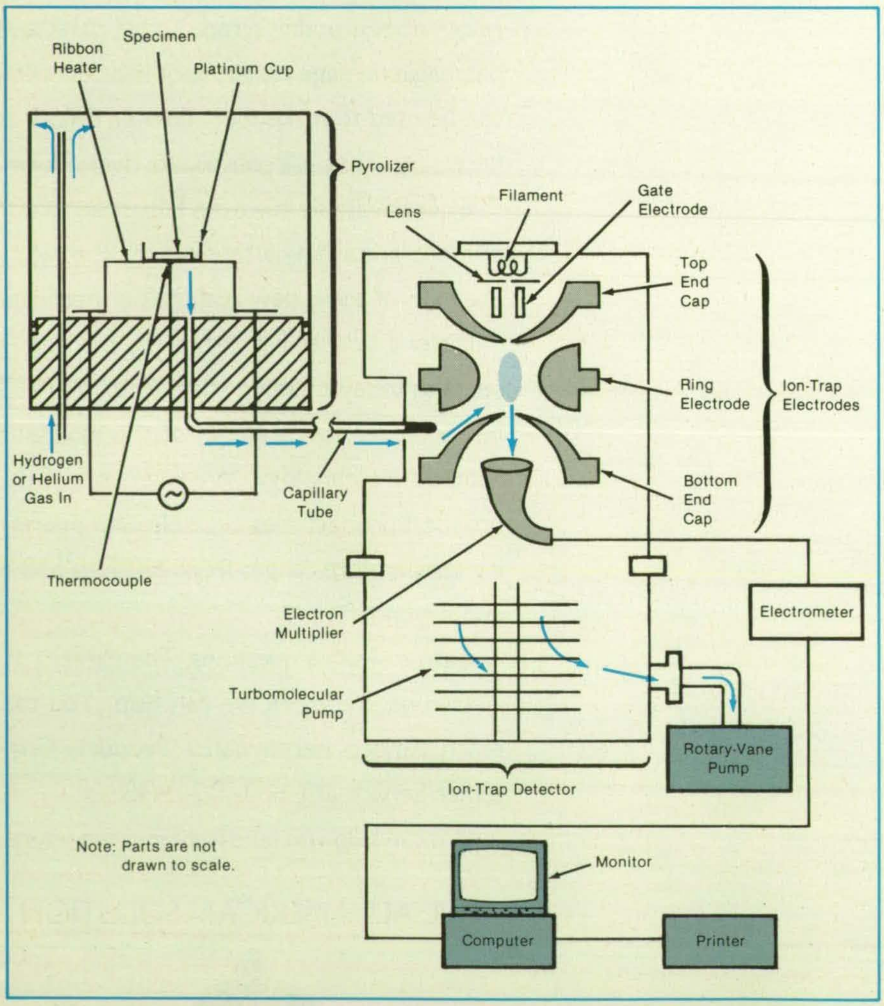

Figure 1. The **Lignin Sensor** includes a flash pyrolizer and an ion-trap detector that acts as a mass spectrometer. The apparatus measures the amount of molecular fragments of lignin in the pyrolysis products of samples.

Diagnosis of a Pressure-Modulator-Radiometer Cell

A lead-salt tunable diode laser provides the required monochromatic radiation.

NASA's Jet Propulsion Laboratory, Pasadena, California

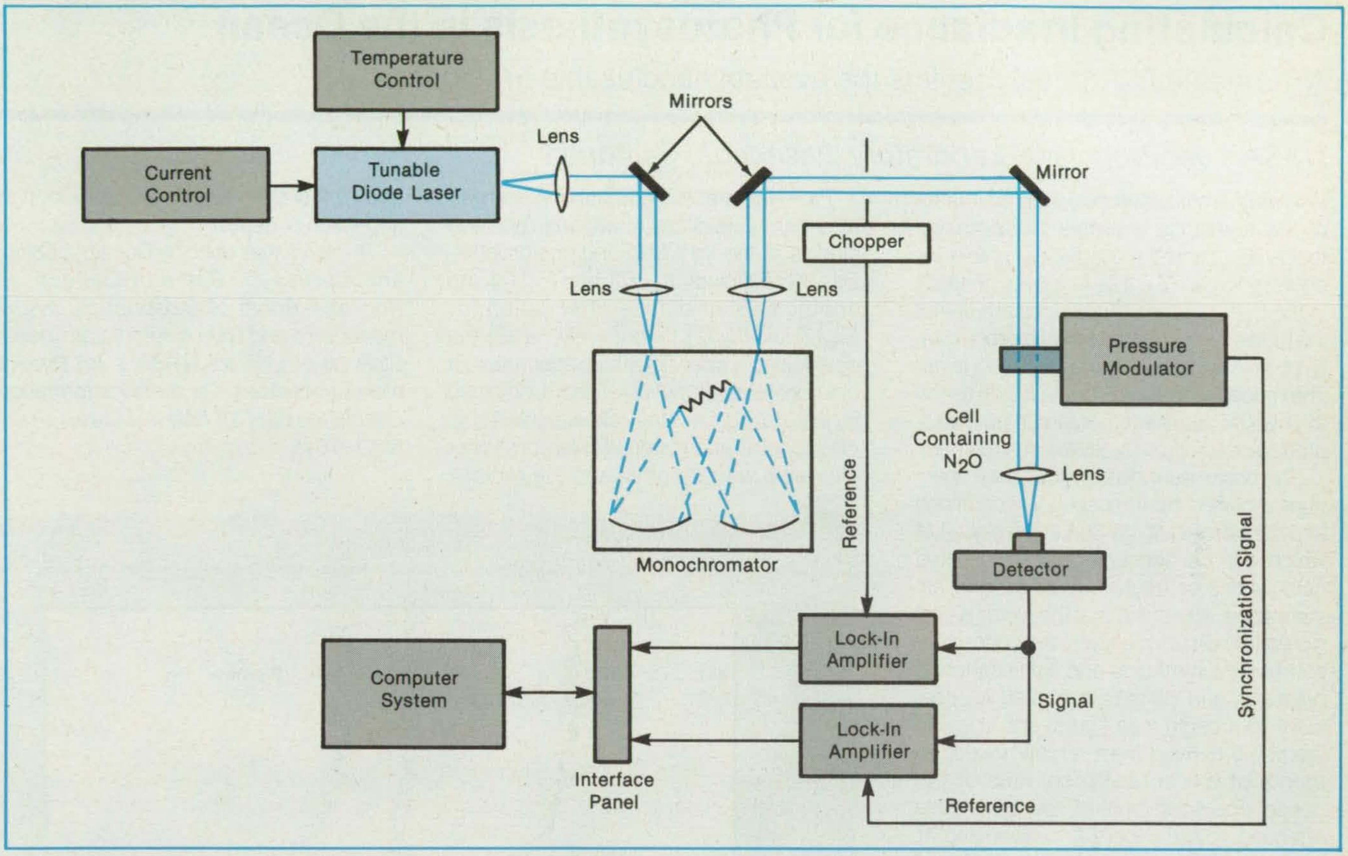

Figure 1. The **Lead-Salt Tunable Diode Laser** provides the monochromatic radiation needed to measure the spectral transmission function of the pressure-modulator-radiometer cell.

The spectral response of a pressure-modulator-radiometer cell has been measured with the help of a lead-salt tunable diode laser. Heretofore, the spectral responses of pressure-modulator-radiometers have been inferred from theoretical calculations and white-cell transmission measurements. However, direct measurement of the spectral response of such an instrument would enable the formulation of more-precise atmospheric-transmission functions, thereby enabling the extraction of better information from the readings taken with the instrument.

A lead-salt tunable diode laser was chosen because of the narrow bandwidths [2×10^{-4} (cm)$^{-1}$] and relatively high powers (up to 1 mW continuous) of such lasers and because they are available for wavelengths from 3 to 30 μm. The pressure-modulator-radiometer cell used in the experiment had a path length of 0.15 cm and a compression ratio of about 2. The cell contained N_2O, which was chosen because its spectrum has already been well characterized.

The apparatus is shown schematically in Figure 1. The diode laser was tuned to the P(15) spectral line of the ν_1 band of N_2O at 1,271.9668 (cm)$^{-1}$. After passing through a monochromator for selection of the mode, the laser beam was mechanically chopped at 385 Hz, directed along the axis of the modulator cell, and then focused onto a cooled HgCdTe detector. A lock-in amplifier locked to the chopper recorded the mean transmission of the cell, while a second lock-in amplifier locked to the modulator (frequency about 30 Hz) simultaneously recorded the modulated transmission function of the cell. A complete scan over the effective shape of the spectral line took approximately 5 min, and data were transferred to a computer system for processing and plotting. Measurements were taken at mean cell pressures of about 10, 20, and 30 torr (1.3, 2.6, and 3.9 kPa, respectively). At each mean pressure, line transmission profiles were recorded at two different pressure-modulator amplitudes.

Figure 2 shows records of the time-averaged and the modulated cell transmission spectra at a mean pressure of 30.5 torr (4.07 kPa). Under these conditions, the collision-broadened half width of the line

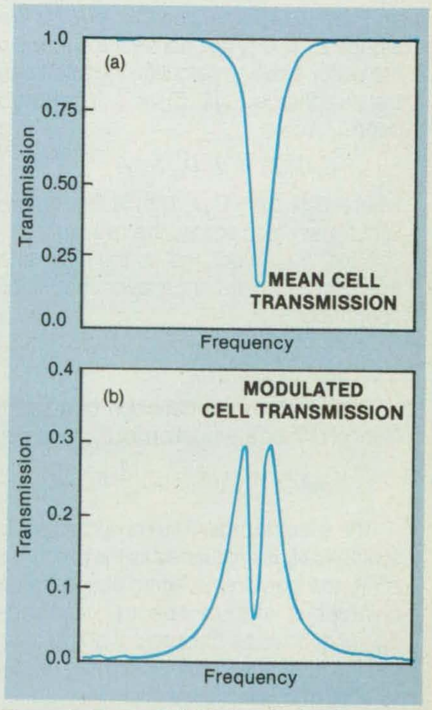

Figure 2. These **Cell Transmission Spectra** were obtained in the apparatus of Figure 1.

(110 MHz) is about three times the diode-laser spectral half width (38 MHz), which is comparable to the Doppler spectral half width (35 MHz). Traditionally, the mean transmission spectrum of a pressure-modulator radiometer is represented by the transmission due to an effective mean pressure, and the modulated transmission spectrum is represented by the difference in transmission between two effective pressure extremes. These models fit the recorded spectra within 2 percent at all points.

This work was done by Randy D. May, Daniel J. McCleese, David M. Rider, John T. Schofield, and Christopher Webster of Caltech for **NASA's Jet Propulsion Laboratory**. *For further information, Circle 99 on the TSP Request Card.*
NPO-17528

Calculating Irradiance for Photosynthesis in the Ocean

A mathematical model predicts the available and usable irradiances.

NASA's Jet Propulsion Laboratory, Pasadena, California

A mathematical model yields estimates of the irradiance available for photosynthesis (E_{par}) and the irradiance usable for photosynthesis (E_{pur}) as functions of depth in the ocean. These irradiances are useful in studies of the photosynthetic productivity of phytoplankton in the euphotic layer. The model describes E_{pur} and E_{par} in terms of spectral parameters that can be measured remotely (from satellites or airplanes).

The ocean is irradiated with a solar spectrum modified by atmospheric conditions and the position of the Sun in the sky, all of which can be accounted for by detailed calculations or treated by simplifying assumptions. Assuming that the water is well mixed in the surface layer, the concentration of light-absorbing and light-scattering pigments and detritus is treated as constant with depth (see figure) and equal to the value derived from remote measurements of the optical properties of the ocean. The coefficient of spectral diffuse attenuation, $K(\lambda)$ (where λ = wavelength), is calculated from previously-developed empirical models of the light-absorbing and light-scattering properties of the pigments and detritus. Then using the spectral irradiance $E_d(\lambda, 0^+)$ just above the surface of the water, one can calculate the total spectral irradiance $E_0(\lambda, Z)$ as a function of depth Z from

$$E_0(\lambda, Z) = E_0(\lambda, 0^-)e^{-K(\lambda)Z}$$

where $E_0(\lambda, 0^-)/E_d(\lambda, 0^+)$ is the ratio of light transmitted across the sea surface.

Next, E_{par} is defined as the integral of the spectral irradiance over the visible spectrum:

$$E_{par}(Z) = \int_{400\text{ nm}}^{700\text{ nm}} E_0(\lambda, Z)d\lambda$$

This leads to the definition of a coefficient of diffuse attenuation for E_{par}, namely

$$K_{par}(Z) = [1/E_{par}(Z)]\frac{d}{dZ}E_{par}(Z)$$

The spectral radiant flux absorbed photosynthetically is calculated as the product of $a°(\lambda)$, the spectral specific absorption of chlorophyll, and the spectral irradiance. E_{pur} is defined as the integral of this spectral flux over the visible spectrum, divided by $a°(\lambda)$ at a specific wavelength:

$$E_{pur}(Z) = \int_{400\text{ nm}}^{700\text{ nm}} [a°(\lambda)/a°(435\text{ nm})]E_0(\lambda, Z)d\lambda$$

From the preceding equations, one can also calculate other quantities useful in studies of the light field and photosynthesis. These include $K_{par}(Z)$, and $K_{pur}(Z)$, the coefficients of diffuse attenuation for $E_{par}(Z)$ and $E_{pur}(Z)$, respectively; $*a°(Z)$, the coefficient of specific diffuse absorption of chlorophyll as a function of depth, obtained by integrating the spectrally-weighted specific spectral absorption of chlorophyll over all visible wavelengths; and the radiant-energy flux absorbed by phytoplankton as a function of depth.

This work was done by Donald J. Collins and Curtiss O. Davis of Caltech, C. Rockwell Booth of Biospherical Instruments, Inc., and Dale A. Kiefer and Casson Stallings of USC for **NASA's Jet Propulsion Laboratory**. *For further information, Circle 2 on the TSP Request Card.*
NPO-17645

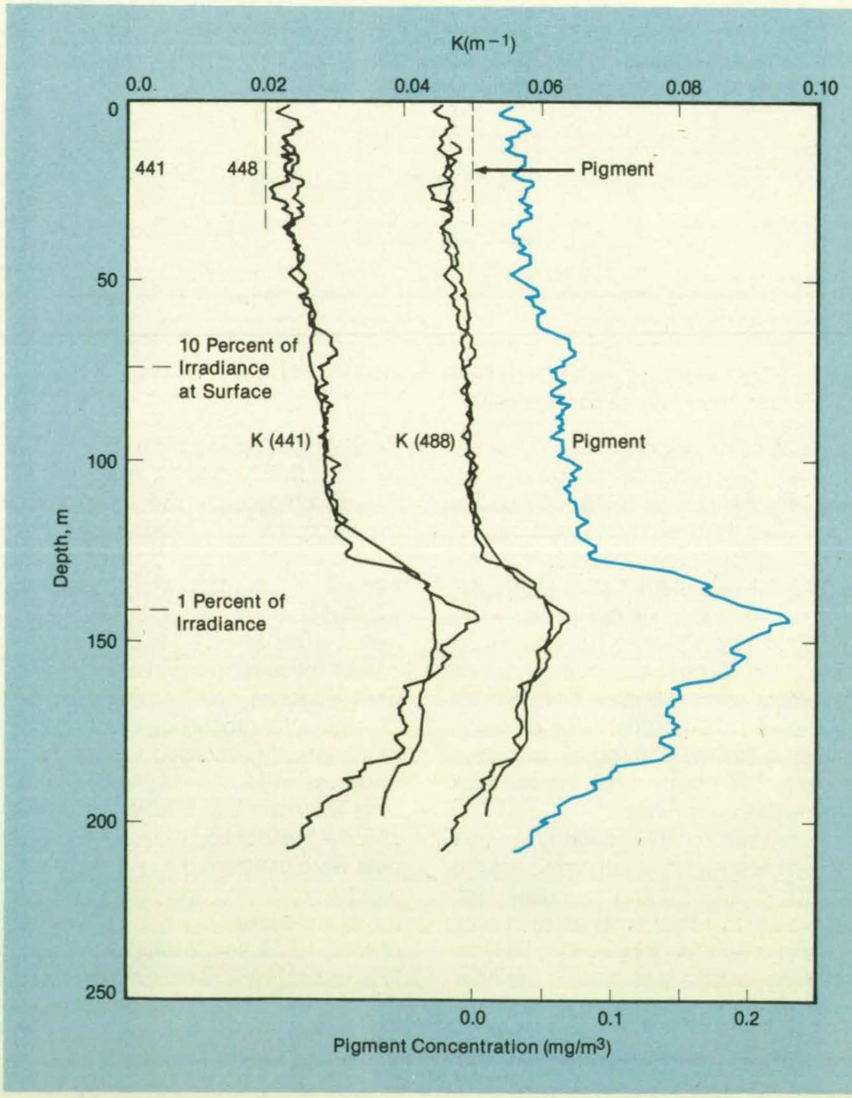

The **Concentration of Pigment** is assumed to be constant with depth for purposes of the model. As these measurements from the tropical Pacific Ocean show, the concentration varies somewhat, but the assumption can be invoked because most of the light is absorbed at depths above where the concentration begins to depart sharply from the nearly constant value of about 0.03 mg/m^3.

Books and Reports

These reports, studies, handbooks are available from NASA as Technical Support Packages (TSP's) when a Request Card number is cited; otherwise they are available from the National Technical Information Service.

Terrestrial-Imaging Spectroscopy

Progress to date is reviewed.

A report reviews the history and the state of the art of terrestrial imaging spectroscopy. This field encompasses the use of airborne and spaceborne imaging spectrometers to generate specialized maps for use in agriculture, geology, ecology, and related disciplines. The report discusses the history, design, and performance of the Airborne Imaging Spectrometer (AIS), which is the pioneering sensor for terrestrial high-resolution remote sensing. It concludes with a discussion of plans for the future of imaging spectroscopy of the Earth.

The main text begins by discussing the motivation for imaging spectroscopy. The spectrum of interest includes the visible and the near infrared. In laboratory and field spectrometers and spectroradiometers, the spectral intensities of one hundred or more wavelength bands each of which is 10 nm wide in each picture element yield sufficient information for the reconstruction of the reflectance spectrum, which is useful in the identification of minerals. Research on the use of spectral reflectance to identify types, constituents, and conditions of plants is also underway.

The next topic is the AIS, which was designed primarily as a test bed on which future spaceborne imaging spectrometers will be based. The development of the AIS took advantage of a new generation of arrays of HgCdTe infrared detectors on small chips, each of which contains more than 1,000 detector elements. In the AIS, each picture element is sensed simultaneously in as many spectral bands as there are detector elements in each line of a two-dimensional array. The array is swept across the scene to produce the multiple (as many as 200) spectral images simultaneously. The flight history, performance, and engineering problems revealed by the flight tests of the AIS are described.

The extraction of information from the spectral-image data is a major challenge. Visual inspection is useful in exploratory analysis. Visual inspection can be enhanced by advanced display techniques like time-sequenced projection of images in the spectral direction and cursor-designated spectral plots of single picture elements. The next problem is the multispectral classification of scenes by use of feature-extraction operators, which could involve linear or nonlinear transformations that reduce the dimensionalities of spectral images while preserving sufficient information for the identification of spectral signatures.

The report discusses recent developments described in the literature of imaging spectroscopy from three points of view: techniques for the handling and analysis of spectral-image data, geological research, and botanical research. The report concludes by restating the broad themes in the development of imaging spectroscopy, describing recent experience with the Airborne Visible/Infrared Imaging Spectrometer (a successor to the AIS), and describing the new Portable Instant Display and Analysis Spectrometer, which is a lightweight, rugged instrument designed to be carried in the field.

This work was done by Gregg A. Vane of Caltech and Alexander F. H. Goetz of the University of Colorado for **NASA's Jet Propulsion Laboratory**. *To obtain a copy of the report, "Terrestrial Imaging Spectroscopy," Circle 28 on the TSP Request Card.*
NPO-17432

Materials

Hardware, Techniques, and Processes

66 Lightweight, Thermally Conductive Composite Material
66 $YBa_2Cu_3O_x$ Superconductors Doped With AgO

Books and Reports

67 Tribological Properties of Ceramics

Lightweight, Thermally Conductive Composite Material

Aluminum reinforced with carbon fibers is superior to copper in some respects.

Lewis Research Center, Cleveland, Ohio

A lightweight composite material has high thermal conductivity. The material consists of an aluminum matrix containing graphite fibers, all oriented in the same direction. It is available as sheets, tubes, and bars. Its thermal conductivity is highest along the fibers. The conductivity across the fibers is about two-thirds that of the aluminum matrix.

At temperatures from −20 to +140 °C, the thermal conductivity of the material along the fibers is greater than that of copper (see figure). Per unit weight, the material is approximately 4 times as conductive as pure copper, twice as conductive as pure aluminum, and 2.6 times as conductive as 6061 structural aluminum alloy.

The graphite/aluminum composite will most likely be useful in a variety of heat-transfer applications in which the reduction of weight is critical. For example, it can be used to conduct heat in high-density, high-speed integrated-circuit packages for computers and in base plates for electronic equipment. It can also be used to carry heat away from the leading edges of wings in high-speed airplanes.

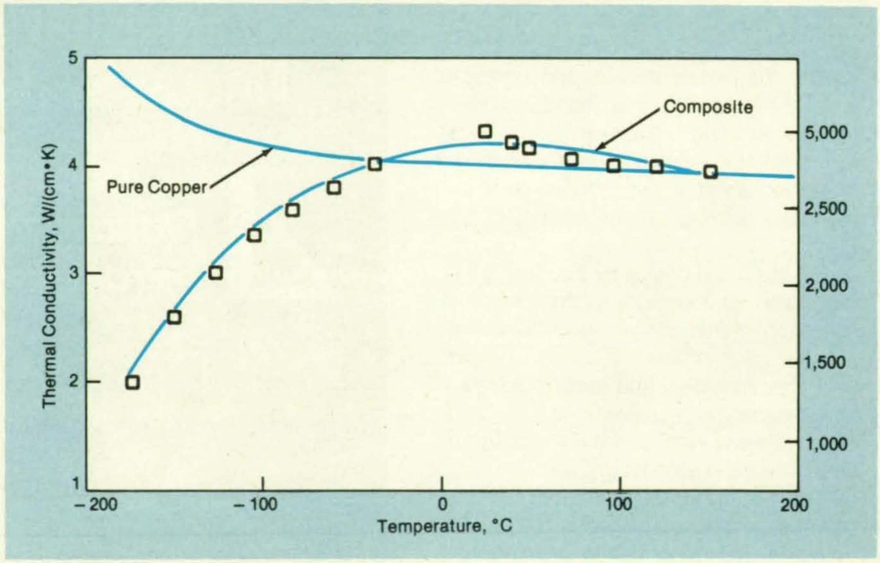

The **Thermal Conductivity of the Composite** along the fibers rises above that of pure copper over a substantial range of temperatures.

This work was done by G. Richard Sharp of **Lewis Research Center** *and Timothy A. Loftin of DWA Composite Specialties, Inc.*

For further information, Circle 98 on the TSP Request Card.
LEW-14814

$YBa_2Cu_3O_x$ Superconductors Doped With AgO

Magnetic properties are unlike those of any other superconductor.

Marshall Space Flight Center, Alabama

Improved superconductive materials have been made by doping the compressed powder destined to become $YBa_2Cu_3O_x$ superconductors with AgO prior to heat treatment. While the new materials have critical temperatures near those of other $YBa_2Cu_3O_x$ superconductors, they have magnetic properties unlike those of any previous high-temperature superconductors.

It had been hypothesized that during the heat treatment of the powder in oxygen to form the superconductor, the AgO would decompose. The oxygen thus freed would assist in preventing the grains of $YBa_2Cu_3O_x$ from becoming deficient in oxygen. The silver thus freed might coat the many intergrain surfaces and fill the intergrain voids, both of which make poor superconducting contacts that limit critical currents and degrade performance. As a result, the intergrain resistances in the normally conducting state should be less, and the critical current densities should be increased.

The properties of the new materials observed thus far support the hypothesis. A specimen was found to be suspendable below as well as above magnets, and the suspension proved to be stable as long as the material remains superconductive. These magnetic properties suggest the existence of very high currents that shield against magnetic fields as high as 20 T. Circuits of great length still show limited critical currents, but this is believed to be because of short portions that have low critical currents. If these "weak links" could be eliminated, long circuits that have high critical currents should be possible.

This work was done by Palmer N. Peters and Maw-Kuen Wu of **Marshall Space Flight Center**. *For further information, Circle 131 on the TSP Request Card.*

Inquiries concerning rights for the commercial use of this invention should be addressed to the Patent Counsel, Marshall Space Flight Center [see page 22]. Refer to MFS-26078

Books and Reports

These reports, studies, handbooks are available from NASA as Technical Support Packages (TSP's) when a Request Card number is cited; otherwise they are available from the National Technical Information Service.

Tribological Properties of Ceramics

Properties of materials for advanced engines and machine tools are examined.

A report reviews the adhesion, friction, and micromechanical properties of ceramics — properties that are becoming increasingly important as more ceramic materials are used in bearings, seals, and gears in advanced engines and in cutting tools and extrusion dies. The report considers the effects of contaminating surface films, temperature, and chemical interactions.

The report examines ceramics, in both monolithic and coating form, in contact with themselves, with other harder materials, and with metals. It first discusses the pulloff force (adhesion) and the shear force between surfaces in contact. It then proceeds to abrasion of ceramics.

Surface films are found to affect the tribological behavior of ceramics. For example, carbon adsorbed on a silicon carbide surface decreases interfacial bond strength and friction. Heating silicon carbide to high temperature can cause a thin layer of graphite to form on the surface, with a consequent reduction of adhesion and friction. In contrast, oxygen on metals in sliding contact with oxide ceramics increases both adhesion and friction.

In metal-to-ceramic contacts, the surface chemistry becomes extremely important. In transition metals, the higher the fraction of d-valence bonds, the lower the coefficient of friction.

Ceramics, like metals, deform elastically and plastically at surface points of contact under load. Unlike metals, ceramics can fracture when the contact stresses exceed critical values.

This work was done by Kazuhisha Miyoshi of **Lewis Research Center**. *Further information may be found in NASA TM-100782 [N88-17801], "Adhesion, Friction, and Micromechanical Properties of Ceramics."*

Copies may be purchased [prepayment required] from the National Technical Information Service, Springfield, Virginia 22161, Telephone No. (703) 487-4650. Rush orders may be placed for an extra fee by calling (800) 336-4700.
LEW-14833

Computer Programs

68 Analyzing Optical Communication Links
68 Predicting Noise From Wind Turbines
69 Algebraic Generation of Two-Dimensional Grids

COSMIC: Transferring NASA Software

COSMIC, NASA's Computer Software Management and Information Center, distributes software developed with NASA funding to industry, other government agencies and academia.

COSMIC's inventory is updated regularly; new programs are reported in *Tech Briefs*. For additional information on any of the programs described here, circle the appropriate TSP number.

If you don't find a program in this issue that meets your needs, call COSMIC directly for a free review of programs in your area of interest. You can also purchase the annual *COSMIC Software Catalog*, containing descriptions and ordering information for available software.

COSMIC is part of NASA's Technology Utilization Network

COSMIC® — *John A. Gibson, Director,*
(404) 542-3265
The University of Georgia, 382 East Broad Street, Athens, Georgia 30602

Computer Programs

These programs may be obtained at a very reasonable cost from COSMIC, a facility sponsored by NASA to make computer programs available to the public. For information on program price, size, and availability, circle the reference number on the TSP and COSMIC Request Card in this issue.

Electronic Systems

Analyzing Optical Communication Links

Link margins and design-control tables are generated from input parameters supplied by the user.

The Optical Communication Link Analysis Program, OPTI, analyzes optical and near-infrared communication links that use pulse-position modulation (PPM) and direct detection. The program prompts for inputs of parameters of components of a system, modulation format and other parameters of operation, sources of background noise, and the desired bit-error rate of the link. From these inputs, the link margin is determined, and a link design-control table (DCT) is generated. The program also enables the user to save sets of input parameters that define a given link and read them back into the program later. Further, the program can alter automatically any of the input parameters to achieve a desired link margin.

In computing the link margin, the program calculates the received optical signal power, background power, and required signal for the desired level of performance (error rate). Background sources are taken from a list of extended sources (e.g., planets, the Moon, and the Sun) and point sources (stars) contained within the program and from additional sources specified by the user. In the case of additional sources, the user must specify the irradiance (for point sources) or radiance and distance from the source to the receiver (for extended sources). Objects within the program are treated as blackbodies at an appropriate temperature with an overall magnitude scaled to match tabulated data.

The OPTI program is written in FORTRAN 77 and was designed to be used on the IBM PC and PC/AT personal computers. (Note: The 8087/80287 math-coprocessor option is highly recommended for use with this program.) The program will also compile under UNIX 4.3 BSD FORTRAN 77 with minor changes.

This program was written by William K. Marshall and Brian D. Burk of Caltech for **NASA's Jet Propulsion Laboratory**. *For further information, Circle 113 on the TSP Request Card.*
NPO-17444

Machinery

Predicting Noise From Wind Turbines

Effects of turbulence, trailing-edge wakes, and bluntness are taken into account.

The computer program WINDY predicts broadband noise spectra of horizontal-axis wind-turbine generators. This will enable adequate assessment of the impact of broadband wind-turbine noise. The program has practical application in the design and siting of wind-turbine machines that are acceptable to the community. Underlying noise-generating phenomena are discussed in the user's manual of the program.

WINDY predicts total noise based on such input sources as the inflow turbulence to the rotor, the interactions of the turbulent boundary layers on the surfaces of the turbine blades with the trailing edges

of those surfaces, and the wake due to a blunt trailing edge. The total broadband noise generated is the logarithmic sum of these contributions. The effects of the size of the machine, the power output, the bluntness of the trailing edge, and distance to the receiver are incorporated in the program.

The program is partly empirical and is based on acoustic measurements of airfoil models and large wind turbines. For the purposes of validation, predicted frequency spectra were compared with measured data from several machines, including MOD-OA, MOD2, WTS-4, and U.S. Windpower, Inc., machines. Good agreement was obtained between the measured and predicted far-field noise spectra.

The WINDY program is written in GW-Basic. It was designed to operate on IBM Personal Computers and compatibles and has been implemented under DOS 3.1. WINDY was developed in 1987.

This program was written by Ferdinand W. Grosveld of Planning Research Corp. for **Langley Research Center**. *For further information, Circle 133 on the TSP Request Card.*

LAR-13984

Mathematics and Information Sciences

Algebraic Generation of Two-Dimensional Grids

Hermite cubic interpolation is performed between fixed, nonintersecting boundaries.

The Two-Boundary Grid Generation (TBGG) computer program applies an interactive algebraic grid-generation technique in two dimensions. The program incorporates algebraic equations that relate a uniform rectangular computational domain to an arbitrary physical domain. TBGG can be applied to a variety of problems in which discrete techniques are used to solve such partial differential equations as the governing equations of fluid flow.

The underlying mathematical technique used in TBGG is Hermite cubic interpolation, which is applied between two fixed, nonintersecting boundaries. Two points and two inward derivatives define the shape of an Hermite cubic. The boundaries are specified by two ordered sets of points, which are parameterized with respect to arc length. The distributions of grid points along the boundaries that define the Hermite cubic functions are determined interactively by use of smoothing spline functions that relate grid points to arc lengths. Correspondingly, the inward derivatives are orthogonal projections of the tangential derivatives with respect to arc lengths along the boundaries.

The distribution of grid points along the Hermite cubic functions that connect the two boundaries is determined interactively with spline functions in a manner similar to that of the distribution of points along the boundaries. Also, the magnitudes of the derivatives are controlled interactively. Left and right boundaries can also be specified and blended with the Hermite cubic functions. The effect of the side-boundary blending, away from the boundaries, is interactively controlled.

The TBGG program is written in FORTRAN 77. It works in an interactive environment in which computational displays and the user's responses are exchanged quickly. The program has been implemented on a CDC CYBER 170-series computer using the NOS 2.4 operating system, with a central-memory requirement of 151,700 (octal) 60-bit words. TBGG requires a Tektronix 4015 terminal and DI-3000 Graphics Library of Precision Visuals, Inc. TBGG was developed in 1986.

This program was written by Robert E. Smith of **Langley Research Center** *and Michael R. Wiese of Computer Sciences Corp. For further information, Circle 130 on the TSP Request Card.*

LAR-13800

Mechanics

Hardware, Techniques, and Processes

70 Jig for Stereoscopic Photography
70 Static Pressure-Assisted Seal for Helium
72 Liquid-Flow Controller Responds to Pressure
73 Liquid-Flow Controller With Preset Break Pressure
74 Liquid-Flow Controller With Trickle Preflow
74 Fourier Analysis of Vibrations of Round Structures
76 Detecting Boundary-Layer Transition in Cold Environments
76 Electrolysis Bubbles Make Waterflow Visible
78 Adaptive-Control Experiments on a Large Flexible Structure

Books and Reports

80 Vibrational Responses of Structures to Impulses
81 Rolling-Contact Spalling in Bearings
82 Insulation for Cryogenic-Liquid Tanks
83 Perspectives on Dilution Jet Mixing
84 Numerical Analysis of Flows with FIDAP
84 Combining Thermal and Structural Analyses

Jig for Stereoscopic Photography

Separations between views can be adjusted precisely for best effects.

Lyndon B. Johnson Space Center, Houston, Texas

A simple jig can be adjusted to set precisely the distance between the right and left positions of a camera used to make stereoscopic photographs. The jig was devised for a training program that uses stereoscopic views of soldered assemblies to teach standard soldering techniques. In view of the trend toward very-large-scale integration of electronic circuits, the training method and the jig used to make training photographs may be useful to many companies to reduce the cost of training manufacturing personnel.

The camera is preferably a 35-mm single-lens-reflex unit equipped with a closeup lens suitable for the workbench distances in question. It slides laterally in the jig (see figure) between stops. The left (from the point of view of the camera) stop is a fixed pin. The position of the right (from the point of view of the camera) stop can be adjusted by a micrometer.

Experiments can be carried out to determine the optimum distance from the object to the camera as a function of the distance between the right and left camera positions. Ideally, the relationship between these distances should cause the stereoscopic images to overlap about 60 percent, and the distance between the right and left positions should be such as to give a view equivalent to that of a human observer, for whom the interpupillary distance is about 70 mm.

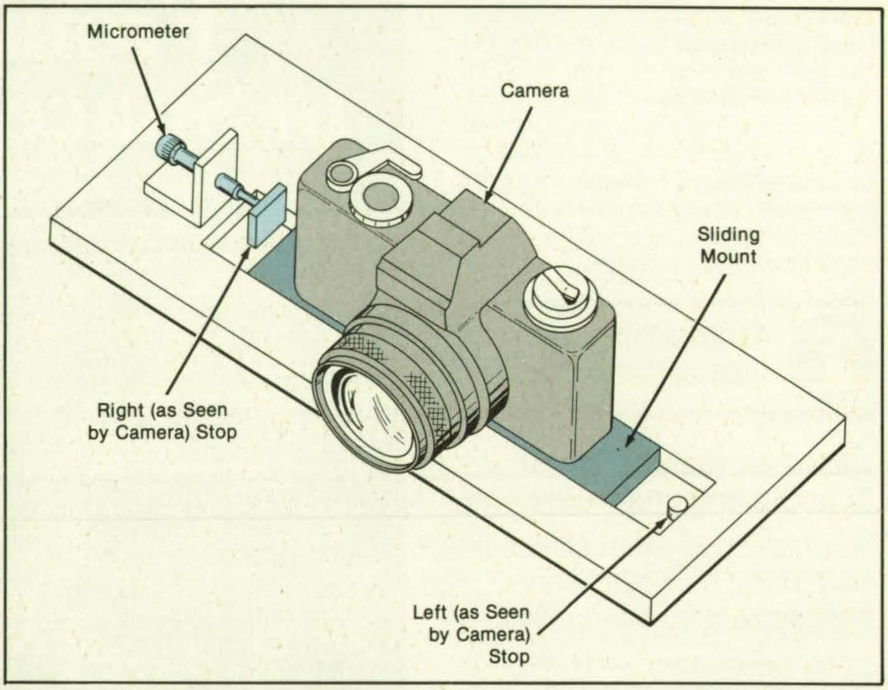

The **Camera Slides in the Slot** between extreme positions, where it takes stereoscopic pictures. The distance between the extreme positions can be set reproducibly with the micrometer.

This work was done by David J. Nielsen of Rockwell International Corp. for **Johnson Space Center**. *No further documentation is available.* MSC-21397

Static Pressure-Assisted Seal for Helium

A metal seal replaces a leaky elastomeric seal.

Marshall Space Flight Center, Alabama

The two-piece, all-metal, pressure-assisted static flange seal shown in the figure holds in pressurized helium satisfactorily at a temperature of −80 °F (−62 °C). The all-metal seal replaces a metal plate with elastomeric inserts on each side (also shown in the figure), which leaked excessively when the operating temperature was reduced from −30 °F (−34 °C) to the new lower temperature.

The new seal is designed to be interchangeable with the old seal and to seal against existing flange surfaces while maintaining the structural integrity of the joint. Thus, the metal plate in the new seal has the same thickness as that of the metal plate in the old seal and has the same bolt-hole configuration.

The new seal is certified for use in flight on the helium joints of the Space Shuttle main engine. Likely terrestrial applications may include laboratory and industrial gas-distribution systems.

This work was done by Donald E. Stuck and Takateru Okabayashi of Rockwell International Corp. for **Marshall Space Flight Center**. *No further documentation is available.*
MFS-29429

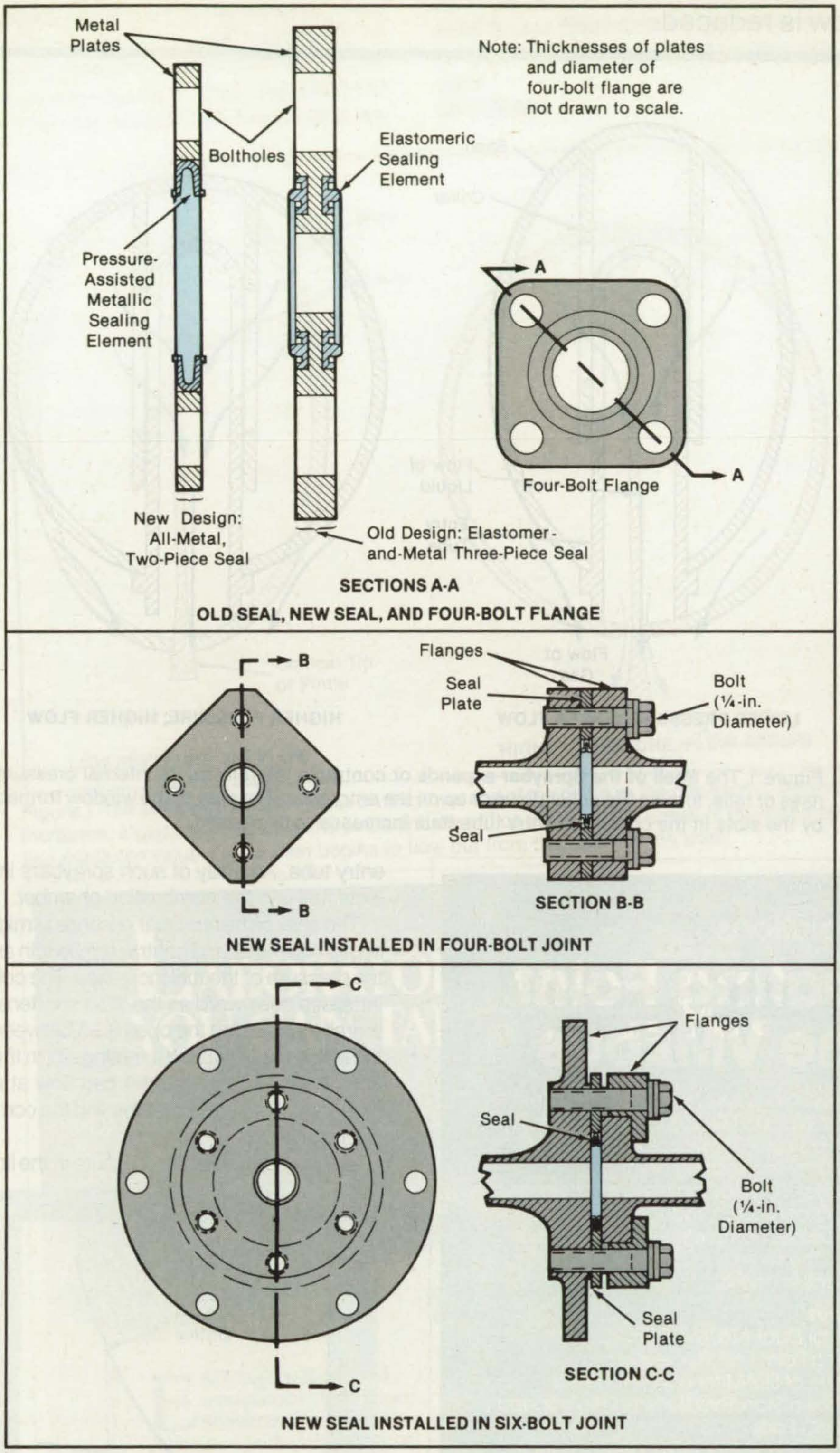

The **Static Seal** is installed between two flanges, which are then bolted together. The old version included two elastomeric sealing elements. The new version includes one pressure-assisted metal sealing element held in place by the metal plate and flanges.

A FREE BROCHURE describes new books, posters, and videotapes available from NASA Tech Briefs. Circle Reader Action Number 700 for your free copy.

Liquid-Flow Controller Responds to Pressure

The variation of pressure with flow is reduced.

Marshall Space Flight Center, Alabama

A mechanism that controls the flow of a liquid in a fuel-spraying head in a combustion chamber responds nonlinearly to the pressure of the liquid. At low pressure, it provides fine control of the spray. As the flow and pressure increase, it provides a larger increase in flow in response to a smaller increase in pressure, thereby keeping the maximum required pressure modest.

The mechanism is part of the fuel-injection system of a rocket engine. It admits liquid fuel into the combustion chamber so that the fuel enters along the flow of gaseous oxidizer. The principle of operation should be applicable to spraying heads for other fluids.

The liquid, fed by a pump, enters a spraybar mounted in a slot in a faceplate. The spraybar includes a flexible shell that forms a cavity around a row of cylindrical collars like the one shown in Figure 1. Each collar slides on an entry tube. The liquid flows into the cavity and through a slot in the collar into the entry tube. It blends with a peripheral flow of oxidizer as it leaves the entry tube. An array of such spraybars injects fuel into the combustion chamber.

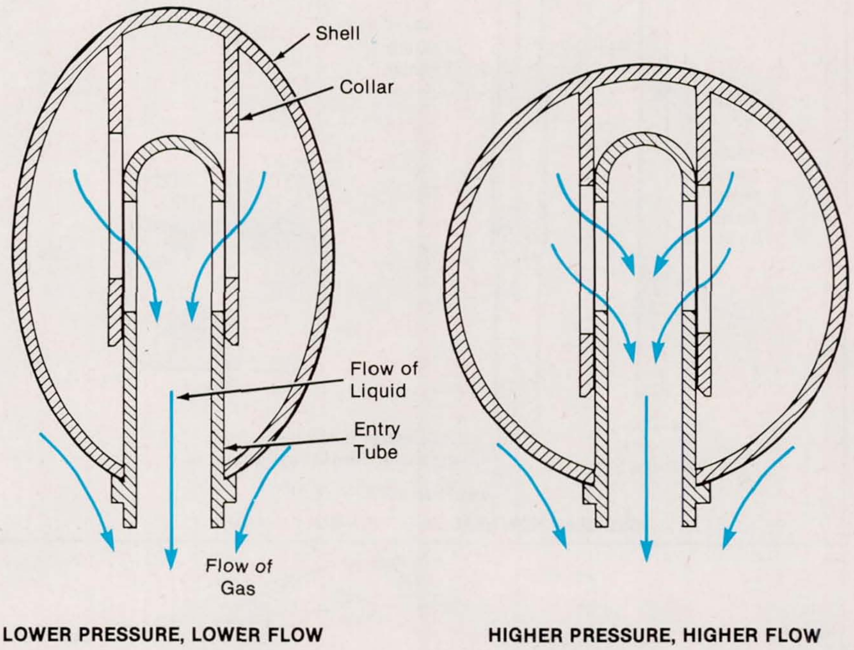

Figure 1. The **Shell of the Spraybar** expands or contracts laterally as its internal pressure rises or falls, forcing the collar down or up on the entry tube. The area of the window formed by the slots in the collar and entry tube thus increases or decreases.

The shell of the spraybar expands in midsection diameter and contracts in length as the pressure of the fuel increases. The collar slides downward as the shell shortens, thereby increasing the open area between the slot in the collar and a mating slot in the entry tube. Thus, propellant can flow at a higher rate into the entry tube and the combustion chamber.

Conversely, when the pressure in the liq-

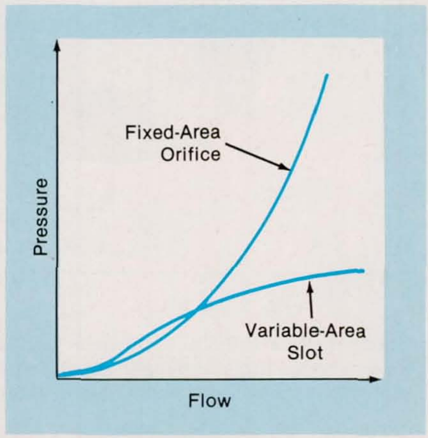

Figure 2. The **Drop in Pressure Through a Variable-Area Orifice** increases much more with flow through the orifice than does the corresponding drop in pressure with flow through a fixed-area orifice. In practical terms, a lower pump pressure is needed with the variable orifice for a given flow of liquid.

mately linearly with pressure. When this mechanism is used to spray fuel in a rocket engine and possibly in other types of combustion chambers, the preset minimum pressure for the initiation of flow prevents "chugging" — unstable combustion at low flow rates. It also allows the spraybar to be prefilled so that the spraying and combustion can be started rapidly. The approximately linear rise of flow with pressure (in contrast with the steeper increase with a fixed-area orifice) reduces the maximum pressure required of the pump at high flow.

This work was done by George B. Cox, Jr., of United Technologies Corp. for **Marshall Space Flight Center**. *For further information, Circle 39 on the TSP Request Card.*

Inquiries concerning rights for the commercial use of this invention should be addressed to the Patent Counsel, Marshall Space Flight Center [see page 22]. Refer to MFS-28330

Liquid-Flow Controller With Trickle Preflow

Pressure increases steeply with flow up to a point, beyond which pressure increases gradually.

Marshall Space Flight Center, Alabama

A liquid-flow controller allows the pressure in the liquid to increase steeply with flow as the flow starts, then provides a more-gradual nearly linear rise of pressure with flow as the flow and pressure increase beyond a preset breakpoint. The controller is an alternative version of the mechanism described in the two preceding articles, "Liquid-Flow Controller Responds to Pressure" (MFS-28329) and "Liquid-Flow Controller With Preset Break Pressure" (MFS-28330).

Like the second version, this version includes a pintle as the metering element in the orifice of a shell. Now, however, the conical tip of the pintle is not solid but contains two cutout sections (see Figure 1).

With no or low pressure in the shell, the orifice rests against the conical surface on the tip of the pintle. As liquid is pumped into the shell, a small amount that can flow trickles out through the cutouts. As the shell becomes full and the pressure inside it increases, the midsection of the shell expands. As pressure increases beyond the breakpoint, the orifice rises away from the cone. The orifice opens wider as the pressure continues to increase, and the flow through the orifice increases accordingly (see Figure 2).

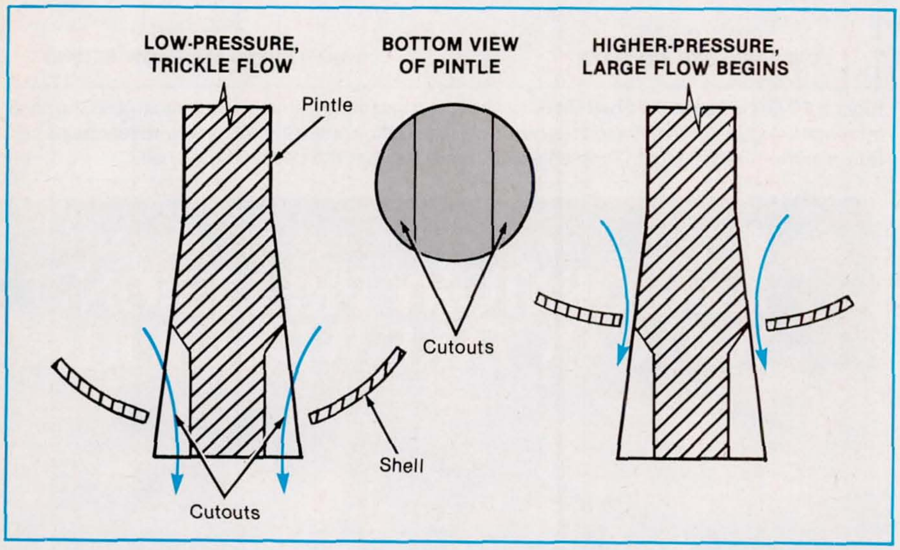

Figure 1. **Material Is Cut Out of the Cone** at the tip of the pintle. Liquid can thus always pass from the shell, albeit at a low rate. When the pressure in the shell is great enough to force the orifice away from the pintle, the liquid flows at a greater rate.

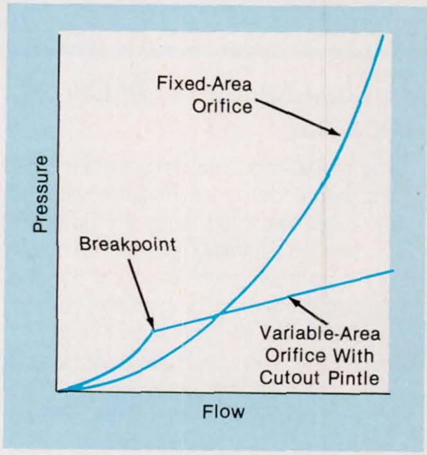

Figure 2. The **Pressure Increases Steeply** with the flow up to the breakpoint, beyond which the increase is more gradual and approximately linear.

This work was done by George B. Cox, Jr., of United Technologies Corp. for **Marshall Space Flight Center**. *For further information, Circle 31 on the TSP Request Card.*
MFS-28331

Fourier Analysis of Vibrations of Round Structures

Complicated vibrations of complicated structures are represented efficiently.

Marshall Space Flight Center, Alabama

A Fourier-series representation has been developed for the analysis of vibrations in complicated, round structures like turbopump impellers. The new Fourier method eliminates the guesswork involved in the characterization of the shapes of vibrational modes. It is an easy way to characterize complicated modes, leading to a determination of the responsiveness of a given mode to various forcing functions.

The shapes of vibrational modes cannot be characterized by viewing geometrical plots of a deformed structure. Previously, it was necessary to conduct an expensive and time-consuming response analysis to determine whether a given vibrational mode could be excited by a given forcing function. Furthermore, there was a tendency to dismiss higher-order modes as being impossible to excite and not to analyze modes that were not characterized as classical diametral modes like those of a flat, circular plate. However, experience teaches that all modes should be regarded as possible (see figure). The new Fourier method facilitates a thorough evaluation of all the modes of a structure.

The new Fourier-series method is used in conjunction with a finite-element numerical simulation of the vibrational modes of a

uid decreases, the shell narrows at its midsection and increases in length. The collar rises on the entry tube and decreases the open area of the slots. Propellant then flows at a lower rate.

If the area of the open slot were constant, the pressure would increase steeply with the flow. The pump would therefore have to generate an increasingly higher pressure for a diminishing increase in flow. With the variable-area slot opening, the required pressure tends to level off at higher flows (see Figure 2). Thus, the pump can provide the required high flow of fuel at reasonable pressure.

This work was done by George B. Cox, Jr., of United Technologies Corp. for **Marshall Space Flight Center**. *For further information, Circle 32 on the TSP Request Card.*

MFS-28329

Liquid-Flow Controller With Preset Break Pressure

Flow starts only after a minimum pressure is exceeded.

Marshall Space Flight Center, Alabama

A spraybar mechanism delivers a liquid at a rate that increases gradually with the pressure of the liquid, once the pressure has exceeded a minimum value. The mechanism is an alternative version of the one described in the preceding article, "Liquid-Flow Controller Responds to Pressure" (MFS-28329). The mechanism includes a flexible shell surrounding a pintle. The enlarged conical tip of the pintle extends through an orifice at the bottom of the shell (see Figure 1).

A pump supplies liquid to the interior of the shell. With no or low pressure in the shell, the tip of the pintle blocks the orifice completely, and no liquid flows from the shell. As the pump increases the pressure, the midsection of the shell starts to expand. The pintle still seals the orifice, however, until the orifice begins to rise on the tip of the pintle toward the narrow end of the cone. At this point, liquid begins to flow from the shell. As the pressure increases further, the orifice opens wider and flow increases.

Thus, no liquid flows until the pressure reaches a predetermined level (see Figure 2). Thereafter, the flow increases approxi-

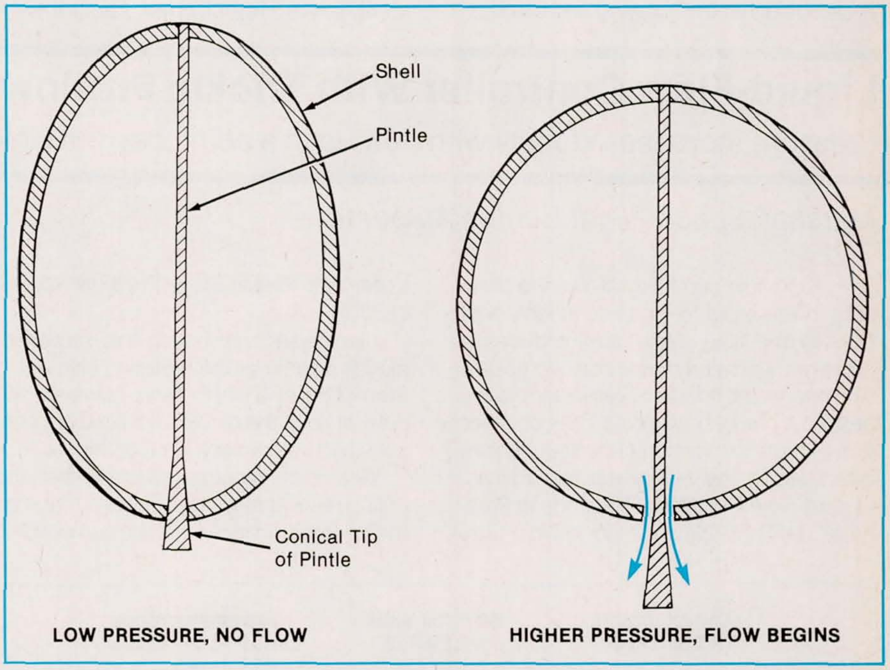

Figure 1. The **Orifice in the Shell Rises** on the lower end of the pintle as the pressure in the shell increases. A gap forms between the pintle and the orifice only after the pressure reaches a certain minimum value. Liquid then begins to flow out from the cavity in the shell.

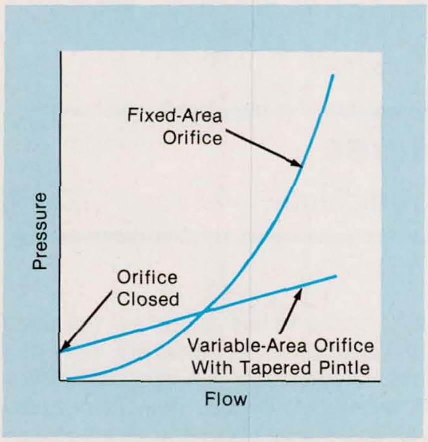

Figure 2. Once the **Minimum Pressure for Flow** is reached, the pressure increases gradually with increasing flow. This contrasts with the behavior of the fluid in a fixed-area orifice, wherein the pressure increases steeply with flow.

Circle Reader Action No. 625

structure. In the case of a turbopump impeller, internal passageways, blades, vanes, and other nonuniformities make it impossible to describe a typical high-order or otherwise complicated mode as a classical diametral mode. Consequently, such a mode is represented as a Fourier sum of classical diametral modes and determined to have some of the properties of each of these component modes. The essence of the method is first to calculate the Fourier coefficients of the displacements of the rim in the mode in question, then to use the relative magnitudes of these coefficients to determine the shape of the mode.

Although the Fourier-series method is trivial for lower-order modes, it becomes indispensable for the examination of the higher-order modes of structures like impellers. In practice, each such mode has many nonzero Fourier coefficients. With knowledge of the relative magnitudes of these coefficients, one can determine what operating speeds are likely to cause excessive vibrations.

This work was done by Gary A. Davis of Rockwell International Corp. for **Marshall Space Flight Center**. *For further information, Circle 117 on the TSP Request Card.* *MFS-29334*

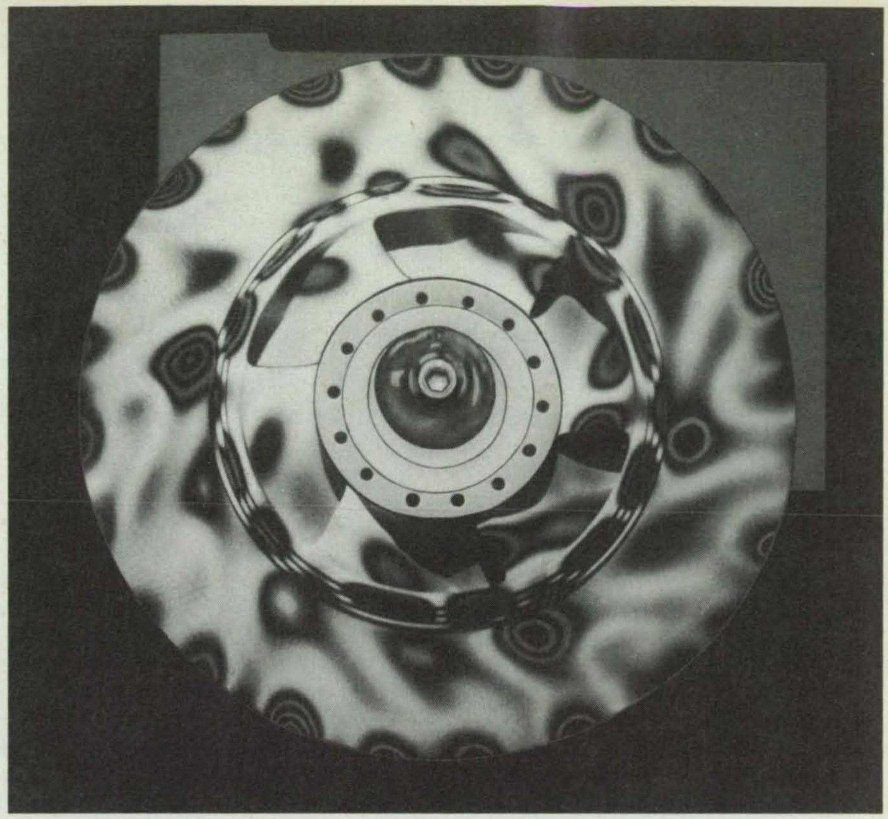

This **Turbopump Impeller** is shown here by holographic interferometry to be vibrating in a flap mode, in which each of the 24 sections of the shroud between the blades of the impeller vibrates independently of the other sections. Such a mode cannot be represented as a single classical diametral mode.

Detecting Boundary-Layer Transition in Cold Environments

Definitive transition Reynolds numbers are obtained for the first time in a cryogenic wind tunnel.

Langley Research Center, Hampton, Virginia

The determination of the location of boundary-layer transition has been a highly desirable adjunct to aerodynamic testing in conventional, ambient-temperature subsonic and transonic wind tunnels. Hot films are reliable and efficient devices for the determination of both the beginning and end of boundary-layer transition in test programs. A transition-detection study was conducted in the Langley 0.3-Meter Transonic Cryogenic Tunnel, using a specialized hot-film system designed specifically for use in cryogenic wind tunnels. The quantitative transition-location data obtained at nearly cryogenic conditions, 360 °R (200 K) represents the first definitive transition Reynolds numbers obtained in a cryogenic wind tunnel. The model was tested at both adiabatic and nonadiabatic wall conditions with a wall-to-wall temperature ratio as low as 0.47.

The vapor-deposited surface hot films and leads and the dielectric substrate were installed on a 12-percent-thick, advanced-technology supercritical airfoil model made of beryllium/copper. Before the hot films and gold connectors could be applied to the surface of the model, a method for carrying the electrical signal from the hot film via the surface gold leads, through the model, and out to the anemometer cables in the plenum of the test section had to be devised. For this purpose, slots were cut in the upper and lower surfaces of the airfoil, and the connecting wires were bonded to the airfoil.

The figure is a block diagram of the multichannel hot-film data-acquisition system. The basic components of the system are the constant-temperature anemometers (CTA's) which provide current to heat the films, a computer, a switching network, a digital multimeter (DMM), a scanner, amplifiers, oscilloscopes, and a frequency-modulation (FM) tape recorder. A desktop computer controls the instrumentation and acquires, stores, and reduces the data. The switching network, under computer control, switches the hot films sequentially into the DMM for resistance measurements. The switches, when disabled, restore the hot films to their respective CTA's. When the CTA's are made operational, the output voltages are scanned and sampled with the scanner and DMM for on-line reduction of data. The output voltages are also viewed on oscilloscopes and recorded on FM tape for further processing and analysis.

Results indicate that the concept for the installation of the specialized hot films and hot-film data-acquisition system will enable on-line determination of boundary-layer transition in such cryogenic wind tunnels as the National Transonic Facility.

This work was done by C. B. Johnson, D. L. Carraway, and P. C. Stainback of **Langley Research Center** *and M. F. Fancher of Douglas Aircraft Co. For further information, Circle 35 on the TSP Request Card. LAR-13830*

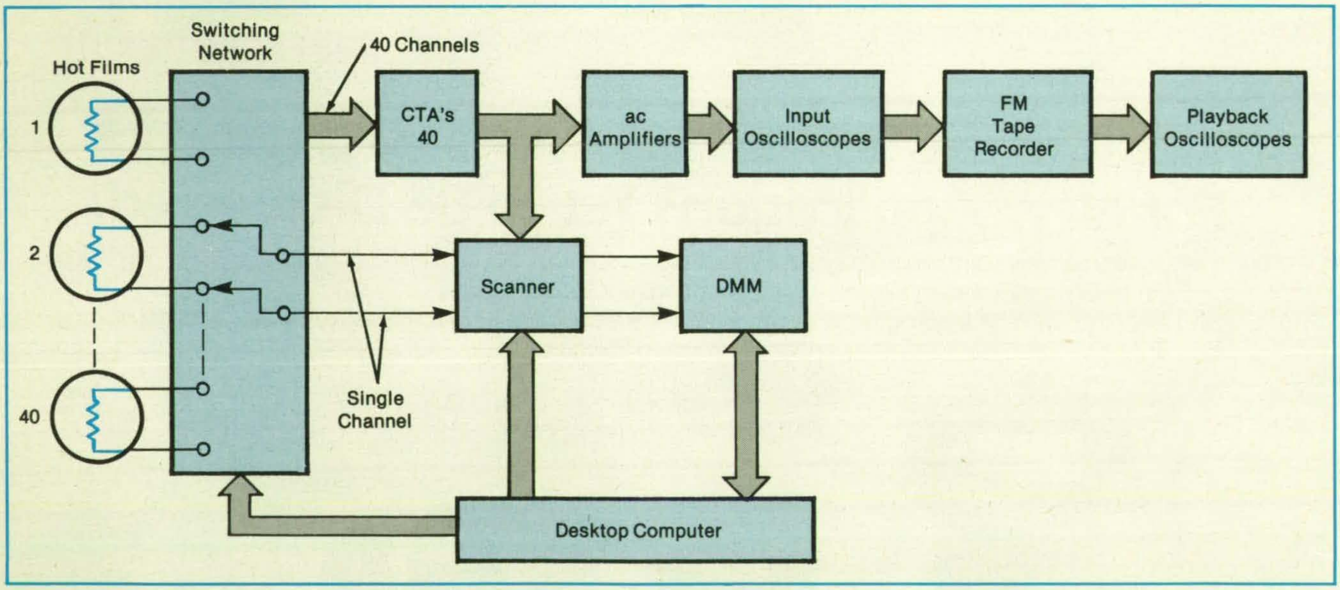

The **Multichannel Data-Acquisition System** processes data from 40 hot-film sensors by use of a desktop computer.

Electrolysis Bubbles Make Waterflow Visible

Traces in photographs are measured to obtain velocities.

Lewis Research Center, Cleveland, Ohio

A technique for the visualization of three-dimensional flow uses tiny tracer bubbles of hydrogen and oxygen made by the electrolysis of water. Strobe-light photography is used to capture the flow patterns, yielding a permanent record that can be measured to obtain the velocities of particles. This technique was used to measure the simulated mixing turbulence in a proposed gas-turbine combustor and could be used in other water-table flow tests.

Figure 1 shows a schematic diagram of the test apparatus, which consisted of an acrylic plastic model of the combustor, a water-electrolysis system, a water-circulation system, and a strobe-lamp-and-camera system. The model was oriented verti-

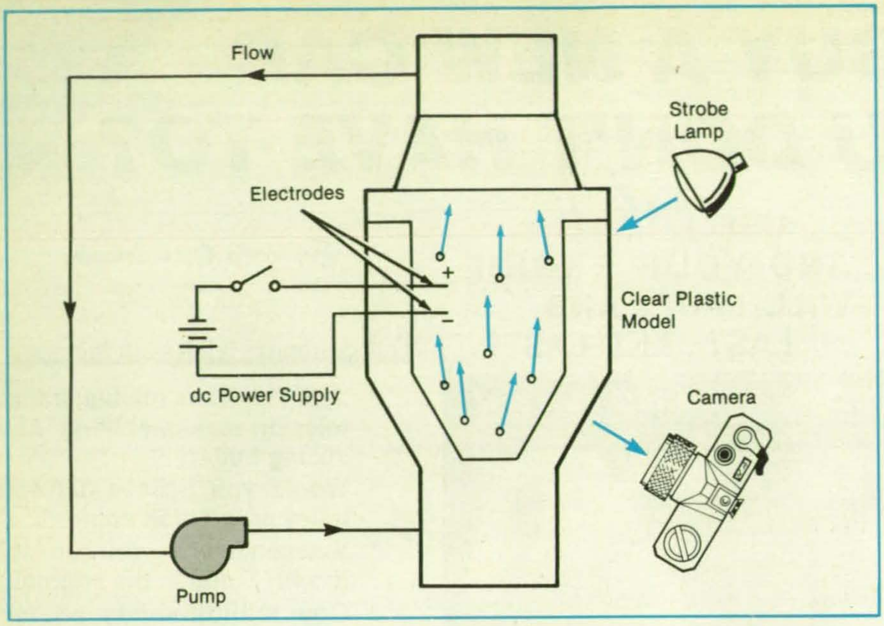

Figure 1. **Bubbles of Hydrogen and Oxygen** are created by electrolysis. Entrained in the flow, they leave traces in photographs that can be measured to determine flow velocities.

cally. The water was made to flow upward in the measurement region to minimize the second-order effect of the buoyancy of the gas bubbles and the tendency of the gas bubbles to stick to the walls of the model.

The electrical conductivity of the water was increased by adding ammonium nitrate to make a 1.0 normal solution. A wetting agent was added to suppress the formation of bubbles on the walls. This solution was then periodically buffered with nitric acid to keep the solution optically clear. (It was speculated that carbon dioxide from contact with air dissolved in the city water creating the observed clouding of the solution through the formation of calcium carbonate.) It was found that a relatively conductive solution enabled the use of single electrodes at most points, provided that in each case the matching electrode was not more than a centimeter or two away.

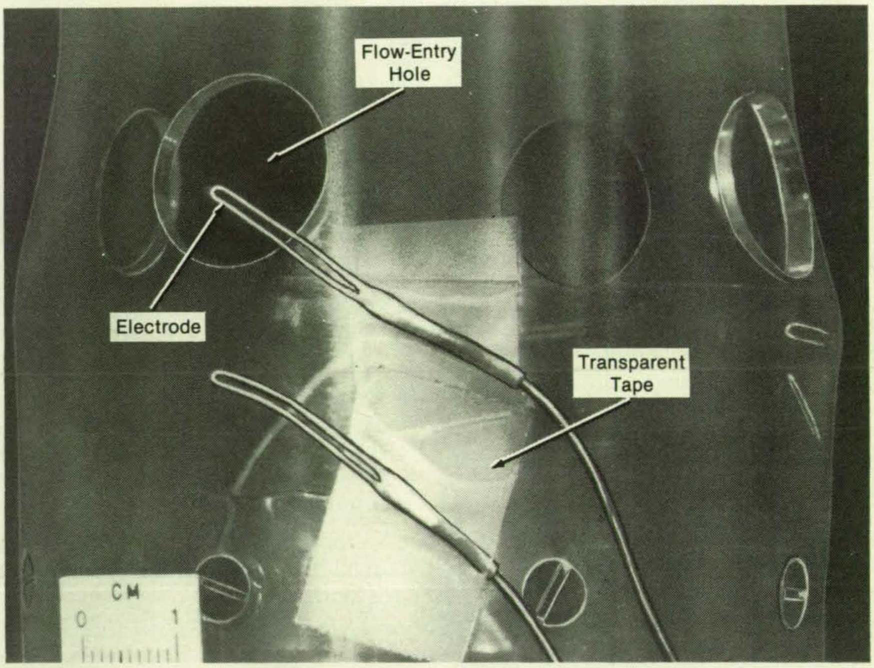

Figure 2. **Electrodes Are Mounted on the Model** to generate bubbles in the flow.

The electrodes, consisting of straight or looped 4.0-cm lengths of 0.13-mm stainless-steel wire, were secured to the model with transparent tape at appropriate flow-entry points as indicated in Figure 2. A 0- to 18-Vdc power source was utilized. The rate of formation of bubbles was varied by varying the electrode voltage. Usually, the higher voltages and bubble-formation rates were used with higher waterflow rates. Switching made it possible to energize various groups of electrodes.

The strobe lamp provided the illumination for the photography, which was done with a conventional 35-mm camera with high-speed film. Measurements of the bubble traces were then coordinated with the waterflow-rate data to obtain final turbulence data.

This work was done by Donald F. Schultz of **Lewis Research Center**. *No further documentation is available.*
LEW-14797

Adaptive-Control Experiments on a Large Flexible Structure

Transient and initial deflections are regulated via sensors, actuators, and a digital control system.

NASA's Jet Propulsion Laboratory, Pasadena, California

An antennalike flexible structure (see Figure 1) has been built for research in advanced technology including the suppression of vibrations and the control of initial deflections. The structure is instrumented with sensors and actuators connected to a digital electronic control system, which is programmed with the control algorithms to be tested. Particular attention in this research is focused on the direct model-reference adaptive-control algorithm based on the command generator tracker theory.

The structure was built to exhibit multiple vibrational modes, low modal frequencies, and low structural damping. The structure was made three-dimensional so that complicated interactions among the components of the structure and the control system could be investigated. The objective of the research is to test the performance of the algorithm and the closed-loop control system under gross uncertainties in the mathematical model of the dynamics of the structure and the environment, including effects that change with time, delays, nonlinearities, and reconfigurations of the system.

The main component of the apparatus consists of 12 ribs attached to a central hub, forming a weblike object 18.5 ft (5.6 m) in diameter. Two rings of pretensioned wires provide coupling of motion in the circumferential direction. Each rib, being

quite flexible and unable to support its own weight without excessive droop, is supported at two locations along its free length by levitators based on pulleys and counterweights. The hub is mounted on a gimbal platform, so that it is free to rotate about two perpendicular axes in the horizontal plane. A flexible boom is attached to the hub and hangs below it, and a feed mass, simulating the feed of an antenna, is attached at the free end of the boom.

Each rib can be individually excited or controlled by a rib-root actuator (see Figure 2). Two hub actuators torque the hub about its two gimbal axes. The hub torquers do not provide torque directly but rather are linear force actuators that provide torque to the hub by pushing at its outer circumference. The placement of these actuators guarantees good controllability of all the flexible modes of motion.

The locations of the sensors are also shown in Figure 2. Each of the 24 levitators is equipped with an incremental optical encoder that provides an indirect measurement of the vertical motion of the corresponding rib at the point of attachment of that levitator. Four evenly-spaced linear variable-differential-transformer rib-root sensors are colocated with four rib-root actuators. The orientation of the hub is measured by two rotary variable-differential transformers mounted directly at the gimbal bearings.

A computer samples the outputs of the sensors, uses these data to update adaptive-control gains and compute appropriate actuation commands, and then sends the signals to the actuators. This cycle is repeated as long as the controller is in operation. The basic idea behind the general model-reference adaptive-control technique is first to design a reference model, the output of which reflects the desired performance of the system, and then to drive the output of the plant to track asymptotically the output of the model via the adaptive-control law. The virtue of the specific technique employed in this research is that it allows the reference model to be of low order even though the order of the actual system is infinite or high, and accurate knowledge of the system is not required in the design of the controller.

In initial proof-of-concept experiments, the adaptive controller has achieved stable regulation of transients with significant improvement over the open-loop performance. The settling time has been reduced by a factor of 3 or more in some cases. In an experiment involving regulation with initial deflection, the outputs of the system followed the highly damped outputs of the reference model closely and converged rapidly.

This work was done by Che-Hang C. Ih, David S. Bayard, Shyh J. Wang, and Daniel B. Eldred of Caltech for **NASA's Jet Propulsion Laboratory**. *For further information, Circle 159 on the TSP Request Card.*
NPO-17478

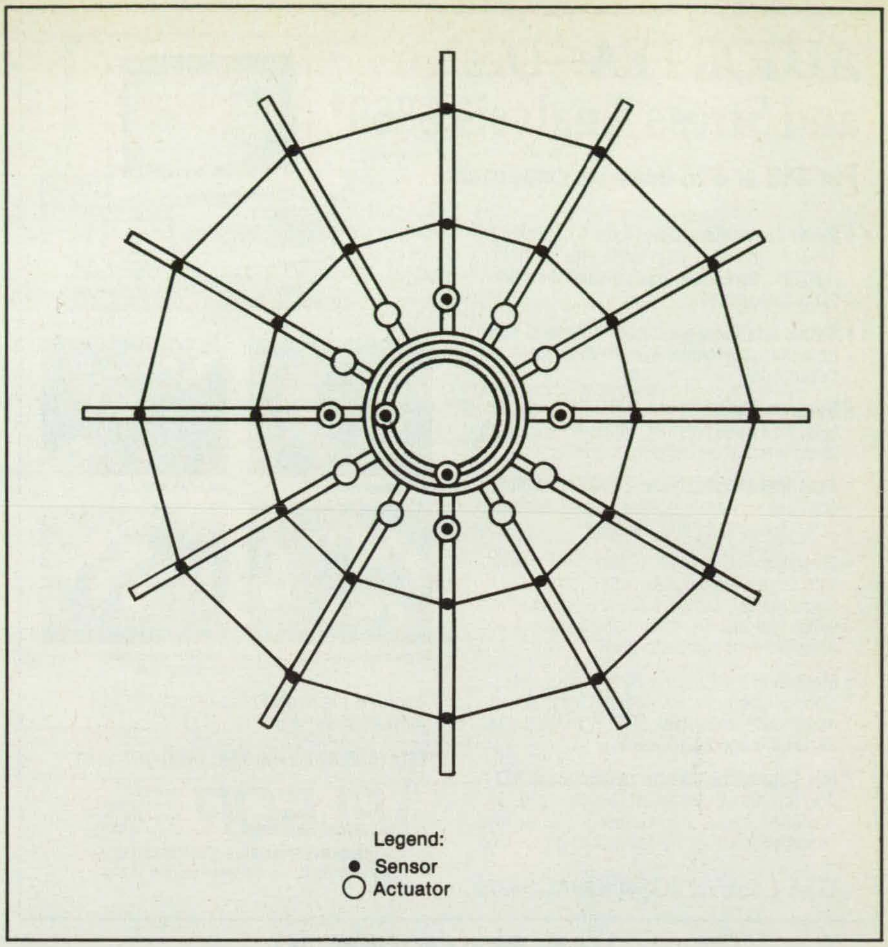

Figure 1. A **Complicated Flexible, Antennalike Structure** exhibits complicated interactions that test the ability of a control system to suppress or regulate deflections.

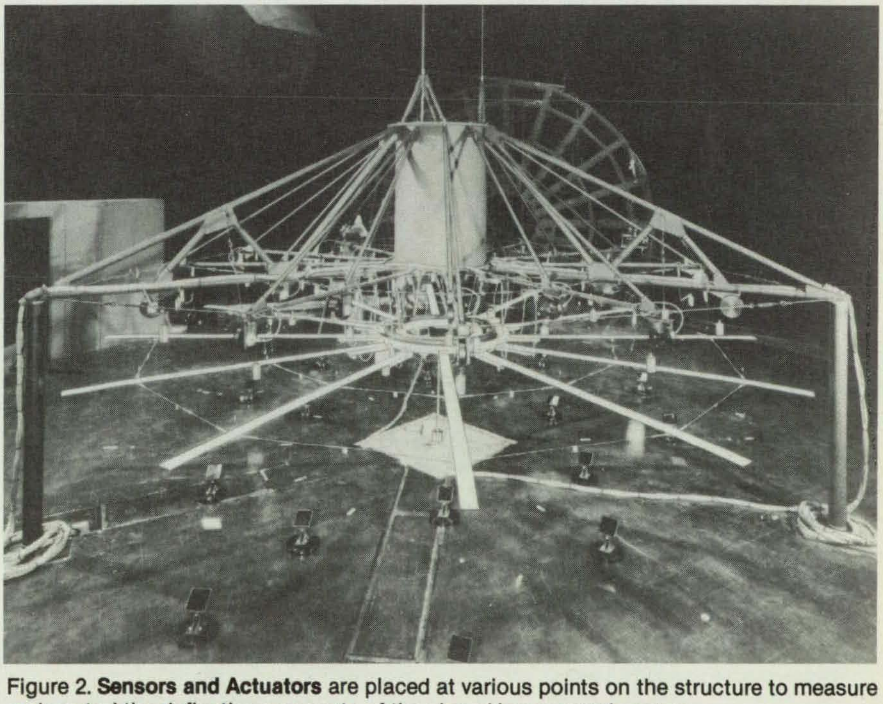

Figure 2. **Sensors and Actuators** are placed at various points on the structure to measure and control the deflections, as parts of the closed-loop control system.

Books and Reports

These reports, studies, handbooks are available from NASA as Technical Support Packages (TSP's) when a Request Card number is cited; otherwise they are available from the National Technical Information Service.

Vibrational Responses of Structures to Impulses

The analysis of transients supplements the usual modal analysis for greater accuracy.

A report discusses the propagation of vibrations in a structure in response to impulsive and/or concentrated loads. The usual finite-element modal analysis is inadequate to describe such phenomena because it does not account for high frequencies that contribute significantly to the vibrations. In the approach taken by the author, the effects of pulsed loads are treated by analyzing the propagation of characteristic vibrational waves explicitly through each member of the structure. This wave-front analysis should be used in combination with the usual finite-element modal analysis to obtain a more accurate representation of the overall vibrational behavior.

The discussion begins with the propagation of pulse excitations in one-dimensional structural members. Excitations include longitudinal, shear, bending, and transverse string vibrational waves, each propagating uncoupled from the others (within a member) at a characteristic speed given by the classical small-vibration equations.

Next, periodic lattice-type structures are considered to be composed of such one-dimensional members with joints characterized by transmission and reflection coefficients for one type of excitation only. Time is nondimensionalized by expressing it in units of the time of propagation along one member. With this formulation, the response of the structure to an initial pulse at the times of arrival of the wave at subsequent members can be expressed by difference equations in matrix form. The solution can be obtained from an initial pulse vector by successive matrix multiplications. The qualitative properties of the solution are defined by the eigenvalues of the fundamental matrix, which plays the same role as that of the stiffness matrix in the finite-element technique.

A real structure is more likely to be aperiodic, with different characteristic speeds and delays in each member. Furthermore, joints can convert one type of deformation into another (e.g., an angle between two rods can convert a longitudinal wave into a longitudinal plus a transverse wave), so that sets of transmission/conversion and reflection/conversion coefficients

are needed. When time is nondimensionalized in terms of the delay for one type of wave in one of the members, a more complicated system of difference equations is obtained. As before, matrix/vector methods are used to obtain the solution.

One of the interesting predictions of this analysis is that unequal delays in members and conversions of waves at joints can cause the vibrational response to a pulse excitation to lose its periodicity and become ergodic. The mathematical instability of a structure under small changes in the propagation speeds and lengths of the members may cause a transition to ergodicity even in a structure for which the analysis initially predicts a periodic response.

This work was done by Michail A. Zak of Caltech for **NASA's Jet Propulsion Laboratory**. *To obtain a copy of the report, "Dynamical Response to Pulse Excitations in Large Space Structures," Circle 97 on the TSP Request Card.*
NPO-17343

Rolling-Contact Spalling in Bearings

The effects of thermal and mechanical stresses are analyzed.

A report describes experimental and theoretical studies of the effects of thermal and mechanical contact stresses and the attendant plastic deformations responsible for rolling-contact spalling of the 440C-steel bearings in a high-pressure-oxygen turbopump. The lives of the bearings are limited by premature spalling of the races and balls.

The experimental part of the study included efforts to promote the growth of fatigue cracks under cyclic torsion in hardened 440C-steel hollow cylinders with circumferential defects. In addition, spalls produced on 440C steel by a three-ball/rod rolling-contact testing machine were studied with scanning electron microscopy. The classical, V-shaped spalls formed with loose flaps, pieces of which broke off from time to time, thus forming wear fragments as the spall cracks grew. Spalls were observed to start growing from the surfaces of uncoated specimens and from points below the surfaces of specimens coated with copper.

The theoretical portion of the study begins with a finite-element stress-vs.-strain analysis without thermal effects. For this purpose, the mathematical model of the contact is a two-dimensional indentation in the otherwise flat surface of a material of idealized stress-vs.-strain behavior called "elastic-linear-kinematic-plastic," the parameters of which are selected to approximate the behavior of 440C steel. This analysis considers Hertzian pressures

of 2.5 to 3.64 GPa and full slip with a coefficient of friction of 0.2 in the absence of local heating. The distortion of the rim, cyclic plastic strains, residual stresses, and the dissipation of energy via plastic deformation are evaluated and compared with the results that would be obtained under the assumptions of pure rolling and perfect plasticity.

Thermal effects are included by means of a coupled temperature-and-displacement finite-element analysis. For this purpose, the indentation is considered to generate heat fluxes at densities up to 8.6×10^4 kW/m^2, which are comparable to those generated in the real bearings. Local temperatures in excess of 1,000 °C are treated. In this case, the stress-vs.-strain behavior is represented by an idealization called "elastic-perfectly-plastic." These calculations reveal that high residual tension remains after the contact is unloaded and cooled.

This work was done by A. M. Kumar, S. M. Kulkarni, B. Bhargava, G. T. Hahn, and C. A. Rubin of the Center for Materials Tribology of Vanderbilt University for **Marshall Space Flight Center**. *To obtain a copy of the report, "Mechanisms of Rolling Contact Spalling," Circle 8 on the TSP Request Card.*
MFS-27201

Insulation for Cryogenic-Liquid Tanks

Rigid foam and radiation shields prevent excessive heating in a variety of environments.

A report describes the design, development, and test of the thermal-protection system for the liquid-oxygen and liquid-hydrogen tanks of the now discontinued Shuttle/Centaur G' project. The Centaur G' spacecraft, with its insulated tanks, would have been launched into orbit around the Earth from the Space Shuttle. The system would have protected the tanks from excessive heat before and during launches, while in orbit around the Earth, and during premature landings from aborted launches.

The system was designed to withstand the stresses of launch and emergency landing, acoustical loads, rapid changes in pressure, and the impingement of rapidly flowing gas near the vents of the cargo bay in the Space Shuttle. One of the primary requirements in the design was that the system present no hazard to the Space Shuttle or its crew.

The tank for liquid hydrogen is insulated with polyimide foam and three radiation shields. The tank for liquid oxygen is insulated with radiation shields only. The foam prevents gases from condensing on the hydrogen tank when it is in the atmosphere of the Earth before and during launch and during reentry. Helium gas flows continuously through the open-cell foam during these phases of flight to remove nitrogen and oxygen from the vicinity of the tank. The flow of helium is contained by the portions of the structure surrounding the tanks, including the forward adapter purge diaphragm, the forward adapter itself, the innermost side-wall radiation shield, and the purge plenum that seals the system on the aft end of the liquid-hydrogen tank. The flow of helium is stopped at lift-off but restarted if a flight is aborted.

Both the purge diaphragm and the innermost radiation shield consist of a high-strength aromatic polyamid cloth sandwiched between two outer layers of polyimide coated with vapor-deposited aluminum (VDA). The outermost radiation sield uses a layer of polytetrafluoroethylene coated internally with VDA as the outer laminate layer. This material gives the ratio of absorptance-to-thermal-emittance required to minimize heating from the Sun and the Earth's albedo while in orbit.

The hydrogen tank foam is 1.5 in. (3.8 cm) thick on the sidewall and 0.75 in. (1.9 cm) thick on the forward bulkhead. The foam is assembled on the tank in panels joined at their edges by twin-pin fasteners. The seams are covered with polyvinyl fluoride tape to seal off convection paths between the radiation shields and the surface of the tank. On the tank, where the panels are arranged in two layers, the seams in the outer layer are offset from those in the inner layer to reduce convection further.

The oxygen tank is warm enough that it does not tend to liquefy the gaseous nitrogen within the Shuttle cargo bay and therefore does not need foam insulation. Like the hydrogen tank, however, it does need shields to protect it from radiated heat in orbit. The tanks are protected by three such shields on the sidewall and four on the aft bulkhead.

This work was done by Richard H. Knoll of **Lewis Research Center** *and Peter N. MacNeil and James E. England of General Dynamics Corp. Further information may be found in NASA TM-89825 [N87-23685], "Design, Development, and Test of Shuttle/Centaur G-Prime Cryogenic Tankage Thermal Protection Systems."*

Copies may be purchased [prepayment required] from the National Technical Information Service, Springfield, Virginia 22161, Telephone No. (703) 487-4650. Rush orders may be placed for an extra fee by calling (800) 336-4700.
LEW-14707

Perspectives on Dilution Jet Mixing

A study identifies effects of flow and geometric parameters on mixing of transverse jets with ducted crossflow.

NASA recently completed a program of measurements and modeling of the mixing of transverse jets with a ducted crossflow, which was motivated by the need to design or tailor the temperature pattern at the combustor exit in gas turbine engines. Problems of jets-in-crossflow have been studied frequently due to their appearance as constituent flows in such diverse applications as pollutant dispersion from chimneys, thermal discharges into rivers and streams, overfire jets in furnaces, engine exhaust from VSTOL (Vertical/Short Takeoff and Landing) aircraft, gas turbine combustor exit temperature pattern control, and fuel injection in high speed propulsion systems. The information obtained in any given study may, in addition to increasing the understanding of the more general problem, be directly relevant to the solution of similar problems in very different applications.

The combustor dilution zone jet-in-crossflow application is a confined mixing problem, with from 10 to 50 percent of the total airflow entering through dilution jets in the aft section of the combustor. The result is that the average temperature of the exiting flow may differ significantly from that of the entering mainstream flow. To control or tailor the exit temperature pattern, it is necessary to be able to characterize the exit distribution in terms of the upstream flow and geometric variables.

The objectives of this program were to identify the dominant physical mechanisms governing the mixing, extend empirical models to provide a near-term predictive capability, and compare numerical code calculations with data to guide future analysis improvement efforts. Mean temperature measurements have been analyzed to identify the principal independent flow and geometric variables affecting the mixing. These measurements are compared with calculations made with both empirical and numerical models for flow and geometric variations typical of many gas turbine combustors.

This work was done by J. D. Holdeman of **Lewis Research Center** *and R. Srinivasan of Garrett Turbine Engine Co. Further information may be found in NASA TM-87294 [N86-32432], "Perspectives in Dilution Jet Mixing."*

Copies may be purchased [prepayment required] from the National Technical Information Service, Springfield, Virginia

22161, Telephone No. (703) 487-4650. Rush orders may be placed for an extra fee by calling (800) 336-4700.

For tutorial slide show, contact J. D. Holdeman at Lewis Research Center.
LEW-14614

Numerical Analysis of Flows With FIDAP

Predictions of FIDAP are compared with other numerical results and with data from experiments.

A report presents an evaluation of the accuracy of the Fluid Dynamics Package (FIDAP) computer program. FIDAP is a finite-element code for the analysis of flows of incompressible fluids and transfers of heat in multidimensional domains. It includes both of the available methods for the treatment of the spurious numerical coupling between the simulated velocity and the simulated pressure; namely, the penalty method and the mixed-interpolation method with variable choices of interpolation polynomials for velocity and pressure. The streamwise upwind (STU) method is included as an option for flows dominated by convection.

In this study, FIDAP was applied to four two-dimensional problems: laminar flow in a wall-driven cavity, laminar flow over a backward-facing step, turbulent flow over a backward-facing step, and turbulent flow through a turnaround duct. In all cases, the nine-node quadrilateral finite element with linear discontinuous interpolations for pressure was used. This approach is known from previous studies to be one of the optimal choices for the treatment of the spurious numerical velocity/pressure coupling in incompressible flow. The penalty parameter was chosen to be 10^{-6}. The flows predicted by FIDAP were compared with the flow predicted by other numerical methods and/or the corresponding measured flows.

The following conclusions were drawn from the study:

- The consistant-integration-penalty, finite-element program with the quadrilateral finite elements described previously can be used to treat the spurious numerical velocity/pressure coupling in the flow of an incompressible fluid.
- When STU is used, the numerical diffusions are too strong in high-Reynolds-number laminar flow, particularly inside a wall-driven cavity.
- When STU is not selected, the numerical results of FIDAP for laminar flow agree well with the predictions of other numerical methods and with measurements.
- STU is essential to the computation of turbulent flow because it stabilizes numerical solutions of the equations of the $k-\varepsilon$ mathematical model of turbulence proposed by Launder and Spalding. However, momentum equations are strongly influenced by STU, and numerical diffusions in the velocity field must, therefore, be minimized by the application of higher-order upwinding techniques to momentum equations.
- The predictions of FIDAP correspond to the general trends in the predictions of other methods for the $k-\varepsilon$ model of turbulence. Discrepancies between the predictions and measurements in both test cases for turbulent flow are caused mainly by the limitations of the standard $k-\varepsilon$ model on recirculating and curved flows. Advanced mathematical models of turbulence should be incorporated into FIDAP to obtain accurate predictions of turbulent flows.

This work was done by Jeong L. Sohn of **Marshall Space Flight Center**. *Further information may be found in NASA CR-179390 [N89-10253], "Numerical Analysis of Laminar and Turbulent Incompressible Flows Using the Finite Element 'Fluid Dynamics Analysis Package (FIDAP)'."*

Copies may be purchased [prepayment required] from the National Technical Information Service, Springfield, Virginia 22161, Telephone No. (703) 487-4650. Rush orders may be placed for an extra fee by calling (800) 336-4700. MFS-27219

Combining Thermal and Structural Analyses

A computer code makes programs compatible so that stresses and deformations can be calculated.

A paper describes a computer code that combines thermal analysis with structural analysis. Called SNIP (for SINDA-NASTRAN Interfacing Program), the code provides an interface between a finite-difference thermal model of a system and a finite-element structural model of it when there is no node-to-element correlation between the models. SNIP eliminates much of the manual work in converting the temperature results of the SINDA (Systems Improved Numerical Differencing Analyzer) program into thermal loads for the NASTRAN (NASA Structural Analysis) program.

SNIP generates thermal-load cards for NASTRAN plate, shell, bar, and beam elements so that thermal deformations and stresses in the structure can be predicted. SNIP uses a geometric search routine and a numerical coding scheme to relate thermal-model nodes to structural-model elements. It then calculates element temperatures according to the weighted averages

of temperatures of the thermal nodes related to each element. Users can vary input parameters to control the correlations between nodes and elements.

SNIP is being used to analyze concentrating reflectors for the solar generation of electric power. Large thermal and structural models are needed to predict the distortion of surface shapes, and SNIP saves considerable time and effort in combining the models.

The code has already been applied to the analysis of thermal deformations of satellite antenna reflectors. It furnished accurate results in a fraction of the time of other model-combining methods. An important side effect was that SNIP induced a high level of communication between thermal and structural modelers, and errors in the models thus became obvious early in the development of the models.

This work was done by Steven R. Winegar of **Lewis Research Center**. *Further information may be found in NASA TM-100158 [N87-27268], "SINDA-NASTRAN Interfacing Program Theoretical Description and User's Model."*

Copies may be purchased [prepayment required] from the National Technical Information Service, Springfield, Virginia 22161, Telephone No. (703) 487-4650. Rush orders may be placed for an extra fee by calling (800) 336-4700.
LEW-14741

Machinery

Hardware, Techniques, and Processes
86 Stowable Mechanical Sound Suppressor
86 Robot Hand Would Adapt to Contours
87 Electrostatic Linear Actuator
Computer Programs
68 Predicting Noise From Wind Turbines

Stowable Mechanical Sound Suppressor

A drive-and-link assembly actuates a system aft of the variable nozzle of an engine.

Langley Research Center, Hampton, Virginia

The concept of redirecting the exhaust gas of a jet engine in thrust-reversal and vectored-thrust applications has been the subject of considerable research and development for many years. Now, with increased emphasis on the suppression of the noise generated by jet engines, a stowable sound suppressor has been conceived for high-speed commercial transport (HSCT) engines. The suppressor is to be located just aft of the variable nozzle of the engine.

During takeoff, when suppression of noise is required, a multisegmented system of separators is rotated out of a center plug across the nozzle stream. Actuation is accomplished by a single ball-screw drive and links, similar to the spokes in an umbrella. With the iris nozzle translated forward, a circumferential row of tubes is exposed. The pattern of tubes and separators form the suppressor configuration. The flow stream through the slots and tubes is sized to the takeoff area.

For positions other than takeoff, the separator portion of the suppressor is rotated back into the tail cone to the stowed position, out of the airstream. The holes in the tube assembly are blocked by a sequenced iris nozzle that also sets the exhaust-throat area. A segmented, spring-loaded door attached to each of the separators blocks the flow of air through the tail cone when the suppressor is in the takeoff position and is translated inward when the suppressor is in the stowed position. In addition to being useful in HSCT engines, the stowable mechanical sound suppressor should be useful on any turbojet engine in which active suppression of sound is a requirement.

This work was done by Edward R. Thompson of United Technologies Corp. for **Langley Research Center**. *No further documentation, is available.* LAR-14158

Robot Hand Would Adapt to Contours

A conceptual device would use hydraulic pressure to activate fingers.

NASA's Jet Propulsion Laboratory, Pasadena, California

Projections on the opposing fingers of a proposed robot hand would automatically conform to the contours of an object on contact. The hand could therefore be used to grasp objects of various shapes and sizes. The conforming process would be passive; the pressure of the object on one or several pad elements would force the other pad elements to touch it. The hand would not use elaborate mechanisms involving motors, cams, and cables.

The projecting elements on each finger would be pistons connected to a common hydraulic reservoir within the finger (see Figure 1). The reservoir is initially filled and sealed, with the pistons at the midpoint of their travel. The application of a force to one piston would cause a pressure to be exerted equally on all the other pistons. The diameters of the pistons near the middle of the finger would be less than the diameters of pistons near the edge. Therefore, the middle pistons would tend to move farther under an increase in pressure in the reservoir and to exert smaller forces. A gimbaled pad at the tip of each piston would tilt to align with the local surface of an object.

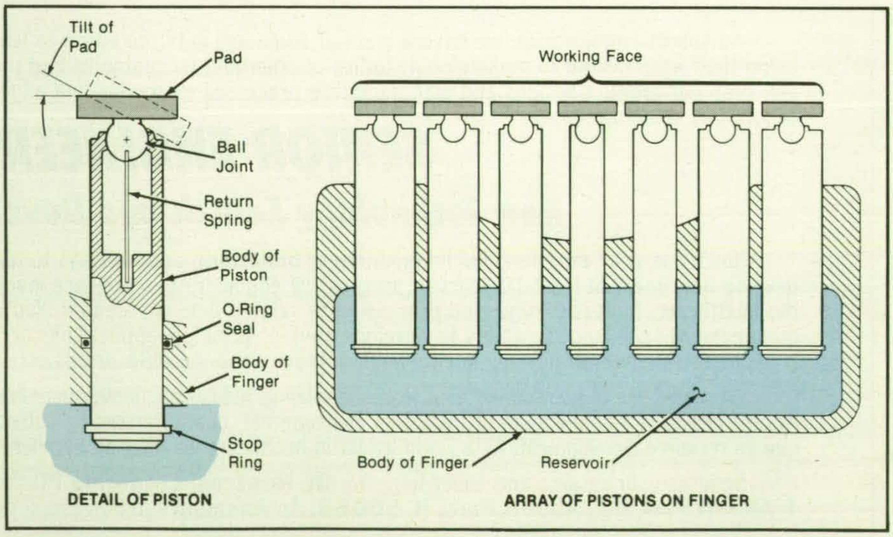

Figure 1. **Pistons Connected to a Common Reservoir** would provide a gentle, firm grip. The fingers would communicate with each other via the hydraulic pressure, without an elaborate control system.

When the finger approached a flat-surfaced object head-on, all pads would contact the object simultaneously (see Figure 2). If the hand approached at an angle, the pistons would push the object into a position in which the pistons would be uniformly displaced, as though the finger had approached head-on.

When the finger approached a small sphere or cylinder, the middle piston would contact the object first. Because of its

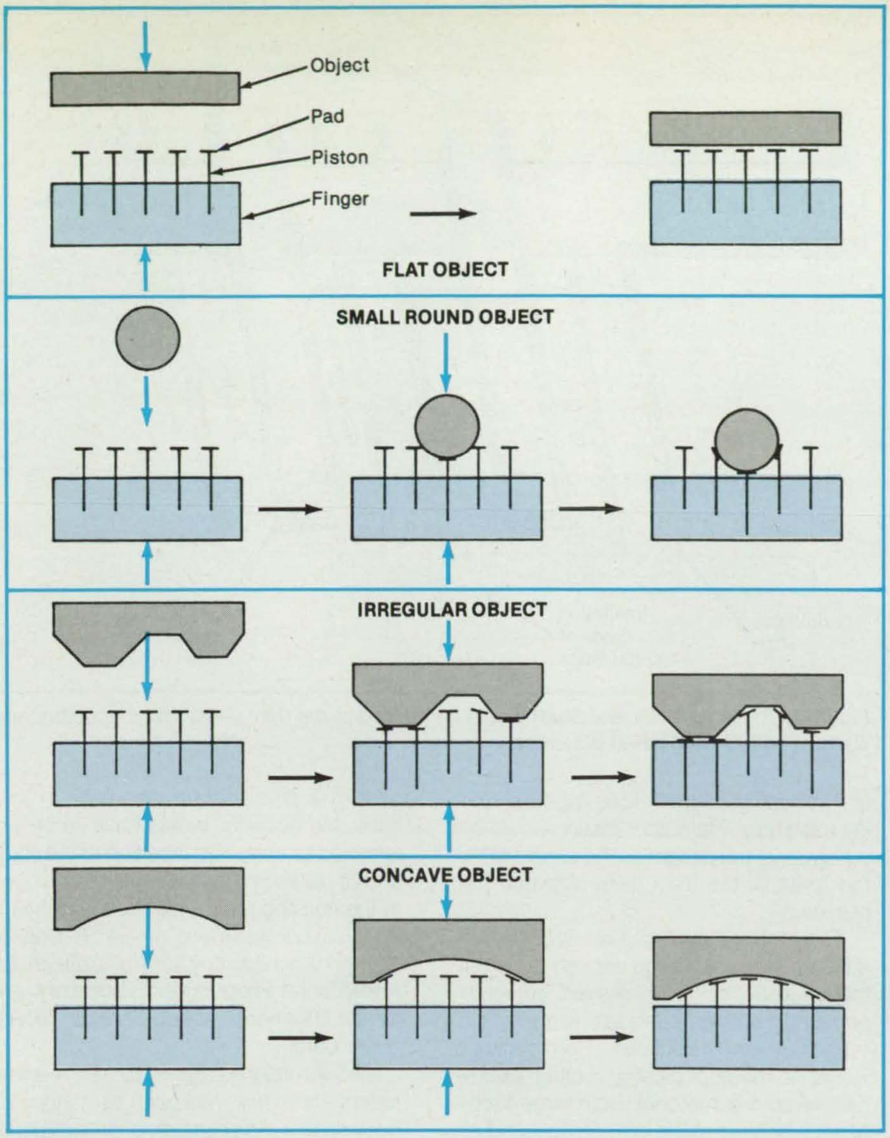

Figure 2. **Pistons Would Move In and Out,** and their tips would slope to match the contour of an object. Their action would tend to center the object on the finger.

small diameter, it would tend to travel farther than the other pistons and would thus allow the round surface to sink in farther for a more secure grip. The hydraulic pressure generated by the middle piston would move its neighbors outward to meet the object. As they made contact, their tip pads would tilt to the local slope of the surface of the object. The pistons would interact similarly in contacting irregular objects and concave objects.

The pistons would tend to center a symmetrical object like one with a spherical or flat surface because the piston forces would decrease toward the middle of the finger. An offcenter object would be subjected to higher forces at the side farthest from the center. The tilted pads would then exert sideways forces that would slide the object inward.

The same gradation of forces would inhibit rolling of an object. The object would become cradled securely in the pads without excessive force.

A sensor could monitor the pressure in the reservoir, and the pressure could be limited to prevent the pistons from damaging an object. No other sensing or control would be needed.

This work was done by Earl R. Collins, Jr., of Caltech for **NASA's Jet Propulsion Laboratory**. *For further information, Circle 1 on the TSP Request Card.*

This invention is owned by NASA, and a patent application has been filed. Inquiries concerning nonexclusive or exclusive license for its commercial development should be addressed to the Patent Counsel, NASA Resident Office-JPL [see page 22]. Refer to NPO-16766.

Electrostatic Linear Actuator

Electrically charged helices would attract or repel each other.

NASA's Jet Propulsion Laboratory, Pasadena, California

A proposed electrostatic linear actuator would be made with intertwined dual helices, which would hold the charge-bearing surfaces. The dual-helix configuration would provide relatively large unbroken facing charged surfaces (and, thereby, relatively large electrostatic force) within a small volume. The spiral form would also make the components more rigid. The actuator was conceived to have few moving parts and to be operable after long intervals of inactivity.

The actuator would include an inner helix on a shaft within an outer helix, resembling a lead screw in a loosely fitting nut (see Figure 1). However, no rotary motion would be involved. The shaft could even be restrained against rotation after in-

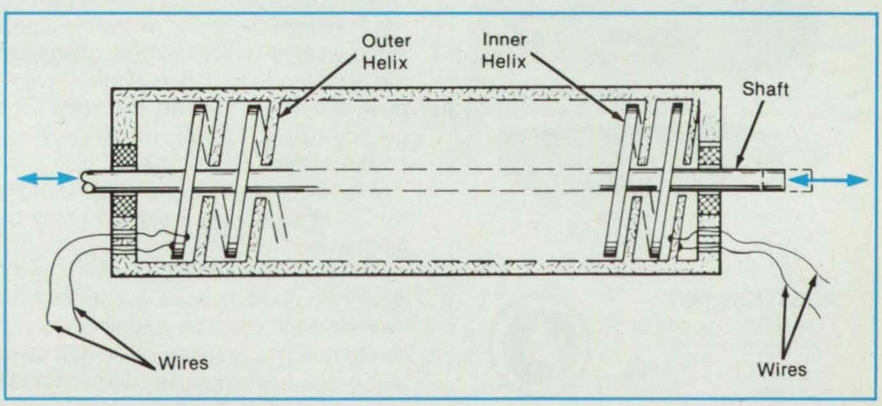

Figure 1. The **Inner Helix Would Slide Axially** in the outer helix in response to voltages applied to the conductors.

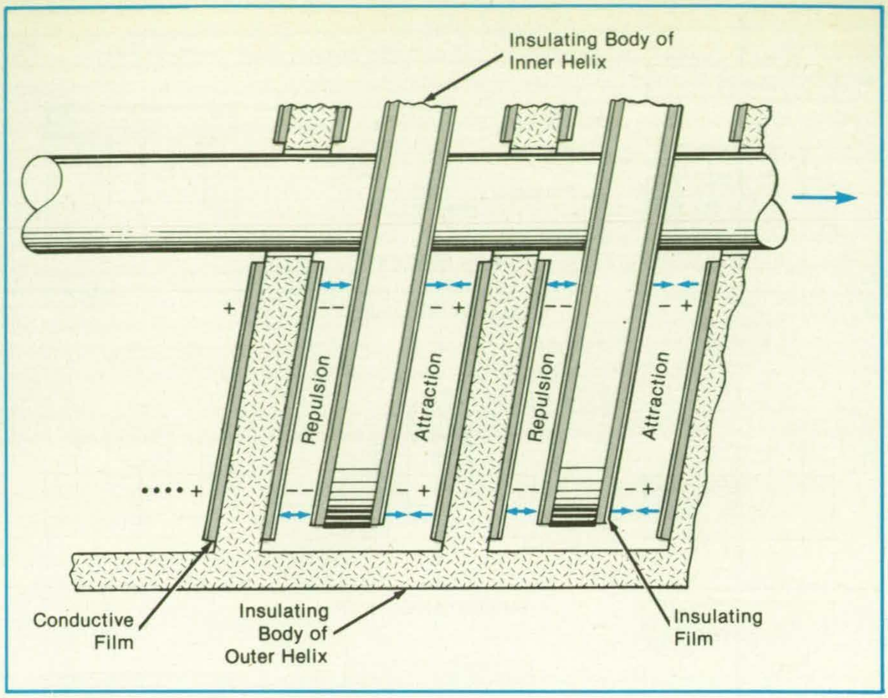

Figure 2. The **Inner Helix and Shaft** would be pushed to the right when the conductors are charged with the indicated polarities.

itial threading of the helices together during assembly. The output motion would be purely axial translation of the shaft, within the limits of the axial gaps between the helices.

The pitch of the helices would be selected to provide gaps large enough to permit the full axial translation desired, yet small enough to provide adequate electrostatic attraction and repulsion. Both helices would be made of plastic or other electrically-insulating material. Both large faces of each helix would be covered by conductive films, which would in turn be covered by thin insulating films to prevent conduction between facing conductive films when the helices touch (see Figure 2). Thus, a substantial electric charge could be stored in the conductor on each face of each helix.

The placement of charges of the appropriate polarities on the conductors would cause attractions and/or repulsions between the conductors, thereby pushing the inner helix along the axis with respect to the outer helix. For example, charges of the polarities indicated in Figure 2 would push the inner helix to the right. The general rule of operation is to place opposite charges (which attract) across a gap that is to be shortened, and like charges (which repel) across a gap that is to be lengthened.

The inner helix could be held so that the outer helix could move, or vice versa. Alternatively, each could be held and released in alternation in synchronization with reversals of charges to obtain a ratcheted crawling motion. In an alternative configuration, the helices could be replaced by flat surfaces perpendicular to the axis, reminiscent of a parallel-plate capacitor. In that case, the actuator would have to be assembled by sideways insertion of the shaft and its plates into longitudinally split halves of the housing and its plates.

This work was done by Earl R. Collins, Jr., and Kenneth C. Curry of Caltech for **NASA's Jet Propulsion Laboratory**. *For further information, Circle 7 on the TSP Request Card.*

This invention is owned by NASA, and a patent application has been filed. Inquiries concerning nonexclusive or exclusive license for its commercial development should be addressed to the Patent Counsel, NASA's Resident Office-JPL [see page 22]. Refer to NPO-17684

Fabrication Technology

Hardware, Techniques, and Processes

89 Quick Check of Butt-Weld Alignment
89 Hot Wax Sweeps Debris From Narrow Passages
90 Preventing Contamination in Electron-Beam Welds
91 Filter Enhances Fluorescent-Penetrant-Inspecting Borescope
92 Connecting Multiple Wires to a Single Through Hole
93 Automatic Tension Adjuster for Flexible-Shaft Grinder

Books and Reports

93 Welding and Cutting a Nickel Alloy by Laser
94 Making Fiber-Reinforced Metal by Rapid Solidification

Quick Check of Butt-Weld Alignment

An optical instrument would show whether plates are aligned or offset.

Marshall Space Flight Center, Alabama

A proposed tool would measure the alignments of plates before they are butt-welded. It would provide a nearly instantaneous check on alignment, thereby facilitating repetitive measurements along the length of the weld joint. It would also reduce the risk of contamination of the weld from dirty measuring tools.

A pair of brackets containing optical fibers would be clamped or rested on the plates on both sides of the joint (see figure). Light would be fed into the fiber in the transmitter bracket. If the plates were perfectly aligned, the light from the transmitter fiber would enter the middle fiber in the receiver bracket and travel to the middle photodetector, which would put out a signal indicative of alignment.

If the plates were poorly aligned, light from the transmitting fiber would enter an upper or lower receiving fiber and would impinge on the corresponding upper or lower photodetector. In this case, a signal in the output of the upper or lower photodetector would indicate misalignment.

This work was done by Matthew A. Smith of Rockwell International Corp. for **Marshall Space Flight Center**. *No further documentation is available.*
MFS-29423

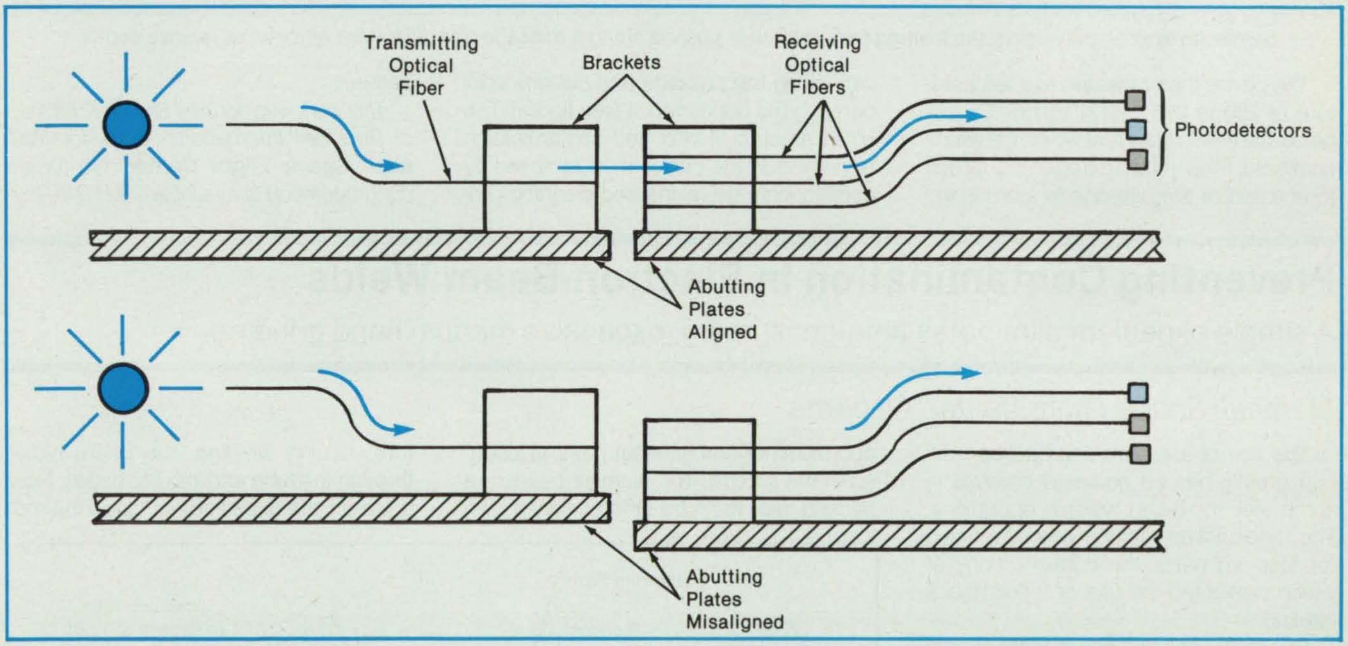

The **Middle Photodetector Would Indicate Acceptable Alignment** when the position of the transmitter fiber precisely matched that of center receiver fiber. If the plates were offset, other photodetectors would signal misalignment.

Hot Wax Sweeps Debris From Narrow Passages

Loose particles are removed from inaccessible places.

Marshall Space Flight Center, Alabama

A safe and effective technique for the removal of debris and contaminants from narrow passages involves the entrainment of the undesired material in a thermoplastic casting material. Devised to clean out fuel passages in the main combustion chamber of the Space Shuttle main engine, the technique could also be applied to narrow, intricate passages in internal-combustion-engine blocks, carburetors, injection molds, and other complicated parts.

First, the debris are located by radiography (which detects metal) or infrared imaging (which detects nonmetallic objects). Next, the part is heated to 300 °F (149 °C), and Rigidax (or equivalent) casting wax, melted in a separate vessel at 300 °F, is poured into the passage in sufficient quantity to reach the debris. The part is allowed to cool at room temperature so that the wax hardens.

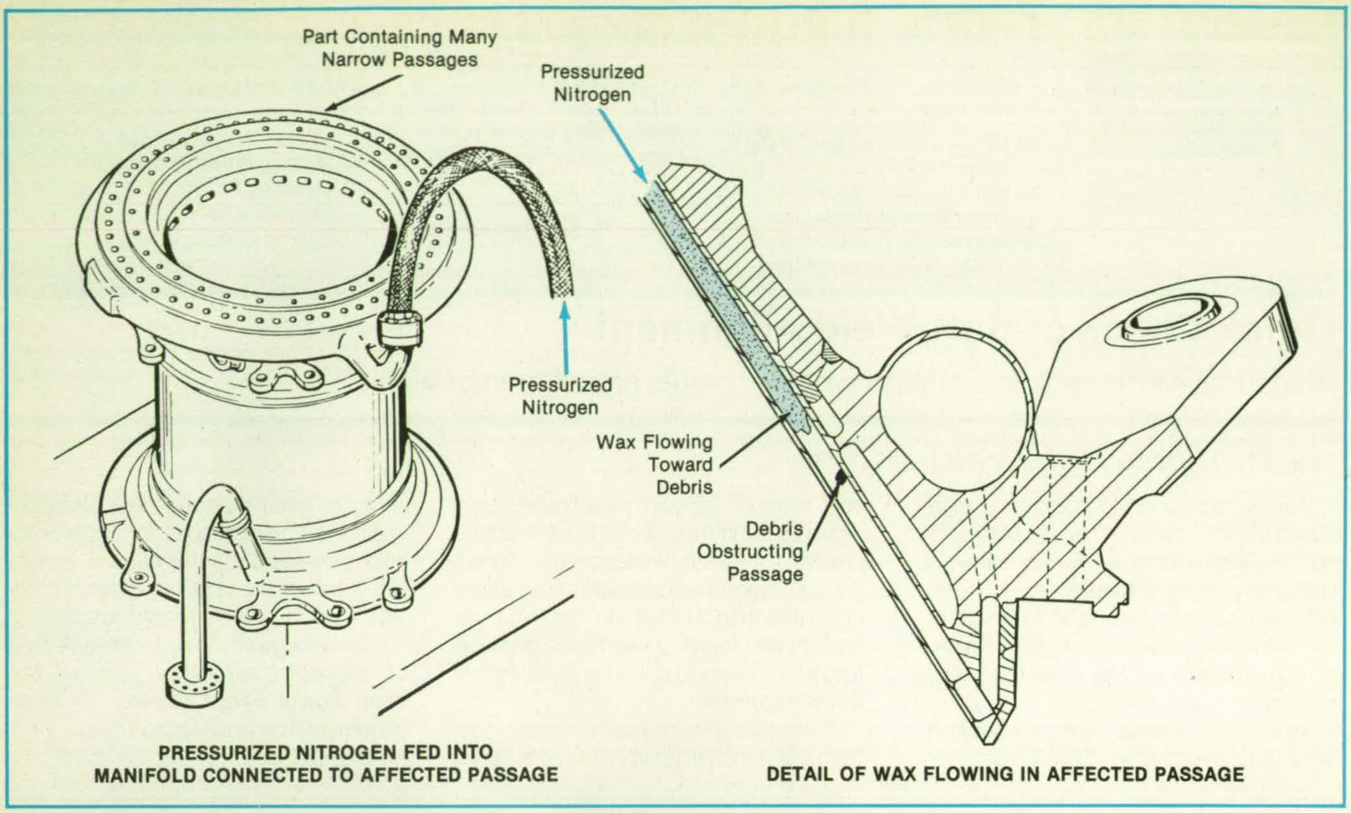

Semisolid Wax slightly below the melting temperature is pushed along a passage by pressurized nitrogen to remove debris.

The part is then reheated to a temperature of 250 to 275 °F (121 to 135 °C), just below the melting point, at which the wax is semisolid. Pressurized nitrogen is supplied to one end of the passage to extrude the wax along the passage and out one end, carrying the debris with it (see figure). The small amount of wax and contamination remaining in the part is then removed by conventional dewaxing and cleaning procedures.

This work was done by Steven K. Ricklefs of Rockwell International Corp. for **Marshall Space Flight Center**. *No further documentation is available. MFS-29462*

Preventing Contamination in Electron-Beam Welds

A simple expedient eliminates time-consuming, expensive manual hand grinding.

Marshall Space Flight Center, Alabama

The use of a groove and backup tube can greatly reduce postweld cleanup in some electron-beam welding operations. The tube-backup method was developed for titanium parts, the configurations of which prevented the use of a solid-block backup.

Previously, alumina beads were placed in the cavity on the root side of the weld to absorb the overpenetrating electron beam (see figure). The beads, about 0.075 in. (1.9 mm) in diameter, were pressed against the parts so that they were in intimate contact with the molten root during welding. As a result, many of the beads adhered to the root when it solidified. Weeks — sometimes months — of grinding by hand were needed to remove the beads and the surface roughness at the root. Additional grinding was needed to remove the roughness on adjacent areas of the parts, caused by the arcing of the electron beam through the beads.

In the new method, a groove is cut in the parts at the root, and a titanium tube, cut approximately in half lengthwise, is inserted in the groove. The alumina beads are packed over the tube in the cavity as before. During welding, the beam blows through the tube and into the beads. Now, however, the beads do not touch the mol-

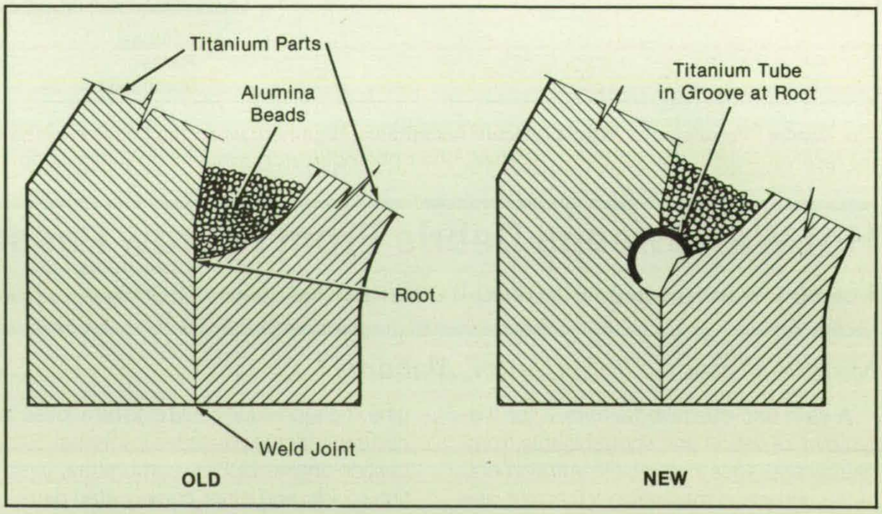

In the **New Welding Configuration** (right), a tube is inserted in a groove to prevent contact between the alumina beads and the molten weld root. In the old configuration (left), the root of the weld joint between the parts became contaminated with beads.

ten root. Moreover, arcing is greatly reduced because the groove and tube diffuse the beam before it reaches the beads. When welding is complete and the beads and tube are removed, only minor spatter remains and can be ground away easily.

This work was done by Wesley D. Goodin, Kevin A. Gulbrandsen, and Carl Oleksiak of Rockwell International Corp. for **Marshall Space Flight Center**. *For further information, Circle 152 on the TSP Request Card. MFS-29428*

Filter Enhances Fluorescent-Penetrant-Inspecting Borescope

A slip-on eyepiece suppresses harmful radiation and seals out ambient light.

Marshall Space Flight Center, Alabama

A slip-on eyepiece for a commercial ultraviolet-light borescope reduces both the amount of short-wave ultraviolet light that reaches the viewer's eye and the apparent intensity of unwanted reflections of white light from surfaces undergoing inspection. The eyepiece fits on the stock eyepiece of the borescope, which illuminates the surface to be inspected with intense ultraviolet light. The surface, which has been treated with a fluorescent dye, emits bright-green visible light wherever the dye has penetrated — in cracks and voids, for instance.

The light source of a borescope generates substantial amounts of undesired short-wave ultraviolet (wavelengths less than 2,000 Å) and visible light along with the desired long-wave ultraviolet light, 2,000 to 3,650 Å in wavelength, that stimulates fluorescence. The visible portion of the extra light reduces contrast so that the fluorescence is more difficult to see, and the short-wavelength ultraviolet portion is harmful to the viewer's eye. It is not practical to filter out the unwanted components at the source because the intensity of the desired long-wavelength ultraviolet would be reduced.

The new eyepiece contains a deep-yel-

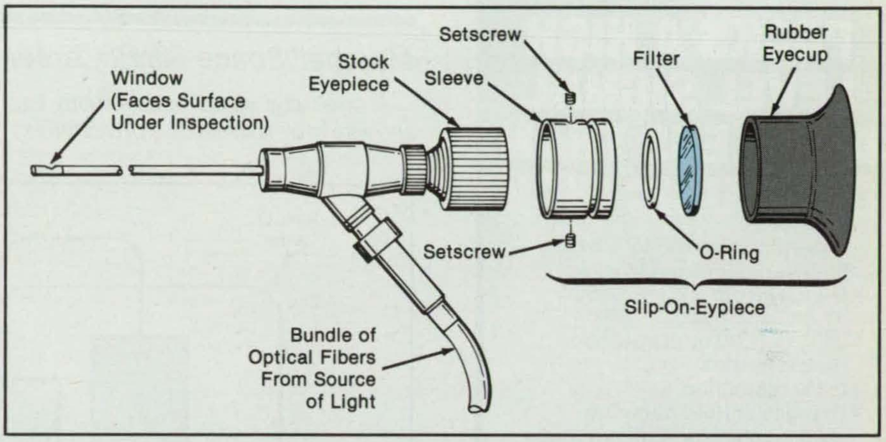

The **Attachment for the Borescope** contains a yellow filter.

low Wratten 15(G) filter, which attenuates the unwanted light strongly but passes the yellow-green fluorescence so that defects can be seen clearly. Other filter colors were tried, including oranges, reds, and greens. Although they attenuated the short-wave ultraviolet somewhat, they adversely affected the appearance of the fluorescent light. The slip-on eyepiece is made of standard parts (see figure). It includes a rubber eyecup that shields the viewer's eye from the room light.

This work was done by Orlando G. Molina of Rockwell International Corp. for **Marshall Space Flight Center**. *For further information, Circle 49 on the TSP Request Card.*
MFS-29379

Connecting Multiple Wires to a Single Through Hole

A solder cup would make it easier to rework printed-circuit boards.

Marshall Space Flight Center, Alabama

A small cup would enable more than one wire to be soldered to a plated through hole in a printed-circuit board. Normally, a through hole can accommodate only one

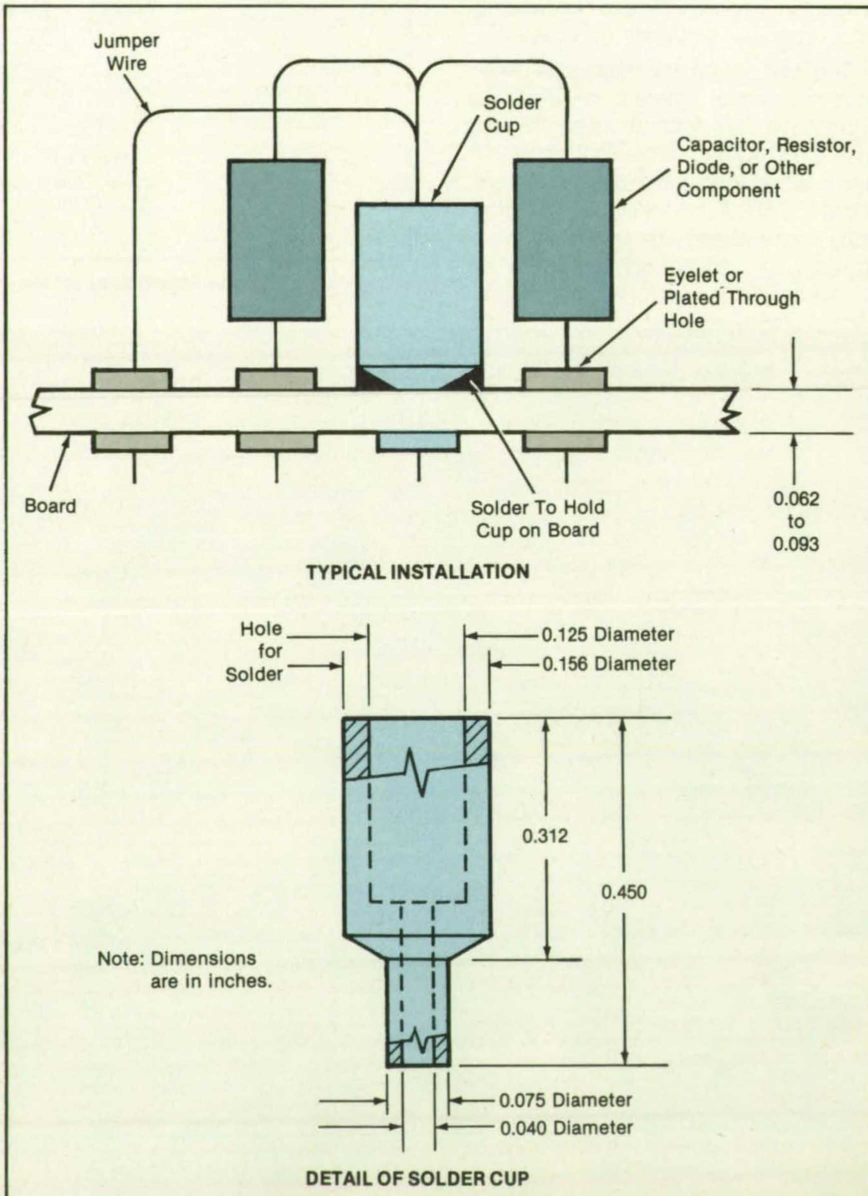

Jumper Wires and Leads from components would be joined to a single through hole by a solder cup.

wire. However, the relatively wide mouth of the cup would hold at least three wires and connect them electrically through its solder contents (see figure).

Cups of this type could be used on breadboard circuits and on newly-manufactured circuit boards. They would be particularly useful in the modification of circuit boards, where they would serve as convenient attachment points for jumper wires and the leads of added components.

The cups would be made of brass plated with silver. They would be inserted in eyelets or plated through holes and swaged onto the boards.

This work was done by Reuben G. Cortes of Rockwell International Corp. for **Marshall Space Flight Center**. *No further documentation is available.*
MFS-29405

Automatic Tension Adjuster for Flexible-Shaft Grinder

A simple pneumatic device reduces wear and increases efficiency.

Marshall Space Flight Center, Alabama

The flexible shaft of a grinding tool is automatically maintained in tension by air pressure. The probelike tool can be bent to reach hard-to-reach areas for grinding and polishing. Unless its shaft is held in tension, however, it rubs against its sheath, overheating and wearing out quickly. By taking up slack in the flexible cable, the tension adjuster reduces friction and enables the tool to operate more efficiently, in addition to lengthening its operating life.

For automatic maintenance of tension, a piston and cylinder are mounted on the two-part handle of the tool (see figure). Air bled from the pressurized supply for the air-driven motor of the tool pressurizes the cylinder, thereby pushing the part of the handle that holds the motor axially away from the part of the handle to which the sheath is attached. The axial separation of the two parts of the handle is restrained by the tension in the flexible shaft, which pulls the bearing surface of the grinding ball onto the end of the sheath. The tension remains constant even as the bearing surface at the end of the sheath erodes.

An orifice in the piston serves as a controlled leak to regulate the pressure on the piston. The air that flows through the orifice passes into the sheath and along the flexible shaft, thereby cooling it. The air leaves the sheath through a small hole near the outer end.

This work was done by Richard K. Burley and William S. Hoult of Rockwell International Corp. for **Marshall Space Flight Center**. *For further information, Circle 9 on the TSP Request Card.*
MFS-29351

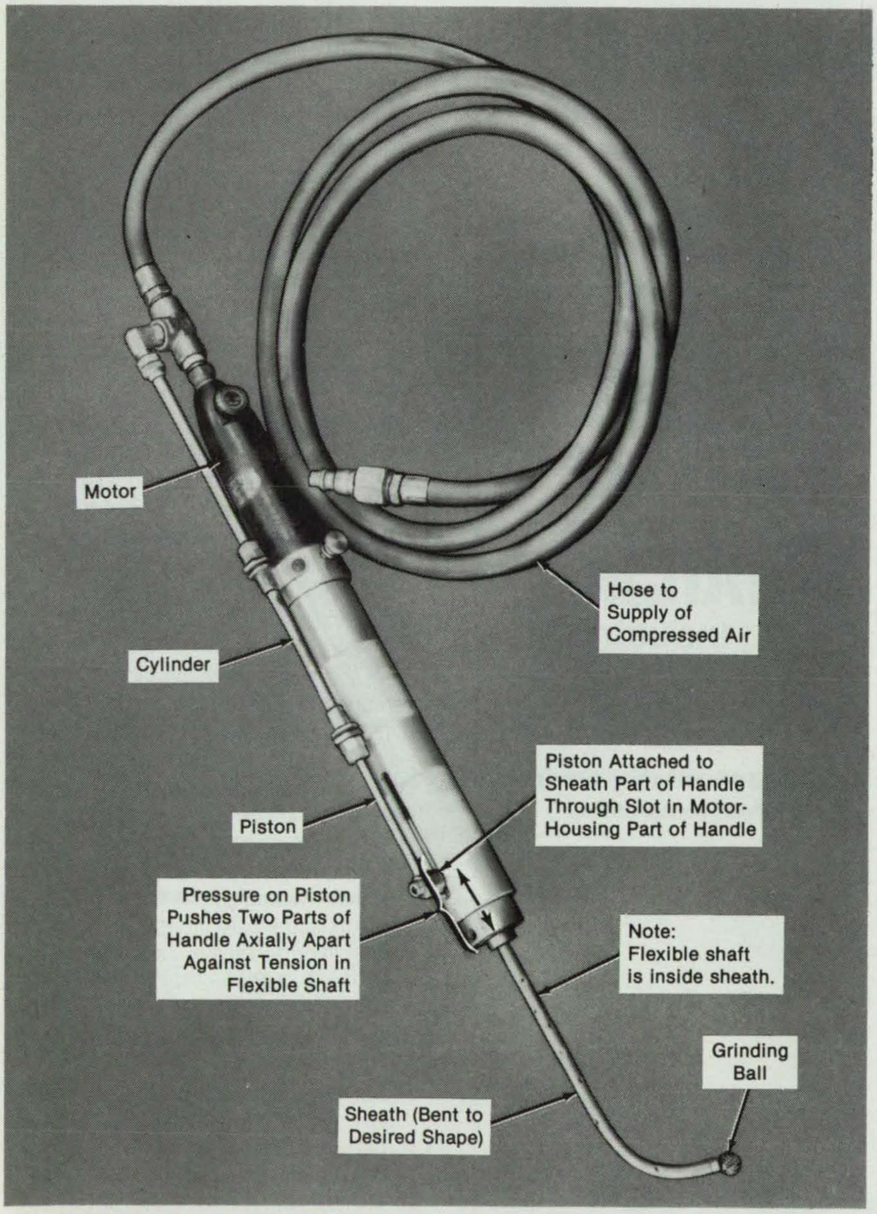

An **Air Supply**, in addition to turning the motor of the tool, pressurizes a small cylinder in the handle. This puts the flexible shaft in tension, holding the grinding ball on the end of the sheath.

Books and Reports

These reports, studies, handbooks are available from NASA as Technical Support Packages (TSP's) when a Request Card number is cited; otherwise they are available from the National Technical Information Service.

Welding and Cutting a Nickel Alloy by Laser

The technique can be effective and energy-efficient.

A report describes an evaluation of laser welding and cutting of Inconel* 718. The report notes that electron-beam welding processes have been developed for In-718, but they can be difficult to use on large or complex structures. Laser welding would be an attractive alternative if microfissuring can be avoided and if the method can match the low specific-energy input and low thermal distortion of electron-beam welding.

The evaluation included the following:

• Development of parameters for cutting

and welding conditions;
- Welding and cutting test panels on the basis of selected parameters;
- Radiographic, metallographic, and mechanical evaluations of the test panels;
- Evaluation of damage on the weld underbead; and
- Evaluation of weld-gap tolerance and filler requirements.

The report concludes that laser welding is an effective joining method for In-718 in up to ½-in. (1.27-cm) thicknesses. It produces a high joint efficiency (welded joints retain about 90 percent of the strength of the unwelded alloy) and narrow welds having high depth-to-width ratio. It requires low specific-energy input, and thermal distortion is minimal.

To obtain autogenous welds with good bead reinforcement, it is necessary to fit together the faying surfaces within 3 percent of the thickness of the material. Components closer than 1 in. (2.54 cm) to the underbead can be severely damaged during high-power welding.

Furtner development is needed to reduce porosity defects, particularly in material one-half in. (1.27 cm) thick. More work is also needed to analyze microfissuring in restrained weldments.

Cutting of In-718 by laser is fast and produces only a narrow kerf. The cut edge requires dressing, however, if it is to endure fatigue.

*"Inconel" is a registered trademark of the INCO family of companies.

This work was done by C. M. Banas of United Technologies Corp. for **Marshall Space Flight Center**. *To obtain a copy of the report, "Laser Welding and Cutting of In-718 Nickel Alloy," Circle 96 on the TSP Request Card.* *MFS-27208*

Making Fiber-Reinforced Metal by Rapid Solidification

The present role and future potential of rapid solidification are discussed.

A report highlights the advantages and versatility of rapid-solidification technology in the fabrication of fiber-reinforced metal-matrix composites. It discusses the present role and future potential of the technology. It includes tables that compare the rapid-solidification methods and provides an extensive list of references.

Regardless of the end product — whether a flat panel or a turbine blade — composite monotapes are the building blocks from which continuous-length, fiber-reinforced metal-matrix composites are made. Consisting of single layers of continuous fibers embedded in metal tapes, monotapes are built up and pressed together to form the part.

The report describes a variety of methods for making monotape. Common to all is rapid solidification of the liquid metal — "rapid" meaning cooling rates of 10^4 to 10^6 K/s. Among the methods are the following:
- Powder cloth,
- Foil/fiber,
- Plasma spraying, and
- Arc spraying.

All of the methods for the fabrication of fiber/metal composites described in the report maintain accurate fiber/matrix volume proportions and accurate distributions of fibers. This is a significant advantage over such conventional powder-metallurgy techniques as extrusion or infiltration of metal.

This work was done by Ronald D. Noebe of **Lewis Research Center** *and Ivan E. Locci of Case Western Reserve University. Further information may be found in NASA TM-101450 [N89-15201], "The Role of Rapid Solidification Processing in the Fabrication of Fiber Reinforced Metal Matrix Composites."*

Copies may be purchased [prepayment required] from the National Technical Information Service, Springfield, Virginia 22161, Telephone No. (703) 487-4650. Rush orders may be placed for an extra fee by calling (800) 336-4700.
LEW-14918

Mathematics and Information Sciences

Hardware, Techniques, and Processes

95 Autonomous-Control Concept for Instrument Pointing System

100 Automatic Monitoring of Complicated Systems

100 Software Model of Software-Development Process

101 Markov Chains for Testing Redundant Software

Computer Programs

69 Algebraic Generation of Two-Dimensional Grids

Autonomous-Control Concept for Instrument Pointing System

Advanced control adaptation strategies are synthesized.

NASA's Jet Propulsion Laboratory, Pasadena, California

The integrated payload articulation and identification system (IPAIDS) is a conceptual system to control the aiming of instruments aboard a spacecraft of the proposed Earth Observation Systern (EOS). The principal features of this concept include advanced control strategies intended to assure the robustness of performance over a wide range of uncertainties in the characteristics of the spacecraft and instrument system. Though intended originally for application to a spacecraft system, the IPAIDS concept has potential utility on Earth; for example, the automatic control of autonomous (robotic) vehicles or of remote sensing systems.

The basic problem is to aim multiple instruments simultaneously at targets of op-

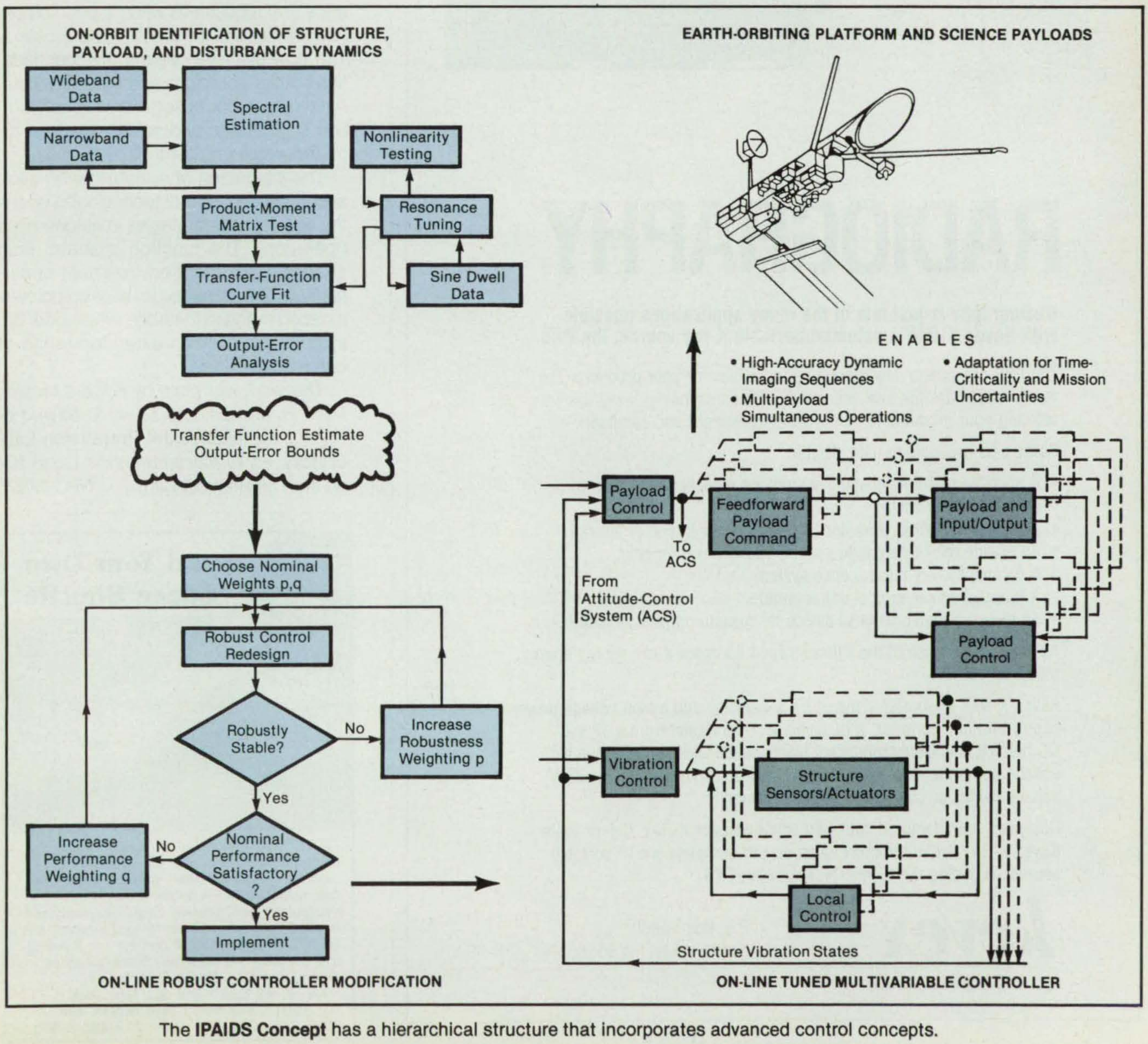

The **IPAIDS Concept** has a hierarchical structure that incorporates advanced control concepts.

portunity. These instruments will have to function accurately in an environment of dynamic disturbances, including structural vibrations. Moreover, the instruments supported by their articulation devices and structures are dynamically complex and interactive. The control system must be highly accurate and capable of robust adaptation to the dynamics of various scenarios, to poorly predicted interactions between instruments and the rest of the dynamic system, and to limitations of mathematical models of the system and of tests performed on the ground.

The IPAIDS controller-adaptation feature is provided by the following hierarchy of strategies for modification and tuning: (1) detection of the predicted operating regime change and insertion of robust controller predesigns; (2) on-orbit identification of the parameters and other features of the mathematical model of the system, with online robust controller redesign; and (3) modern indirect adaptive control. These functions are coordinated to provide maximum performance under a variety of operational scenarios, depending on the degree of performance desired and the relative degree of time criticality involved. In particular, predesigned changes in the robust controller are adequate in scenarios where immediate control-modifying actions are required but where high performance is not crucial. In contrast, scenarios that require high performance but allow sufficient time for testing and computation invoke the on-orbit identification and on-line robust controller redesign function. Finally, situations critical in both time and performance require a modern indirect-adaptive-control approach.

The Integrated Identification and Control system contains and updates programmable parameters that are used by the Control subsystem software and hardware. The active elements include a parameter-identification function, a model-adjust function, and a control tuning function.

The figure portrays autonomous on-orbit identification in support of robust controller tuning. The approach utilizes a combination of parametric and non-parametric identification techniques in conjunction with control strategies that incorporate H_2-based tuning heuristics. These heuristics allow for intelligent tradeoffs to be made between control-system performance and robustness with respect to confidence levels of the identified parameters. The flow diagram depicts this identification-control paradigm and the multi-input, multi-output controllers for carrier-vibration suppression and science-payload articulation/pointing control.

The integration of system-identification and advanced control technologies opens the way for new strategies in autonomous operations. The function space of time criticality and plant/environment uncertainty vs. performance is more completely mapped by these methods, which offer the system designer an extended range of control capabilities.

This work was done by Edward Mettler, Mark H. Milman, and David S. Bayard of Caltech for **NASA's Jet Propulsion Laboratory**. *For further information, Circle 107 on the TSP Request Card.* *NPO-17521*

BMDP

the statistician's choice ... the researcher's edge!

For over twenty years **BMDP** has been regarded as **the most reliable and complete** statistics package available. Today, it remains **the choice of professional statisticians**--industry wide. In 1990, we carry on this tradition by offering the most advanced statistical library available for mainframe, mini, and microcomputer platforms.

No matter what software you're currently using for database management or graphics, **BMDP is your statistical edge!** While other packages offer only general procedures to cover the variety of advanced techniques, BMDP provides specific programs that quickly test even the most sophisticated multivariate models.

Advanced Programs for 1990

- *New* **Maximum Likelihood Estimation**
- *New* **Polychotomous Logistic Regression**
- *New* **Multiway Correspondence Analysis**
- **Stepwise Regression**
- **Stepwise Logistic Regression**
- **Stepwise Discriminant Analysis**
- **All Possible Subsets Regression**
- **Derivative-free Non-linear Regression**
- **Spectral Analysis**
- **Box-Jenkins Time Series**
- **Life Tables & Survival Functions**
- **Survival Analysis-Cox Models**
- **Missing Data Estimation & Correlation**
- **Repeated Measures ANOVA/ANCOVA**
- **Repeated Measures (w/ missing trials)**
- **Multivariate ANOVA & ANCOVA**
- **General Mixed Model ANOVA**
- **Regression on Principal Components**
- **Polynomial Regression**
- **Partial Correlation Regression**
- **Canonical Correlation**
- **Log-linear Modeling**
- **Linear Scores for Preference Pairs**
- ***And Much More!***

Call (213) 479-7799
Get BMDP Free For 30 Days!

BMDP Statistical Software, Inc.
1440 Sepulveda Boulevard Los Angeles, California 90025 FAX (213) 312-0161

Circle Reader Action No. 421

Automatic Monitoring of Complicated Systems

Computers can perform routine analysis of operations, alerting human operators to signs of trouble.

NASA's Jet Propulsion Laboratory, Pasadena, California

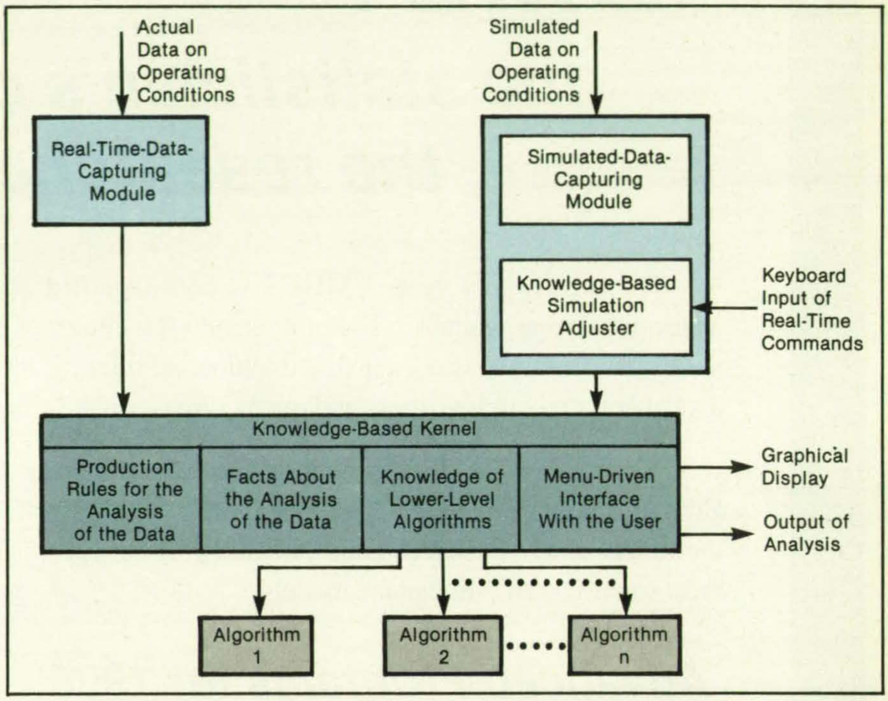

The **Prototype System** monitors incoming data and compares them to simulated data that have been adjusted to reflect recent and unsimulated real-time commands.

A collection of computer programs is being developed for an expert computer system that will perform the complicated, tedious, and repetitive portions of the analysis of telemetry data from spacecraft. By relieving human operators of these tasks, the system will not only provide nonstop, accurate surveillance of the incoming data but will also free the operators to concentrate their expertise on unexpected, abnormal operating conditions. The general software concept has obvious potential for use in such terrestrial systems as production lines, power-distribution networks, chemical processes, large airplanes, and other assemblies of interdependent equipment.

The prototype system (see figure) performs real-time verification of all incoming data. When the system is unable to explain discrepancies with certainty as resulting from data out of synchronization or other false-alarm conditions, the system triggers alarm devices to request assistance from designated individuals.

The system incorporates a knowledge base, currently estimated to contain several hundred relevant facts and rules for performing the analysis. The system also contains a powerful inference engine (software for performing reasoning and logical deduction). The system incorporates standard programs for the processing of numbers, for which expert-system/artificial-intelligence techniques are unsuitable. The system can be overriden by individuals with appropriate knowledge, experience, and permission to do so.

The system is implemented hierarchically by use of a commercial expert-system-shell computer program that serves as the framework for the knowledge-based portion of the system. One top-level C program accepts the incoming data through a serial input port and buffers the data for use as needed. Another top-level program both receives data from the telemetry-simulation facility and accepts, from an operator keyboard, input containing information on real-time commands that have been issued and that are not accounted for in simulation.

The two top-level programs feed streams of actual and simulated data to the knowledge-based kernel of the program, which resides at the second level of the hierarchy. The knowledge-based kernel calls lower-level algorithmic routines as they are needed to process numbers. The results are returned to the kernel from the lower-level routines. These results constitute additional inputs that, in conjunction with production rules, assist the knowledge-based kernel in producing an analysis for each line of real-time telemetry.

The hierarchical organization of this program provides for automated supervision of the analysis process. For the longer term, this organizational modularity will also enable integration of the prototype system into a larger future system of cooperating experts that will be responsible for a larger set of monitoring and maintenance tasks.

This work was done by Ursula M. Schwuttke of Caltech for **NASA's Jet Propulsion Laboratory**. *For further information, Circle 11 on the TSP Request Card.*
NPO-17409

Software Model of Software-Development Process

Costs, times, and other quantifiable attributes of development of large computer programs are estimated.

NASA's Jet Propulsion Laboratory, Pasadena, California

A collection of computer programs constitutes a software tool for the simulation of medium- to large-scale software-development projects. The tool is intended to aid managers in planning, managing, and controlling software-development processes by reducing the uncertainties in budgets, required personnel, and schedules.

To make an adequate mathematical model of a complicated development process, it is necessary to quantify characteristics that are usually difficult to quantify and/or identify, like human factors and feedback loops. Of course, it is also necessary to include easily identifiable and more-readily quantifiable characteristics like costs, times, and numbers of errors. A mathematical model that incorporates these and

other factors of the dynamics of the software-development process is implemented in the Software Life Cycle Simulator (SLICS) computer program.

SLICS is composed primarily of staff, product, and budget subsystems. The staff subsystem models the functions that determine the required level of the work force. The product subsystem models the functions that describe progress in developing the software product. These functions are determined by the productivity and the rework activities that are needed when requirements are changed or errors are detected.

The budget subsystem includes functions that model various expenditures and the total cost in relation to the available budget. The budget subsystem controls both the staff and the product subsystems according to the status of the budget. The staff and product subsystems are linked through information on the assignment of personnel and through the status of progress toward the completed product.

SLICS is integrated with an input expert system, an output expert system, and a knowledge-based management system, to obtain the overall software collection called the Hybrid Expert Simulation System (HESS) for software-development processes (see figure). The input expert system (IES) verifies the compatibility of the components of the input vector. The IES alerts the user to any erroneous input vectors before the vectors are inserted into SLICS. The IES also makes recommendations as to which components of the input vector should be altered.

The output expert system makes recommendations regarding the software-development process, based on analysis of the output from SLICS, the characteristics of the input vector, and, if applicable, the characteristics of the initial design of the software-development process undergoing simulation. The output expert system also suggests how to alter the input vector to make the recommendations more desirable.

The knowledge-based management system is a data-based management system composed of knowledge-based records. Each knowledge-based record is composed of a vector of input data (i.e., input vector) and its respective set of recommendations. After each simulation run, the user decides whether to add the resulting knowledge-based record to the knowledge-based management system.

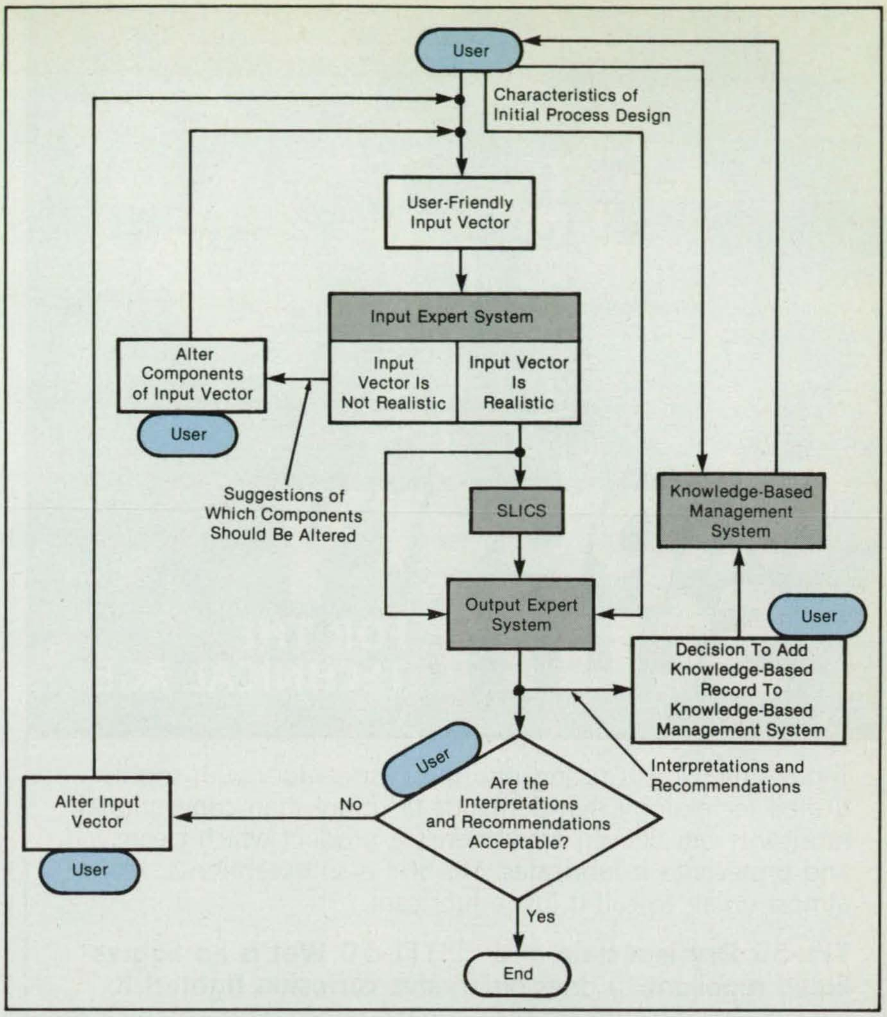

SLICS simulates the dynamics of a software-development process. In combination with input and output expert software systems and a knowledge-based management software system, it develops information for use in managing a large software-development project.

In combination with the other programs in HESS, SLICS can be used for any or all of the following:

- To test various management actions, policies, options, and procedures;
- To test the impacts of various assumptions, scenarios, and environmental factors on the software-development process;
- To predict the consequences of management actions on the interrelationships among components and flows of the software-development process; and
- To examine the sensitivity of the software-development process to various internal and external factors.

This work was done by Chi Y. Lin and Debra J. Synott of Caltech and Reuven R. Levary of St. Louis University for **NASA's Jet Propulsion Laboratory**. *For further information, Circle 101 on the TSP Request Card.*
NPO-17424

Markov Chains for Testing Redundant Software

The reliability of multiple-version process-control software is verified.

Langley Research Center, Hampton, Virginia

A preliminary design has been developed for a validation experiment (actually, a numerical simulation) that addresses problems unique to assuring the extremely high quality of multiple-version programs in process-control software. In addition, the approach takes into account the inertia of the controlled system in the sense that it can take more than one failure of the control program to cause the controlled system to fail.

The verification procedure consists of two steps: experimentation (that is, numerical simulation) and computation, with a Markov model for each step. The experimental step consists of running the programs through many simulated missions and recording the states of the programs

for each iteration of the control loop. The states in the Markov chain represent the number of programs that give correct answers during the current iteration of the control loop, and the transitions are the probabilities of changing states for the next iteration. The estimates of the transition probabilities, together with confidence limits, result from an analysis of these data.

This procedure makes no assumptions about independent failures of the programs. It includes the effect of the operating environment where the next input is a function of external forces (or the mathematical equivalent of forces) and previous control reactions. It captures the possible lingering effect of a previous failure of a program and the possible effect of an input region on such a failure.

The computational step modifies the Markov chain used in the experimental step by adding more states and rearranging some of the transition probabilities. The additional states express the fact that it is necessary for the majority of programs to fail several times in a row before the controlled system is finally made to fail. The values for the transition probabilities are those determined by the experiment, but they occur somewhat differently in the structure of the new chain. The probability of the failure of the system due to faults in the multiple-version software is computed from this modified model.

Although the actual operation is carried out as described, the pre-experimental design phase proceeds in reverse order. An analysis of the second Markov model reflecting the inertia of the controlled system is made to determine what values of transition probability give the required reliability. In general, confidence intervals depend on the number of trials. Because one of the goals is a procedural efficiency greater than that of natural life testing, this number is chosen so that the increase in efficiency is about one order of magnitude.

The most important aspect of this technique is that the approach offers an efficient method for verification of the reliability of multiple-version control software with no assumption of the failures of independent programs. It includes a confidence level and realistically includes the effect of the control environment on the reliabilities of programs.

This work was done by Allan L. White of **Langley Research Center** *and Jon A. Sjogren of the U.S. Army Avionics Research and Development Activity. For further information, Circle 25 on the TSP Request Card.* LAR-13812

New on the Market

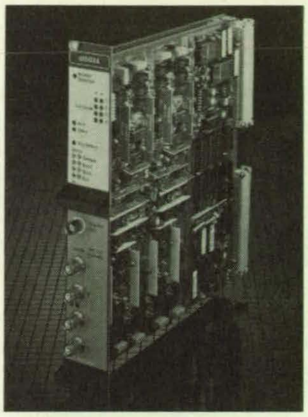

The DL6024 **data acquisition system** from Lucas Industrial Instruments, Severna Park, MD, provides multichannel sampling capability in one module, enabling higher channel density per system at a lower cost per channel. Designed for applications requiring 72 dB dynamic range and low distortion, the DL6024 can sample at speeds up to 100 MHz and synchronously sample up to 200 channels.
Circle Reader Action Number 778.

The new PtSi **infrared imaging system** from Eastman Kodak Company's Federal Systems Div., Rochester, NY, features a detector array with 640 x 486 pixels, signal processing electronics for 30 frames/sec. imaging, 12 bit digital output, and freeze frame capability. The PtSi camera is available in a liquid nitrogen Dewar configuration offering more than eight hours hold time, or in a closed-cycle Stirling cooler configuration that accomodates application-specific filters.
Circle Reader Action Number 780.

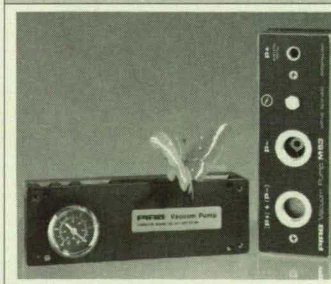

PIAB Vacuum Products, Hingham, MA, has introduced a new line of compact **vacuum pumps** for such applications as part handling, packaging, lifting, and suctioning operations. Designed with a unique multi-ejector system that minimizes air consumption and increases efficiency, the pumps can reach suction capacity ranges up to 900 scfm with a minimal amount of energy. They contain no moving parts, generate no heat, and are whisper quiet.
Circle Reader Action Number 788.

WaferScale Integration Inc., Fremont, CA, has introduced the industry's fastest 1-megabit word-wide **CMOS EPROM**, with access times of 120 to 200 ns. When used with 16- or 32-bit bus microprocessors, the word-wide architecture of the WS27C210L offers a 16 to 38 percent reduction in board space requirements compared to byte-wide solutions. The new EPROM enables microprocessors such as Intel's 80386 and Motorola's 68040 to incorporate operating systems and applications software into EPROM, eliminating tedious downloading into RAM. It is also suited for non-volatile program storage in embedded control applications such as laser printers and telecommunications equipment. Packaging options include CERDIP, plastic leaded chip carrier (PLCC), ceramic leadless chip carrier (LCC), and the ceramic leaded chip carrier (CERQUAD).
Circle Reader Action Number 782.

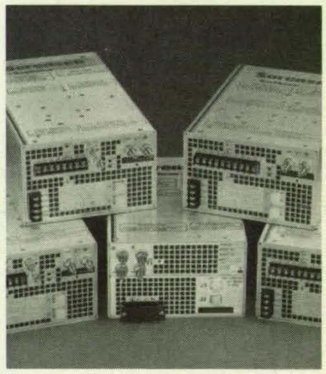

The S series of **power supplies** from the Sorensen Company, Chicago, IL, features models with one to five outputs and power levels of 500, 750, 1000, 1250, 1500, and 2000 watts. The devices have a power MOSFET design for high reliability and higher efficiencies, and a modified forward converter topology that eliminates inverter transformer core saturation and permits fast load response. The "S" series operates at switching frequencies up to 144 kHz.
Circle Reader Action Number 784.

Plus 5, Santa Monica, CA, has introduced a credit card sized **memory card** that records and stores up to 1024KB with an access time better than 160 nanoseconds. Called the PCard, the TTL-compatible device is available as SRAM, EPROM, and EEPROM and can be used with the IBM PC/AT bus or an RS232 interface. Applications include hand-held terminals, data acquisition, process control, and portable computerized stock control systems.
Circle Reader Action Number 786.

New on the Market

Image Analyst™ 7.1, a new **image processing and analysis software package** from Automatix Inc., Billerica, MA, features a graphical user interface designed to reduce training and support costs, a menu structure that enables applications to be installed without programming, and a standard computer platform for increased performance with third-party products. The software outputs dimensional and process data in spreadsheet format for simplified analysis. Image Analyst runs on a Macintosh-based workstation and is available on factory-hardened Autovision 90 platforms—for product inspection, gauging, and flaw detection.
Circle Reader Action Number 796.

VOYAGER™, a new **x-ray microanalysis system** from Tracor Northern Inc., Middleton, WI, features an integral SPARC-based workstation, UNIX multitasking operating system, high-resolution monitor, and windowing display capability. The new system includes the Proza™ Microvolume analysis program, for improved resolution and extended spectral range, and the Labnote™ report generation program which enables users to produce custom reports combining text with tabular data, spectral data, and images directly from VOYAGER screens. Output is via a laser printer.
Circle Reader Action Number 798.

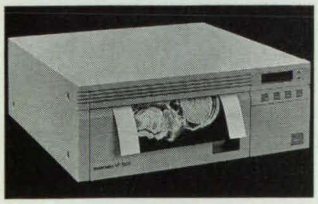

The VP-3500 **video printer** from Seikosha America Inc., Mahwah, NJ, produces 64-tone gray-scale prints with a resolution of up to 1280 lines and a line rate high enough to satisfy MR, CT, and Cath Lab requirements. Designed for business, scientific, engineering, and medical applications, the VP-3500 requires no software and produces hardcopy printouts from most video monitors that display data from imaging systems, microscopes, PCs, optical disk systems, or virtually any device with a video output. The VP-3500 retails for $6700.
Circle Reader Action Number 800.

The LAD **large area display system** from Greyhawk Systems Inc., Milpitas, CA, offers 7500 x 5000 pixels resolution, 1500 lumen light output, and flicker free, full continuous tone color images. It accepts industry-standard raster and vector data formats and features a screen two meters high by three meters wide. Based on Greyhawk's proprietary Liquid Crystal Light Valve (LCLV) technology, the LAD system is ideal for applications involving the display of high information content images, such as mapping, command and control, network management, 3D modeling, spatial light modulator systems, printed circuit board fabrication systems, and color printers.
Circle Reader Action Number 794.

Spectrum Coatings Laboratories Inc., Providence, RI, has introduced a series of chemical- and corrosion-resistant **epoxy primers** for treated and untreated metal surfaces. Suited for marine, aviation, industrial, and transportation applications, the Series 1006 epoxy primers protect against the effects of salt spray, humidity, solvents, oils, and hydraulic fluids. The two-component primers are formulated to accept all industrial and military specification topcoats and can be applied with electrostatic or high-volume, low-pressure (HVLP) spray equipment. They allow a recoat time of 60 minutes and cure cycles at ambient or elevated temperatures.
Circle Reader Action Number 790.

Intech Corp., Fort Lee, NJ, has introduced Magnet Quick, an automatic **recharging device** that instantly restores full magnetic power to a variety of tools. Magnet Quick first neutralizes any residual magnetism in the tool to create a reservoir capacity that can accept a full magnetic charge. A new charge is then held to ensure optimum magnetic performance.
Circle Reader Action Number 792.

New Literature

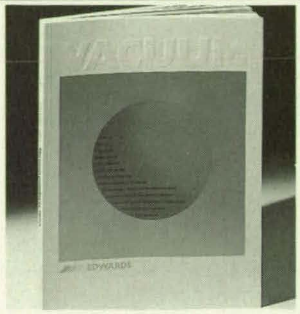

Edwards High Vacuum Intl., Wilmington, MA, is offering a free 250-page catalog on its complete line of **vacuum components and systems**. Products include mechanical rotary pumps, Drystar® oil-free pumps and systems, magnetically-levitated turbomolecular pumps, pressure and flow control instrumentation, thin film deposition systems, leak detection systems, and industrial and laboratory freeze dryers, valves, and fittings.
Circle Reader Action Number 702.

The 1990 PC Data Acquisition Catalog from ADAC, Woburn, MA, features a variety of **PC/XT/AT/386 compatible products**, including plug-in I/O boards, I/O subsystems, industrial PCs, signal conditioning products, and data acquisition and control software. Available free of charge, the catalog contains technical papers on such topics as gain and system resolution, signal conditioning solutions and techniques, and networking PC-based data acquisition systems.
Circle Reader Action Number 710.

Shin-Etsu Silicones of America Inc., Torrance, CA, has published a 20-page product guide on one- and two-component **RTV silicones.** The guide describes 43 products complete with cure systems, colors, and technical specifications such as specific gravity, tensile and dielectric strengths, elongation, viscosity, bond strength, temperature and chemical resistance, and resiliency. It also provides a brief background on the company, as well as information on one-part primers, two-part mixing procedures, and applications for both one- and two-part RTV's.
Circle Reader Action Number 708.

A four-page color brochure from Innovative Imaging Systems Inc., Cleveland, OH, illustrates the VolumeView™ family of industrial **computed tomography x-ray inspection systems** for rapid, nondestructive 3D inspection of manufactured parts. The systems can acquire and reconstruct 3D volume 512 x 512 x 512 points in 120 seconds, with spatial resolutions from 0.005" to 0.05". Benefits include reduced inspection costs, rapid comparison of part dimensions, in-process verification to production standards, automatic flaw detection, and real-time production line inspection capability. The modular units consist of a host computer and data acquisition, image reconstruction, and operator interaction subsystems.
Circle Reader Action Number 712.

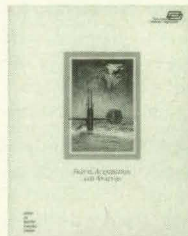

A new brochure from Concurrent Computer Corp., Westford, MA, describes the company's **real-time signal acquisition and analysis products**. The eight-page brochure highlights the company's two product lines: the real-time UNIX Series 6000 with Motorola 68030 CPUs, and the Series 3200 with OS/32 operating system, both of which feature multiple processors and buses. The publication also features third-party hardware and software products and provides case histories in speech processing, radar, and underwater acoustics.
Circle Reader Action Number 704.

A new line of **aerosol and coating products** for construction, industrial maintenance, and field service applications is described in an eight-page bulletin from Panduit Corp., Tinley Park, IL. Product highlights include electrical/electronic cleaners, electrical sealants, greases, lubricants, and coatings. Most Panduit aerosols contain no fluorocarbons; they use carbon dioxide as propellant.
Circle Reader Action Number 706.

New Literature

A free 360-page catalog from National Instruments, Austin, TX, describes the company's line of **hardware and software products for engineering and scientific applications**. The full-color catalog is divided into four product areas: application software, GPIB interfaces, data acquisition, and VXIbus. A new products section includes GPIB-to-serial and GPIB-to-parallel converter boards; GPIB interface kits for Apollo workstations; a five-slot, portable VXI chassis; a low-cost multifunction board for PC/XT/AT and compatibles; and two high-performance boards for the Macintosh II Nubus.
Circle Reader Action Number 726.

Data Translation, Marlboro, MA, is offering two free handbooks that describe its **data acquisition and image/array processing products** on IBM PCs, PS/2, Macintosh II, and other popular microcomputers. The 1990 Data Acquisition Handbook and Image Processing Handbook detail more than 600 boards, software packages, and accessories. They contain data sheets, product summary tables, application stories, and ordering information, as well as technical articles covering image processing and data acquisition from the basics to the state of the art.
Circle Reader Action Number 718.

Ceramic Source '90, a **reference guide for the ceramics field**, is available from the American Ceramic Society Inc., Westerville, OH. The guide consists of a product directory featuring raw materials/ ceramic powders, production equipment, coatings and finishings, testing and evaluation, and ceramic components and devices; a list of organizations, their services, and key contacts; a product tradenames section; a technical data section providing tables on recently published ceramic properties; and an international company directory with more than 3500 listings.
Circle Reader Action Number 716.

Trek Inc., Medina, NY, has published a 36-page catalog describing the company's line of **high voltage operational amplifiers and supplies, noncontacting electrostatic voltmeters, and static measurement and control products**. The brochure lists specifications, applications, and general product data — including power requirements, operating conditions, and dimensions. It also includes product selection charts and a special services section describing Trek's custom design and private labeling services.
Circle Reader Action Number 724.

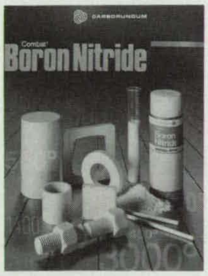

Combat®**boron nitride (BN)**, a synthetic ceramic material that resists temperatures up to 3000° C and has a dielectric strength of 2300 volts per mil, is described in a 12-page brochure from the Carborundum Company, Niagra Falls, NY. The brochure details the electrical, mechanical, thermal, and chemical properties of Combat BN in solid shapes, powders, coatings and aerosol sprays. Combat BN machinable solids are used in electronic applications such as heat sinks, sputtering targets, and electrical insulators, while Combat BN powders, are used as resin additives to increase the thermal and electrical properties without abrading delicate electronic components.
Circle Reader Action Number 720.

A 64-page catalog from Eurotherm Corporation, Reston, VA, features **temperature and process controllers, programmer/controllers, power control products, indicators and alarms, and system products**. Each product section begins with a tutorial, applications data, a glossary, and product selection guides.
Circle Reader Action Number 714.

Subject Index

A

ACTINOMETERS
Field-induced-gap infrared detectors
page 32 NPO-17526

Diagnosis of a pressure-modulator-radiometer cell
page 63 NPO-17528

ACTUATORS
Electrostatic linear actuator
page 87 NPO-17684

ADAPTIVE CONTROL
Adaptive-control experiments on a large flexible structure
page 78 NPO-17478

ADHESIVES
Epoxies bond waveguides to flanges
page 40 NPO-17497

AIRCRAFT NOISE
Stowable mechanical sound suppressor
page 86 LAR-14158

ALGEBRA
Algebraic generation of two-dimensional grids
page 69 LAR-13800

ALIGNMENT
Quick check of butt-weld alignment
page 89 MFS-29423

ALUMINUM GRAPHITE COMPOSITES
Lightweight, thermally conductive composite material
page 66 LEW-14814

AMPLIFIERS
32-GHz wideband maser amplifier
page 38 NPO-17558

ANTENNAS
Wideband microstrip antenna-feeding array
page 26 NPO-17548

ARRAYS
Wideband microstrip antenna-feeding array
page 26 NPO-17548

ARTIFICIAL INTELLIGENCE
Automatic monitoring of complicated systems
page 100 NPO-17409

B

BACKUPS
Preventing contamination in electron-beam welds
page 90 MFS-29428

BEARINGS
Rolling-contact spalling in bearings
page 81 MFS-27201

BOUNDARY LAYER TRANSITION
Detecting boundary-layer transition in cold environments
page 76 LAR-13830

BUTT JOINTS
Quick check of butt-weld alignment
page 89 MFS-29423

C

CERAMICS
Tribological properties of ceramics
page 67 LEW-14833

CIRCUIT BOARDS
Connecting multiple wires to a single through hole
page 92 MFS-29405

CIRCUITS
Concept for generation of long Pseudorandom sequences
page 50 NPO-17241

COMBUSTION CHAMBERS
Perspective on dilution jet mixing
page 83 LEW-14614

COMPOSITE MATERIALS
Lightweight, thermally conductive composite material
page 66 LEW-14814

Making fiber-reinforced metal by rapid solidification
page 94 LEW-14918

COMPUTER PROGRAMS
Numerical analysis of flows with FIDAP
page 84 MFS-27219

CONTAMINANTS
Hot wax sweeps debris from narrow passages
page 89 MFS-29462

CONTROL
Autonomous-control concept for instrument pointing system
page 95 NPO-17521

CONTROLLERS
Disturbance-accommodating controller would aim antenna
page 42 NPO-17631

Programmable direct-memory-access controller
page 54 NPO-17341

COORDINATES
Algebraic generation of two-dimensional grids
page 69 LAR-13800

CRYOGENIC WIND TUNNELS
Detecting boundary-layer transition in cold environments
page 76 LAR-13830

Classifieds

Classified advertising rates and specifications are as follows: Set in 8 point light typeface, with up to five words at beginning of copy in bold caps. Count box numbers as six words.

50 words or less .... $ 180
100 words .... $ 250

Check or money order must accompany order to: Classified Advertising Manager, NASA Tech Briefs, Suite 921, 41 East 42nd Street, New York, NY 10017-5391

A NEW MONTHLY DIGEST from four translated Soviet electronics journals for $200/year. Indispensable for specialists in Soviet technical intelligence, thesis advisors and front-end researchers. For a free sample write to Soviet Electronics Digest Dissemination Service, P.O. Box 857, Burtonsville, MD 20866

CRYOGENIC ROCKET PROPELLANTS
Insulation for cryogenic-liquid tanks
page 82 LEW-14707

CUBIC EQUATIONS
Algebraic generation of two-dimensional grids
page 69 LAR-13800

D

DATA CONVERSION ROUTINES
Peripheral equipment interchanges bytes of data
page 48 MFS-29478

DATA LINKS
Analyzing optical communication links
page 68 NPO-17444

DEBRIS
Hot wax sweeps debris from narrow passages
page 89 MFS-29462

DEMODULATORS
Digital demodulator for advanced receiver
page 44 NPO-17628

DIGITAL DATA
Peripheral equipment interchanges bytes of data
page 48 MFS-29478

DIGITAL SYSTEMS
Concept for generation of long Pseudorandom sequences
page 50 NPO-17241

DIGITAL ELECTRONICS
Digital demodulator for advanced receiver
page 44 NPO-17628

DOPPLER EFFECT
Doppler-shifted Raman spectroscopy measures flows
page 58 LAR-14133

E

EARTH OBSERVING SYSTEM (EOS)
High-resolution imaging spectrometer
page 52 NPO-17624

EARTH OBSERVATION (FROM SPACE)
Autonomous-control concept for instrument pointing system
page 95 NPO-17521

ELECTRIC CONNECTORS
Connecting multiple wires to a single through hole
page 92 MFS-29405

ELECTRIC MOTORS
Balanced-bridge feedback control of motor
page 52 NPO-17430

Electrostatic linear actuator
page 87 NPO-17684

ELECTROLYSIS
Electrolysis bubbles make waterflow visible
page 76 LEW-14797

ELECTRON BEAM WELDING
Preventing contamination in electron-beam welds
page 90 MFS-29428

ENDOSCOPES
Filter enhances fluorescent-penetrant-inspecting borescope
page 91 MFS-29379

ENTRAINMENT
Hot wax sweeps debris from narrow passages
page 89 MFS-29462

EPOXY RESINS
Epoxies bond waveguides to flanges
page 40 NPO-17497

EXPERT SYSTEMS
Automatic monitoring of complicated systems
page 100 NPO-17409

Software model of software-development process
page 100 NPO-17424

F

FEEDBACK CONTROL
Balanced-bridge feedback control of motor
page 52 NPO-17430

FIELD EFFECT TRANSISTORS
Gallium arsenide domino circuit
page 36 NPO-17417

FINITE ELEMENT METHOD
Numerical analysis of flows with FIDAP
page 84 MFS-27219

Combining thermal and structural analyses
page 84 LEW-14741

FLEXIBLE BODIES
Adaptive-control experiments on a large flexible structure
page 78 NPO-17478

FLOW CHARACTERISTICS
Numerical analysis of flows with FIDAP
page 84 MFS-27219

FLOW MEASUREMENT
Doppler-shifted Raman spectroscopy measures flows
page 58 LAR-14133

FLOW REGULATORS
Liquid-flow controller responds to pressure
page 72 MFS-28329

Liquid-flow controller with preset break pressure
page 73 MFS-28330

Liquid-flow controller with trickle preflow
page 74 MFS-28331

FLOW VISUALIZATION
Electrolysis bubbles make waterflow visible
page 76 LEW-14797

FLUORESCENCE
Filter enhances fluorescent-penetrant-inspecting borescope
page 91 MFS-29379

FOURIER ANALYSIS
Fourier analysis of vibrations of round structures
page 74 MFS-29334

FUEL SPRAYS
Liquid-flow controller with preset break pressure
page 73 MFS-28330

FUEL FLOW REGULATORS
Liquid-flow controller responds to pressure
page 72 MFS-28329

Liquid-flow controller with trickle preflow
page 74 MFS-28331

G

GALLIUM ARSENIDES
Gallium arsenide domino circuit
page 36 NPO-17417

GAS TURBINE ENGINES
Perspective on dilution jet mixing
page 83 LEW-14614

GERMANIDES
Ge/Si integrated circuit for infrared imaging
page 28 NPO-17397

GRINDING MACHINES
Automatic tension adjuster for flexible-shaft grinder
page 93 MFS-29351

H

HELICAL WINDINGS
Electrostatic linear actuator
page 87 NPO-17684

HELIUM
Static pressure-assisted seal for helium
page 70 MFS-29429

HIGH TEMPERATURE SUPERCONDUCTORS
$YBa_2Cu_3O_x$ superconductors doped with AgO
page 66 MFS-26078

I

IMAGING SPECTROMETERS
High-resolution imaging spectrometer
page 52 NPO-17624

INCONEL (TRADEMARK)
Welding and cutting a nickel alloy by laser
page 93 MFS-27208

INFRARED IMAGERY
Ge/Si integrated circuit for infrared imaging
page 28 NPO-17397

INFRARED DETECTORS
Field-induced-gap infrared detectors
page 32 NPO-17526

Tunable-quantum-well infrared detector
page 34 NPO-17361

INSTRUMENT ORIENTATION
Autonomous-control concept for instrument pointing system
page 95 NPO-17521

INSULATION
Insulation for cryogenic-liquid tanks
page 82 LEW-14707

IRRADIANCE
Calculating irradiance for photosynthesis in the ocean
page 64 NPO-17645

J

JET MIXING FLOW
Perspective on dilution jet mixing
page 83 LEW-14614

JET ENGINES
Stowable mechanical sound suppressor
page 86 LAR-14158

JIGS
Jig for stereoscopic photography
page 70 MSC-21397

JOINTS (JUNCTIONS)
Static pressure-assisted seal for helium
page 70 MFS-29429

L

LIGNIN
Lignin sensor based on flash-pyrolysis mass spectrometry
page 62 NPO-17592

LOGIC CIRCUITS
Gallium arsenide domino circuit
page 36 NPO-17417

M

MANAGEMENT PLANNING
Software model of software-development process
page 100 NPO-17424

MANIPULATORS
Robot hand would adapt to contours
page 86 NPO-16766

MARKOV CHAINS
Markov chains for testing redundant software
page 101 LAR-13812

MASERS
32-GHz wideband maser amplifier
page 38 NPO-17558

MASS SPECTROMETERS
Lignin sensor based on flash-pyrolysis mass spectrometry
page 62 NPO-17592

MEMORY (COMPUTERS)
Programmable direct-memory-access controller
page 54 NPO-17341

METAL MATRIX COMPOSITES
Making fiber-reinforced metal by rapid solidification
page 94 LEW-14918

METAL GRINDING
Automatic tension adjuster for flexible-shaft grinder
page 93 MFS-29351

MICROMECHANICS
Tribological properties of ceramics
page 67 LEW-14833

MICROSTRIP ANTENNAS
Wideband microstrip antenna-feeding array
page 26 NPO-17548

MICROWAVE AMPLIFIERS
32-GHz wideband maser amplifier
page 38 NPO-17558

MONITORS
Automatic monitoring of complicated systems
page 100 NPO-17409

MOTORS
Balanced-bridge feedback control of motor
page 52 NPO-17430

MULTISPECTRAL RESOURCE SAMPLER
Terrestrial-imaging spectroscopy
page 65 NPO-17432

N

NICKEL ALLOYS
Welding and cutting a nickel alloy by laser
page 93 MFS-27208

NOISE SPECTRA
Predicting noise from wind turbines
page 68 LAR-13984

NOISE REDUCTION
Stowable mechanical sound suppressor
page 86 LAR-14158

O

OCEANS
Calculating irradiance for photosynthesis in the ocean
page 64 NPO-17645

OPTICAL COMMUNICATION
Analyzing optical communication links
page 68 NPO-17444

OPTICAL FILTERS
Filter enhances fluorescent-penetrant-inspecting borescope
page 91 MFS-29379

P

PARABOLIC ANTENNAS
An optimal design for steerable dish antenna with BWG
page 33 NPO-17429

Disturbance-accommodating controller would aim antenna
page 42 NPO-17631

PERIPHERAL EQUIPMENT (COMPUTERS)
Peripheral equipment interchanges bytes of data
page 48 MFS-29478

PHOTOSYNTHESIS
Calculating irradiance for photosynthesis in the ocean
page 64 NPO-17645

PINTLES
Liquid-flow controller with preset break pressure
page 73 MFS-28330
Liquid-flow controller with trickle preflow
page 74 MFS-28331

PNEUMATIC EQUIPMENT
Automatic tension adjuster for flexible-shaft grinder
page 93 MFS-29351

POSITIONING DEVICES (MACHINERY)
Jig for stereoscopic photography
page 70 MSC-21397

PRESSURE MODULATOR RADIOMETERS
Diagnosis of a pressure-modulator-radiometer cell
page 63 NPO-17528

PRINTED CIRCUITS
Connecting multiple wires to a single through hole
page 92 MFS-29405

PROCESS CONTROL (INDUSTRY)
Markov chains for testing redundant software
page 101 LAR-13812

PROPELLANT SPRAYS
Liquid-flow controller responds to pressure
page 72 MFS-28329

PSEUDORANDOM SEQUENCES
Concept for generation of long Pseudorandom sequences
page 50 NPO-17241

PULSE POSITION MODULATION
Analyzing optical communication links
page 68 NPO-17444

PYROLYSIS
Lignin sensor based on flash-pyrolysis mass spectrometry
page 62 NPO-17592

Q

QUANTUM WELLS
Tunable-quantum-well infrared detector
page 34 NPO-17361

R

RADIATION MEASURING INSTRUMENTS
Tunable-quantum-well infrared detector
page 34 NPO-17361

RADIO ANTENNAS
An optimal design for steerable dish antenna with BWG
page 33 NPO-17429

RADIOMETERS
Diagnosis of a pressure-modulator-radiometer cell
page 63 NPO-17528
Field-induced-gap infrared detectors
page 32 NPO-17526

RAMAN SPECTROSCOPY
Doppler-shifted Raman spectroscopy measures flow
page 58 LAR-14133

RAPID QUENCHING (METALLURGY)
Making fiber-reinforced metal by rapid solidification
page 94 LEW-14918

RECEIVERS
Digital demodulator for advanced receiver
page 44 NPO-17628

REFLECTOR ANTENNAS
Disturbance-accommodating controller would aim antenna
page 42 NPO-17631

REMOTE SENSING
High-resolution imaging spectrometer
page 52 NPO-17624
Terrestrial-imaging spectroscopy
page 65 NPO-17432

ROBOTS
Robot hand would adapt to contours
page 86 NPO-16766

ROLLER BEARINGS
Rolling-contact spalling in bearings
page 81 MFS-27201

S

SCHOTTKY DIODES
Ge/Si integrated circuit for infrared imaging
page 28 NPO-17397

SEALS (STOPPERS)
Static pressure-assisted seal for helium
page 70 MFS-29429

SILVER OXIDES
$YBa_3Cu_3O_x$ superconductors doped with AgO
page 66 MFS-26078

SOFTWARE (COMPUTERS)
Markov chains for testing redundant software
page 101 LAR-13812

SOFTWARE ENGINEERING
Software model of software-development process
page 100 NPO-17424

SPALLING
Rolling-contact spalling in bearings
page 81 MFS-27201

SPECTROSCOPY
Terrestrial-imaging spectroscopy
page 65 NPO-17432

STEERABLE ANTENNAS
An optimal design for steerable dish antenna with BWG
page 33 NPO-17429

STEREO-PHOTOGRAPHY
Jig for stereoscopic photography
page 70 MSC-21397

STRUCTURAL ANALYSIS
Combining thermal and structural analyses
page 84 LEW-14741

STRUCTURAL VIBRATION
Fourier analysis of vibrations of round structures
page 74 MFS-29334
Vibrational responses of structures to impulses
page 80 NPO-17343

SUPERCONDUCTORS
$YBa_3Cu_3O_x$ superconductors doped with AgO
page 66 MFS-26078

T

TELEOPERATORS
Robot hand would adapt to contours
page 86 NPO-16766

THERMAL ANALYSIS
Combining thermal and structural analyses
page 84 LEW-14741

NASA Tech Briefs, ISSN 0145-319X, USPS 750-070, copyright © 1990 in U.S., is published monthly by Associated Business Publications Co., Ltd. 41 E. 42nd St., New York, NY 10017-5391. The copyrighted information does not include the individual Tech Briefs which are supplied by NASA. Editorial, sales, production and circulation offices at 41 E. 42nd Street, New York, NY 10017-5391. Subscriptions for non-qualified subscribers in the U.S., Panama Canal Zone, and Puerto Rico, $75.00 for 1 year; $125.00 for 2 years; $200 for 3 years. Single copies $10.00. Remit by check, draft, postal or express orders. Other remittances at sender's risk. Address all communications for subscriptions or circulation to NASA Tech Briefs, 41 E. 42nd Street, New York, NY 10017-5391. Second-class postage paid at New York, NY and additional mailing offices.

POSTMASTER: please send address changes to NASA Tech Briefs, 41 E. 42nd Street, Suite 921, New York, NY 10017-5391.

THERMAL CONDUCTORS
Lightweight, thermally conductive composite material
page 66 LEW-14814

THERMAL PROTECTION
Insulation for cryogenic-liquid tanks
page 82 LEW-14707

THREE DIMENSIONAL FLOW
Electrolysis bubbles make waterflow visible
page 76 LEW-14797

TRANSIENT RESPONSE
Vibrational responses of structures to impulses
page 80 NPO-17343

TRANSONIC WIND TUNNELS
Detecting boundary-layer transition in cold environments
page 76 LAR-13830

TRIBOLOGY
Tribological properties of ceramics
page 67 LEW-14833

TURBINE PUMPS
Fourier analysis of vibrations of round structures
page 74 MFS-29334

TURBINES
Predicting noise from wind turbines
page 68 LAR-13984

V

VERY LARGE SCALE INTEGRATION
Programmable direct-memory-access controller
page 54 NPO-17341

VIBRATION DAMPING
Adaptive-control experiments on a large flexible structure
page 78 NPO-17478

VIBRATION
Vibrational responses of structures to impulses
page 80 NPO-17343

W

WAVEGUIDES
Epoxies bond waveguides to flanges
page 40 NPO-17497

WELDED JOINTS
Quick check of butt-weld alignment
page 89 MFS-29423

WELDING
Preventing contamination in electron-beam welds
page 90 MFS-29428

Welding and cutting a nickel alloy by laser
page 93 MFS-27208

WIND TURBINES
Predicting noise from wind turbines
page 68 LAR-13984

Advertiser's Index

3-D Visions .... (RAC 669) 113
AISN Software .... (RAC 399) 110
AMP .... (RAC 657) 19
Abbott Laboratories .... (RAC 376) 85
Aerospatiale .... (RAC 658) 29
Algor Interactive Systems, Inc. .... (RAC 361) 80
Amco Engineering Co. .... (RAC 500) .... COV III
American Precision Industries .... (RAC 329) 106
Amoco Performance Products .... (RAC 336) 60-61
Anritsu America, Inc. .... (RAC 407) 9
Astro-Med, Inc. .... (RAC 405) 35
Austron, Inc. .... (RAC 304) 88
BMDP Statistical Software, Inc. .... (RAC 421) 100
Bruel & Kjaer Instruments, Inc. .... (RAC 319) 43
Burr-Brown Corporation .... (RAC 313) 72
COSMIC .... (RAC 334) 68
Capacitec .... (RAC 385) 110
Carley Lamps .... (RAC 409) 105
Caramaseal .... (RAC 415) 107
DSP Development Corporation .... (RAC 652) 23
David Sarnoff Research Center .... (RAC 604) 2-3
Digital Equipment Corporation 24-25
Eighteen Eight Laboratories .... (RAC 675) 81
Electro '90 .... (RAC 413) 109
Electro Scientific Industries, Inc. .... (RAC 625) 73
Extrude Hone/Surfex Division .... (RAC 426) 111
Fluoramics, Inc. .... (RAC 364) 77
Ford Aerospace 37
General Dynamics .... (RAC 305) 53
Grumman Data Systems .... (RAC 363) 11
Gulf State Utilities Co. .... (RAC 417) 107
Hardigg Industries, Inc. .... (RAC 492) 67
Hillman Rollers .... (RAC 325) 111
Humphrey, Inc. .... (RAC 626) 92
Hydra-Electric Co. .... (RAC 427) 111
IBM Corporation 46-47
IOtech, Inc. .... (RAC 303) 71
Illbruck .... (RAC 466) 83
Inco Alloys International .... (RAC 569) 7
Inco Specialty Powder Products .... (RAC 452) 59
Information Handling Services .... (RAC 546,419) 17,55
Instrumentation Marketing Corporation .... (RAC 448) 91
Integrated Inference Machines .... (RAC 307) 12
Integrated Systems Inc. .... (RAC 557) 45
International Robots & Vision Automation Show & Conference .... (RAC 456) 103
John Fluke Manufacturing Co. .... (RAC 668) 30-31
Kevex X-Ray Tube Division .... (RAC 531) 96
Kewaunee Scientific Corporation .... (RAC 430) 104
KineticSystems Corporation .... (RAC 458) 10
Lincoln Laser Company .... (RAC 593) 75
Link Flight Simulation Division .... (RAC 460) 5
MTI Instruments .... (RAC 365) 106
MathSoft, Inc. .... (RAC 628) 13
Micro Way .... (RAC 566) .... COV IV
Microstar Laboratories .... (RAC 552) 82
Mikron Instrument Co., Inc. .... (RAC 390) 108
Mobay Corp., Plastics and Rubber Division 41
Molecu Wire .... (RAC 388) 57
NUPRO Company .... (RAC 378) 39
National Instruments .... (RAC 681) 111
National Technical Systems .... (RAC 358) 69
New England Affiliated Technologies .... (RAC 547) 110
Nicolet Instruments .... (RAC 696) 27
Nordex .... (RAC 600) 110
Odetics Precision Time Division .... (RAC 346-348) 81,83,85
Omega Engineering, Inc. .... (RAC 617,619) .... COV II-1
Oracle Federal Division .... (RAC 494) 20-21
Primavera Systems, Inc .... (RAC 663) 80
RGB Spectrum .... (RAC 467) 8
RemGrit Corporation .... (RAC 320) 102
Rexham Industrial .... (RAC 369) 94
Rolyn Optics Co. .... (RAC 551) 110
SAMPE .... (RAC 503) 114
STN International .... (RAC 464) 49
Science Applications International Corporation .... (RAC 692) 65
Seikosha America, Inc. .... (RAC 462) 51
Servometer Corporation .... (RAC 490) 111
Silicon Composers, Inc. .... (RAC 679) 110
Small Parts Inc. .... (RAC 400) 110
Space Shuttle Models 96
Stat-Ease Inc. .... (RAC 393) 68
Sutrasoft .... (RAC 450) 111
Tescom Corporation .... (RAC 545) 108
The J.M. Ney Company/ NEYTECH Division .... (RAC 605) 110
The Lee Company .... (RAC 597) 105
Tiodize .... (RAC 422) 67
VAT Incorporated .... (RAC 518) 84
Videk .... (RAC 470) 4
Videotapes 88
World Precision Instruments .... (RAC 585) 110

***RAC** stands for **Reader Action Card.** For further information on these advertisers, please circle the RAC number on the Reader Action Card elsewhere in this issue. This index has been compiled as a service to our readers and advertisers. Every precaution is taken to ensure its accuracy, but the publisher assumes no liability for errors or omissions.

Five Centuries Ago, Shielded Enclosures Were Custom Made.

Some Still Are.

The crusading spirit is alive and well at AMCO. We have the proven capability, experience, and willingness to work with you on the more difficult shielding applications encountered today.

In 1962 AMCO designed and built the first Modular Shielded Enclosure System. Used by NASA on the Saturn Booster Program it remains today one of the most reliable on the market.

AMCO has made many advancements since then:

- ❒ Modular Shielded Enclosure Systems for FCC & Commercial Applications.
- ❒ Shielded Cabinets compatable to Tempest NACSIM-5100A.
- ❒ Custom or Modified Standard Shielded Enclosures for those very special needs – including Siesmic, Environmental, Drip Proof, Shock & Vibration.

For free catalogs call **1-800-833-3156**.
In Illinois call **708-671-6670**.
Ask for Commercial Catalog 650 and/or Heavy Duty Catalog 203.
For free initial consultation call **708-671-6670** and ask for The Performance Evaluation Lab-Extension 232.

amco®

AMCO Engineering Co.
3801 N. Rose Street
Schiller Park, Illinois 60176

See us at: Interface – Dallas, TX – 3/6-3/8 Booth #561
Southcon – Orlando, FL – 3/20-3/22 Booth #323-325
NAB – Atlanta, GA 3/21-4/3 Booth #2009-2013

Circle Reader Action No. 500

Weitek Your 386/486!

The new 4167 delivers up to 10 Megaflops when driven by NDP Fortran-486 and is supported by dozens of scientific, engineering and CAD applications. MicroWay provided the tools to develop many of these applications and supplies the interface cards required to use Weitek coprocessors in conjunction with with an 80387, in both standard AT bus and MicroChannel machines.

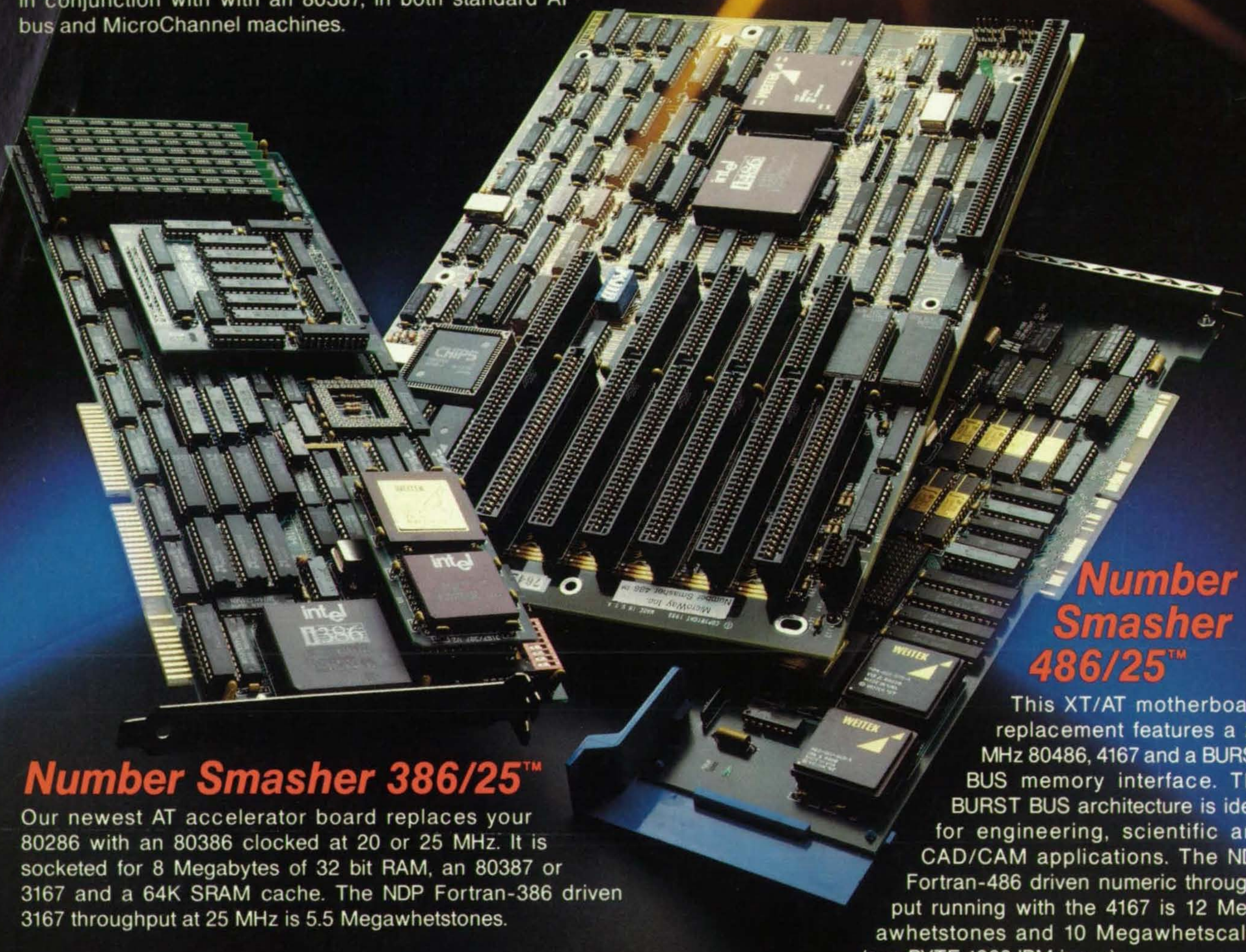

Number Smasher 486/25™

This XT/AT motherboard replacement features a 25 MHz 80486, 4167 and a BURST BUS memory interface. The BURST BUS architecture is ideal for engineering, scientific and CAD/CAM applications. The NDP Fortran-486 driven numeric throughput running with the 4167 is 12 Megawhetstones and 10 Megawhetscales (see BYTE 1989 IBM issue).

Number Smasher 386/25™

Our newest AT accelerator board replaces your 80286 with an 80386 clocked at 20 or 25 MHz. It is socketed for 8 Megabytes of 32 bit RAM, an 80387 or 3167 and a 64K SRAM cache. The NDP Fortran-386 driven 3167 throughput at 25 MHz is 5.5 Megawhetstones.

mW3167/387

This popular daughterboard (shown on the Number Smasher 386/25) lets you plug a 3167 and an 80387 into a 386 system that has a single EMC socket.

mW3167/MCA

Our MCA Weitek card runs in the IBM Model 70 and 80. At 20 MHz, its performance is 2 to 3 times that of an 80387.

NDP Fortran-486 and C-486 are globally optimized mainframe compilers that have been fine tuned for the 80486 and 4176.

3167/4167 Numeric Performance

	3167/MCA	NS 386/25	NS/486/25
Megawhetstones	3.4	5.5	12.2
Megawhetscales	1.6	3.1	9.9

Weitek 3167 amd 4167 are trademarks of Weitek Corp., MicroWay and Number Smasher are registered trademarks of MicroWay, Inc., 80386, 80387, 80486 are trademarks of Intel Corp.

MicroWay

World Leader in PC Numerics

Corporate Headquarters: P.O. Box 79, Kingston, MA 02364 USA (508) 746-7341
32 High St., Kingston-Upon-Thames, UK., 01-541-5466